RESEARCH & REVIEWS IN SCIENCE AND MATHEMATICS

GECE AKADEMİ

Book Title	:	**Research & Reviews in Science and Mathematics**
Publisher	:	Gece Kitaplığı
Editor in Chief	:	Doç. Dr. Atilla ATİK
Cover&Interior Design	:	Melek ZORLUSOY
Social Media	:	Arzu ÇUHACIOĞLU
Preparing for publication	:	Gece Akademi Dizgi Birimi
Puplisher Certificate No	:	15476
Certificate No	:	34559
ISBN	:	978-605-7631-45-9

Editor

Prof. Dr. Rıdvan KARAPINAR

Gece Publishing
ABD Adres/ USA Address: 387 Park Avenue South, 5th Floor, New York, 10016, USA
Telefon/Phone: +1 347 355 10 70

Gece Akademi
Türkiye Adres/Turkey Address: Kocatepe Mah. Mithatpaşa Cad. 44/C Çankaya, Ankara, TR
Telefon/Phone: +90 312 431 34 84 - +90 555 888 24 26

web: www.gecekitapligi.com —www.gecekitap.com
e-mail: geceakademi@gmail.com

CONTENTS

CHAPTER 1: Geostatistics for Conserving Marine Species
OLGU AYDIN, EYLEM KABA, AKİYUKİ KAWASAKI **5**

CHAPTER 2: Weather Early Warning System by Stream Processing Rainfall and Wind Sensor Data
ÖZGÜR YILMAZEL **23**

CHAPTER 3: General Screening of Propolis Around The World: Chemical Composition and Its Polyphenol Concentration
MERVE KESKİN, ŞABAN KESKİN, SEVGİ KOLAYLI **33**

CHAPTER 4: Getting Information From Human-Based Signals
ÖZGÜR AFŞAR **49**

CHAPTER 5: Importance of Algae as Biomass Energy
BETÜL KUT GÜROY, SİBEL BAYIL OĞUZKAN **59**

CHAPTER 6: Null Curve Evolution and Geometric Phase
NEVİN GÜRBÜZ **69**

CHAPTER 7: Usage of Pleurotus Ostreatus Fungal Biomass as A Biosorbent for Removal of Cr(VI) İons
ASLI GÖÇENOĞLU SARIKAYA **77**

CHAPTER 8: A Survey on The Historical Perspective of Soft Set Theory
GÜZİDE ŞENEL **85**

CHAPTER 9: On a New Approximation for Weighted Integral-Type Inequalities in VELS
LÜTFİ AKIN **93**

CHAPTER 10: On Some Properties of Hardy-Littlewood Maximal Operators on Hardy Spaces Built upon BFS
LÜTFİ AKIN **111**

CHAPTER 11: The Cobalt Diffusion in Mgb_2 Superconductors During Heat Treatment
ASAF TOLGA ÜLGEN **125**

CHAPTER 12: Nearness and Near Sets via Normal Subgroups
NURETTİN BAĞIRMAZ, HATİCE TAŞBOZAN **137**

CHAPTER 13: In Vitro Synthesis of mrna For Gene Therapy Applications
BETÜL AYDIN **147**

Geostatistics for Conserving Marine Species

Olgu AYDIN[1]

Eylem KABA[2]

Akiyuki KAWASAKI[3]

CHAPTER 1

1 Department of Geography, Faculty of Humanity, Ankara University

2 General Directorate of State Hydraulic Works

3 Department of Civil Engineering, The University of Tokyo

INTRODUCTION

Much of applied ecology is increasingly revolving around the need to manage ecosystems for biodiversity (Heywood 1995, Pearson and Carroll 1998). Therefore, species conservation, planning, and management need monitoring data in order to gather critical information about where a species occurs and its density (Underhill and Gibbons 2002). To this end, quantitative models of distribution enable assessment of major factors influencing distribution or prediction of where a given species should occur (Lawton and Woodroffe 1991). Recently, numerous techniques for obtaining basic quantitative information on species distribution have been developed (Phillips et al. 2006, Elith and Leathwick 2009, Leathwick et al. 2005, Leatwick et al. 2006). These new methodological approaches not only provide a better understanding of species–environment relationships but also allow the prediction of species distribution across unsampled locations.

The Mediterranean Sea is a marine diversity hot spot. It includes 7% of the world's marine species (approximating 17,000 marine species) for an area that represents less than 1% of the world's ocean surface (UNEP/MAP-Plan Bleu 2009). The recent marine biota in the Mediterranean Sea are primarily derived from the Atlantic Ocean. However, the wide range of climate and hydrology has contributed to the co-occurrence and survival of both temperate and subtropical organisms (Sara` 1985, Bianchi and Morri 2000). A large percentage of the Mediterranean marine species are endemic (Boudouresque 2004, Tortonese 1985). This sea also has its own set of emblematic species that are of conservation concern. There are several unique and endangered habitats including the seagrass meadows of the endemic Posidonia oceanica, the vermetid reefs built by the endemic gastropod *Dendropoma petraeum*, coralligenous assemblages, and deep-sea and pelagic habitats that support unique species. Among sensitive habitats that exist within the coastal ecosystems, vermetids are a gregarious species of gastropods living in lower intertidal habitats (Silenzia et al. 2004). They commonly colonize abrasion platforms generated by wave action and the edge of the resulting structure is frequently eroded, taking the shape of a continuous vertical wall 0.4–1-m high. (Lambeck et al. 2004). *Dendropoma petraeum* also resides in warm temperature areas of the world. It is not uniformly distributed along the northwest coast of Sicily between Cefalù (province of Palermo) and Trapani (Lunetta and Damiani 2002) and is not found in other places along the Sicilian coast because of inappropriate surface temperatures and rock sedimentation (Lunetta and Damiani 2002).

Dendropoma petraeum principally lives in the infralittoral/upper-circalittoral of temperate and tropical seas; some species can form solid organic reefs at the main sea level. These formations, being generally restricted to a very narrow belt, have been utilized as biological sea-level indicators (Bio SLI) (Laborel 1986, Laborel and Laborel-Deguen 1996, Antonioli et al. 1999) with a precision of 0.5–1.0 m (Laborel 1986). Among all the available Bio SLI organisms, the level of precision for vermetids is known to be high, thus representing one of the most reliable tools in paleo sea-level reconstruction. Numerous studies have been conducted to reconstruct sea-levels using *Dendropoma petraeum* in various locations such as Bermuda Islands, Brazil, Curacao, and Gran Cayman in the tropical Atlantic, Senegal, and the Hawaiian Island (Silenzia et al. 2004).

Bioconstructions such as *Dendropoma petraeum* are also modulators of coastal geomorphological processes because they protect rocks against erosion by generating extensive abrasion platforms. Furthermore, they act as biological engineers creating new habitats along the narrow lower intertidal fringe, thereby increasing its complexity and biodiversity (Calvo et al. 2009). Therefore, *Dendropoma petraeum* is a very sensitive species.

Understanding the spatial variations of any species is particularly important for conversation planning of areas in order to achieve a high degree of protection (Myers et al. 2000). Geostatistics is a branch of applied statistics that focuses on the detection, modeling, and estimation of spatial patterns (Rossi et al. 1992). In many situations, understanding a phenomenon and interpreting its nature depends on determining a spatial or geographical relationship with the phenomenon. Spatial data analysis methods supported by statistical tools have been increasingly gaining popularity in the exploration and modeling of events. Geographical information systems (GIS) and geostatistical approaches with kriging and cokriging interpolation can be applied to spatial mapping. In addition, the databases of many GIS explicitly contain topological relationships between various spatial features (Ungerer and Goodchild 2002). Geostatistical techniques are useful for providing estimates of sampled attributes at unsampled locations from sparse information (Hernandez-Stefanoni and Ponce-Hernandez 2006, Hassan and Atkins 2007, Borrough 2001). These methods are based on knowledge of the spatial structure of a phenomenon, which is obtained through spatial autocorrelation or autocovariance functions such as semivariograms. Estimating the values between measured points follows the semivariogram estimation based on the degree of spatial autocorrelation or covariance found in the data (Hernandez-Stefanoni and Ponce-Hernandez 2006).

González-Gurriarán et al. (1993) have used geostatistical methods to analyze the spatial structure and distribution of three species of brachyurans: *Liocarcinus depurator*, *Macropipus tuberculatus*, and *Polybius henslowii*. In this study, experimental variograms are calculated and fitted to a spherical model that is used to determine the spatial structure of the species. Then, the distributions of the populations are determined by kriging methods. The results indicate the existence of spatial covariance, and the variograms change as a function of population density and geographical area. Maxwell et al. (2009) used 14 years of survey data to map the distribution of plaice, sole, and thornback ray in three hydrographic regions comprising parts of the Irish Sea, the Celtic Sea, and the English Channel using the hybrid regression-kriging technique, which combines regression models with geostatistical tools. In this study, logistic generalized linear models (GLMs) are developed using environmental variables such as depth, bottom temperature, bed shear stress, and sediment type. GLMs using the mean squared error of prediction estimated by cross-validation are selected and geostatistical analysis of the residuals is conducted to incorporate spatial structure in the predictions.

Because fish species tend to be organized in structures and their distribution is not random in space and time, researchers have used geostatistics to evaluate the spatial structure of populations, estimate biomass and abundance of populations, and identify cohorts in several areas and resources (Maynou et al. 1998, Roa and Tapia 2000, Petitgas 2001, Rueda 2001, P´erez-Casta˜neda and Defeo 2004).

Turkey's south coast Fethiye-Gocek and its islands, which are a part of the Mediterranean Sea, contain numerous habitats including *Dendropoma petraeum* that play a crucial role in the sustainability of the ecosystem. Therefore, *Dendropoma petraeum* is protected under the regulation of the Turkish Ministry of Environment. To date, there are no reports on the demonstration and modeling of the spatial distribution of *Dendropoma petraeum* in Fethiye-Gocek. The aim of this study is to apply spatially continuous data analyzing methods for exploring and modeling the distribution of *Dendropoma petraeum* in Fethiye-Gocek. In addition, environmental effects on the distribution are examined to support the idea that temperature and content of the water are related to the fauna of this species. Kriging and cokriging methods are applied over the entire study area and their results are compared. Cokriging interpolator yielded the most accurate estimates of the species values. This interpolator not only provided the most accurate estimates but also provided additional useful interpretation of the spatial variability structure of this species through the interpretation of its semivariogram. This additional role was found very useful to support decisions in conservation planning.

A Case Study of Dendropoma Petraeum on the Coasts of The Mediterranean Using Geostatistical Technics

The study area was the Gulf of Fethiye, which is a branch of the Mediterranean Sea in southwest Turkey. The cities of Fethiye and Gocek enclose this gulf. Fethiye-Gocek is a special environmentally protected region that consists of Mugla, Fethiye town and its six sub-districts, and six villages. The area is located on the borders of the Mediterranean and the southeast part of Mugla city. It is approximately 120 km away on the southeast of Mugla (Fig. 1).

The amount of *Dendropoma petraeum* per square meter area and other parameters were obtained from the Ministry of Environment and Urban Planning. This research obtained various species measurements from 245 locations. Fig. 2 shows the locations where *Dendropoma petraeum* individuals are observed. Measurements of various chemical parameters were obtained from 15 stations, apart from the 245 locations. These parameters include aluminum (Al), iron (Fe), manganese (Mn), lead (Pb), copper (Cu), zinc (Zn), nickel (Ni), cobalt (Co), chromium (Cr), cadmium (Cd), mercury (Hg), phosphorus (P), nitrogen (N), carbon (C), temperature, density, and salinity. The parameters related to spatial variation of *Dendropoma petraeum* were selected from among the measurements from these 15 stations. The boundary was also obtained from the Ministry of Environment and Urban Planning; however, the territory was extracted from the research area for further analysis. Spatial data analysis was performed using ArcGIS software, version 9.3 (ESRI, Redlands, CA), and SPSS 15 (SPSS, Chicago, IL) was used for correlation analysis.

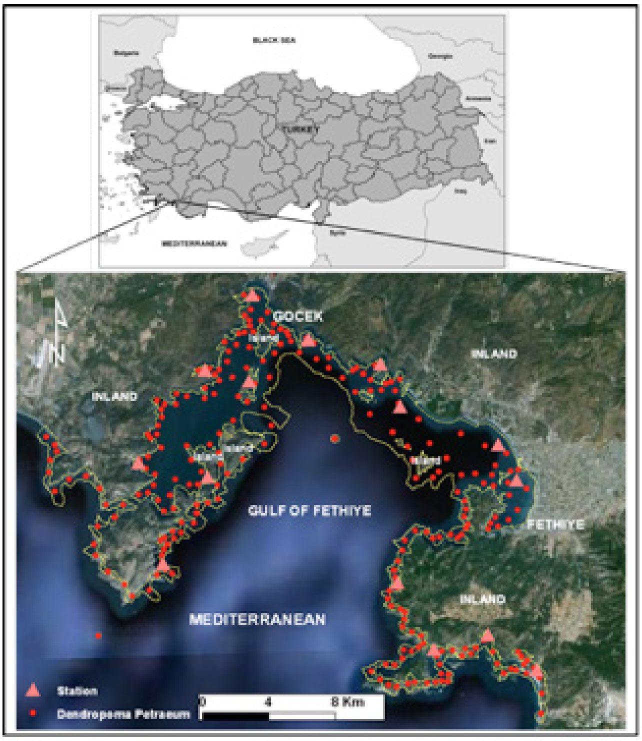

Figure 1. Map of the Fethiye-Gocek Special Environmentally Protected Region, Turkey.

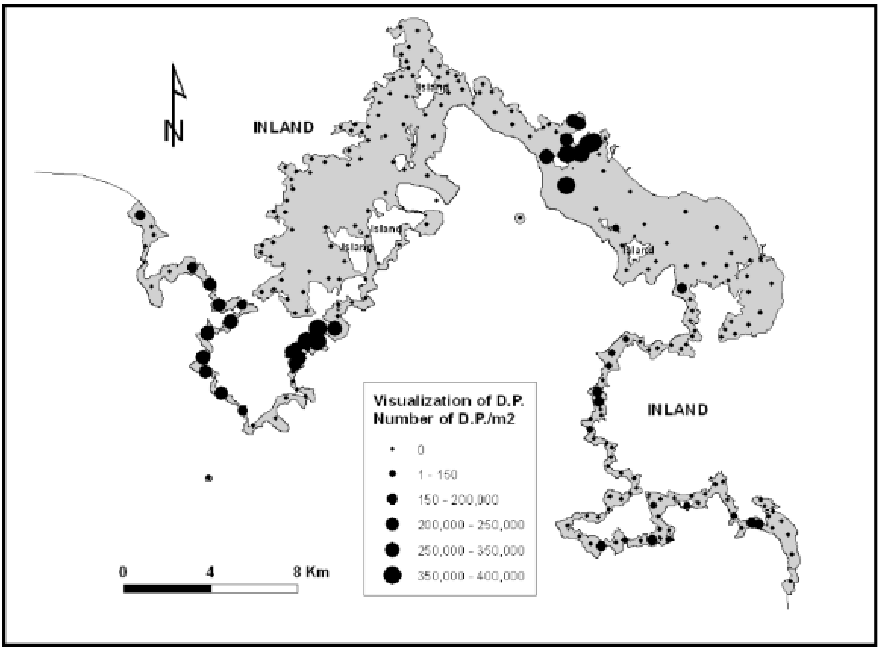

Figure 2. Proportional symbol map of Dendropoma petraeum at the special environmentally protected region of the Gulf of Fethiye. Note: The highest population density of this species is at station numbers 6, 41, and 43, where 400,000 individual/m2 have been identified. The frequency index value is 17.93% (EPASA, 2010:294).

Spatial Analysis

The first step of geostatistics is analyzing the spatial structure of variables from historical characteristics by deriving a sample variogram. A functional model is fitted to the sample variogram that contains information that can be used for interpolation (kriging technique) to estimate the characteristics at unsampled locations and extend the findings for the regional behavior of natural phenomena. Prior to spatial analyzing, a map of the study area showing the distribution of *Dendropoma petraeum* was created using Arc GIS.

To understand the variations in spatially continuous data, a map that shows such continuity is required. Then, the spatially continuous pattern was examined using spatial moving averages and Voronoi maps. A spatial moving average is a simple way to estimate heterogeneity in the mean value of the attribute, $\mu(S)$, by the average of the values at the neighboring sampled data points (Bailey and Gatrell 1995). Various neighborhood search radii (1000, 2000, 2500, and 3000 m) for the rectangle representations were examined. The suitable rectangle size was selected to be 3000 m as it covered the entire study area, thus providing a better presentation. Voronoi maps were constructed from a series of polygons formed around the location of a sample point. They were created such that each location within a polygon is closer to the sample point in the polygon than to the other sample points. After the polygons were created, neighbors of a sample point were defined as any sample point whose polygon shares a border with the selected sample point.

As mentioned in Section 2.1, Al, Fe, Mn, Pb, Cu, Zn, Ni, Co, Cr, Cd, Hg, P, N, C, temperature, density, and salinity were measured. Then, correlation analysis was performed to determine whether these parameters were correlated. Temperature, density, and salinity showed a high correlation. Because *Dendropoma petraeum* is more sensitive to temperature compared with density and salinity, only temperature was selected as a secondary variable for cokriging analysis.

Histogram, qq plot, trend analysis, semivariogram clouds

To make better decisions before creating a surface, data should be examined. Geostatistical techniques provide many data exploration tools including examining data distribution, identifying the trends in data, and understanding the spatial autocorrelation and directional influences. A histogram and QQ plot were applied to examine the data distribution. The histograms displayed skewness and kurtosis for all parameters.

Because the data had a skewed distribution of attributes and was not suitable for logarithmic transformation, trend analysis was performed to identify data trends.

Semivariogram/covariance cloud analysis was applied for understanding spatial autocorrelation and directional influences. The semivariogram/covariance cloud was necessary to examine the spatial autocorrelation between the measured sample points.

Variogram fitting

In this part of the analysis, the spatial structure of *Dendropoma petraeum* was modeled using geostatistical tools. A semivariogram and variogram are the basic tools for the analysis of spatial structures. Structural analysis involves describing and modeling the estimated variogram. A variogram (γ) is a graph or formula describing the expected squared difference between the values of sample pairs with a given orientation. It describes the between-population variance within a distance class according to the geographical distance between pairs of populations (Fig. 3A) . We fitted a variogram to determine a suitable method. Trend removal was applied, but data transformation was not applied to the data. Semivariogram parameters were calculated. Each distance and half of the squared differences of values were estimated in Excel (Microsoft, CA, USA). A common method for averaging γ at specific distances is to bin the distances into intervals (called lag distances), i.e., use all points within some bin width around a given distance value. Spherical, exponential, circular, gaussian, and linear variogram model's sill, range, and nugget values were obtained from the semivariograms (Table 1) with a lag size of 1700 m and 10 lags. Thus, a semivariogram could fit up to 17 km. For each variogram model, values were estimated for each distance. Then, a spherical model was selected for further analyses by kriging and cokriging methods. The spherical model has the following form:

$$\gamma(h,\theta) = c_0 + c_s\left\{1.5\frac{h}{a} - 0.5\left(\frac{h}{a}\right)^3\right\} \text{ for } 0 < h \le a, \qquad \textbf{(Eq.1)}$$

$$\gamma(h,\theta) = c_0 + c_s \text{ for } h \ge a, \text{ for } h \ge a,$$

where c_0 is the "nugget effect" arising from variability between replicates (the microstructures that remain undetected because of the sample size, or errors in measurement or location) and c_s is the "sill" minus the "nugget effect," where the sill is that value of semivariance achieved with a value of $h = a$, i.e., the range, and represents the maximum distance at which spatial effects are detectable.

	Spherical Model*	Exponential Model	Circular Model	Gaussian Model	Linear (Stable) Model
a (range)	10,955.6	14,391.5	9,834.39	9,783.51	16,166.9
c_0 (nugget effect)	3,917,100,000	3,179,700,000	4,030,600,000	4,910,500,000	3,587,200,000
$c_0 + c_s$ (sill)	6,035,100,000	7,286,800,000	5,920,300,000	5,126,100,000	7,114,400,000
c_s	2,118,000,000	4,107,100,000	1,889,700,000	215,600,000	3,527,200,000

Table 1. Variogram parameters from the tested models (spherical, exponential, circular, gaussian, and linear). *According to R^2 results, spherical model fits the data best.

Kriging for Dendropoma petraeum

Most GIS ignore statistical variation, whereas geostatistics uses an understanding of statistical variation as an important source of information to improve the prediction of an attribute at unsampled points, given a limited set of measurements (Borrough 2001). Kriging refers to the geostatistical procedures that require an understanding of the principles of spatial statistics and provide statistically unbiased estimates of surface values from a set of control points. Kriging is a generic term adopted by geostatisticians for a family of generalized least squares regression algorithms. The basic idea is to estimate the unknown attribute value at unsampled areas as a linear combination of the neighboring observations (Diodato 2005).

After determining that the spherical model was a suitable variogram model, kriging interpolation method was applied to *Dendropoma petraeum*. Three different kriging methods were applied: ordinary, simple, and universal, and then, the root mean square (RMS) values obtained from these kriging methods were compared.

A cokriging interpolation method was employed for spatial data analysis. It is a mathematical interpolation and extrapolation tool that can be utilized when measurements have been performed at scattered sampling points (Hassan and Atkins 2007). Cokriging is an extension of kriging in which random variables are simultaneously predicted by utilizing their interrelationships and their spatial codependence (Wu and Murray 2005). It is based on the theory of regionalized variables whose values vary with location. Cokriging gives weights to data that minimize the estimation variance (cokriging variance) (Isaaks and Srivastava 1989).

In addition to the four sets of correlated variables mentioned in section 2.2, another set including P, N, and temperature was built and five different cokriging interpolations were processed. A lag size of 1700, 10 lags, and the spherical model were used for the three cokriging techniques as follows (Fig. 3B). The ordinary, simple, and universal cokriging models were applied.

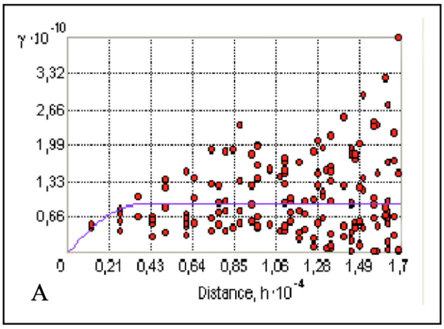

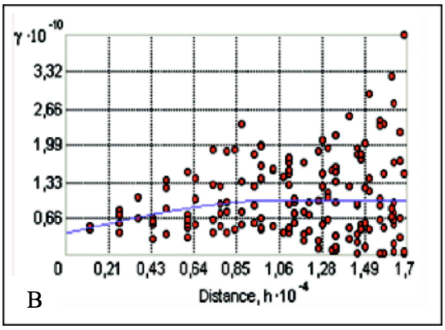

Figure 3. A) Semivariogram of ordinary kriging for Dendropoma petraeum density.B) Semivariogram of simple cokriging for Dendropoma petraeum density.

Preliminary visualization of *Dendropoma petraeum* species was shown in a proportional symbol map (Fig. 2). Moreover, a spatial moving average map created for the study area showed that the western and central regions of the study area have a higher population density (Fig. 4). The Voronoi map also showed the same density pattern as that shown in the spatial moving average (Fig. 5).

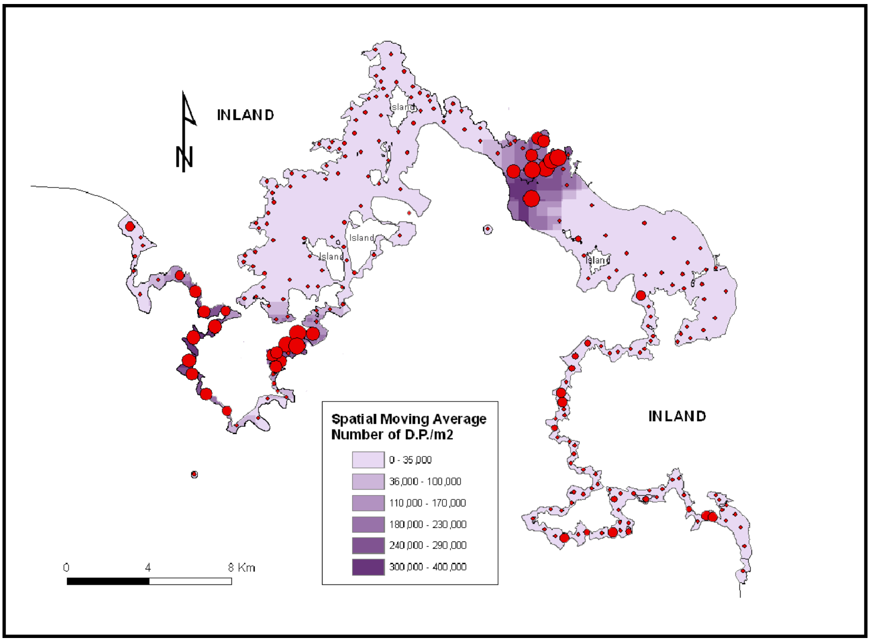

Figure 4. Depiction of concentration of Dendropoma petraeum using the spatial moving average tool.

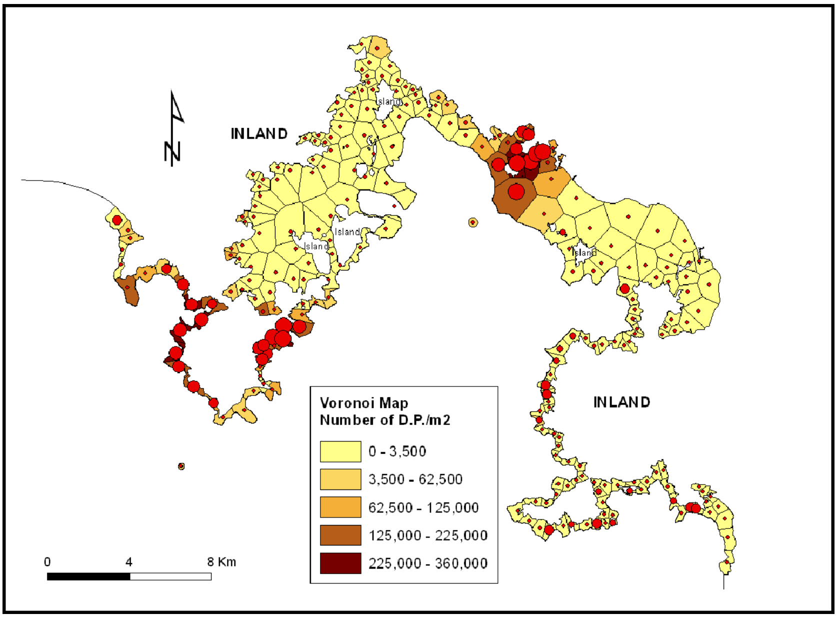

Figure 5. Construction of Voronoi maps using polygons around the location of the sample points and depiction of higher density.

An examination of the surfaces stemming from these techniques explains the global trends in the variation of *Dendropoma petraeum*. The correlation results for the various parameters obtained from the 15 stations are listed in Table 2.

	Al		Fe		Mn		Pb		Cu		Zn		Co		Cr		C		P*		N*	
Cd	X		X		X		X		X		X		X		X		X		X		X	
Hg		X		X		X		X		X		X		X		X		X		X		X
Temp.	X	X	X	X	X	X	X	X	X	X	X	X	X	X	X	X	X	X	X	X	X	X

Table 2. Letter "X" indicates correlation among parameters obtained from 15 stations (*since temperature, nitrogen (N), and phosphorus (P) are remarkable influential factors for Dendropoma petraeum, the N and P groups were selected for further analysis).

Four sets of correlated variables were selected as they were considered to comprehensively explain the distribution of *Dendropoma petraeum*. The first set included P, Cd, and temperature; the second set comprised P, Hg, and temperature; the third set consisted of N, Cd, and temperature; and the fourth set contained N, Hg, and temperature. The histograms displayed skewness and kurtosis for all parameters. According to the QQ plots, the closer the points are to the straight line in the graph, the more normal is the distribution. Trend analysis showed that the entire data exhibited a trend in the east–west and north–south directions. The trend was U-shaped, and therefore, a second-order polynomial was used for the global trend. Table 3 shows R^2 obtained from the semivariogram and the model semivariogram values. R^2 statistics are used to give information about the goodness-of-fit of a model. A higher value of R^2 shows a better fitting of the model. From the table, it follows that the spherical model performed better because it yielded the highest R^2. This spherical model was applied to both kriging and cokriging methods. The results of the three kriging methods were expressed as the RMS values shown in Table 4.

R^2 Spherical Model	R^2 Exponential Model	R^2 Circular Model	R^2 Gaussian Model	R^2 Linear Model
0.006782992	0.005371971	0.0061402	0.003307421	0.002939

Table 3. Model fitting evaluation results (R^2)

Cokriging Methods			
Parameters	**Ordinary Kriging (RMS)**	**Simple Kriging (RMS)**	**Universal Kriging (RMS)**
Phosphorus Temperature Cadmium	6,878.63	69,164	70,154.1
Phosphorus Temperature Mercury	68,778.44	64,620.39	89,456.35
Nitrogen Temperature Cadmium	68,776.33	69,159.17	70,149.26
Nitrogen Temperature Mercury	68,776.42	69,130.11	70,139.31
Phosphorus Nitrogen Temperature	68,778.68	60,410.36	91,588.98
Kriging Methods			
	Ordinary Kriging (RMS)	**Simple Kriging (RMS)**	**Universal Kriging (RMS)**
Dendropoma petraeum	64,697.61	65,331.81	72,925.15

Table 4. Comparison of RMS values of three kriging and cokriging interpolation methods for the sets of parameters selected from correlation analysis. The RMS values indicated in bold are more accurate for modeling the spatial variation.

The ordinary kriging method was selected for the data in this study because it has the lowest RMS value. However, the individual RMS values were extremely high. This shows that this model is not adequate to explain the variation (Fig. 6). From the three cokriging methods, the most suitable model, simple cokriging, was used to create a prediction map as it has the lowest RMS value (Fig. 7). The dark areas indicate a more powerful prediction. These areas also indicate locations where the *Dendropoma petraeum* is most abundant. The prediction standard error map for ordinary kriging and simple cokriging are given in Fig. 8 and 9. These maps demonstrate the accuracy of *Dendropoma petraeum* distribution in unsampled areas. The lower the error values, the more accurate the prediction map. As shown in the figures, the error values of cokriging are lower than those of kriging, thus a better prediction map was obtained by the cokriging method.

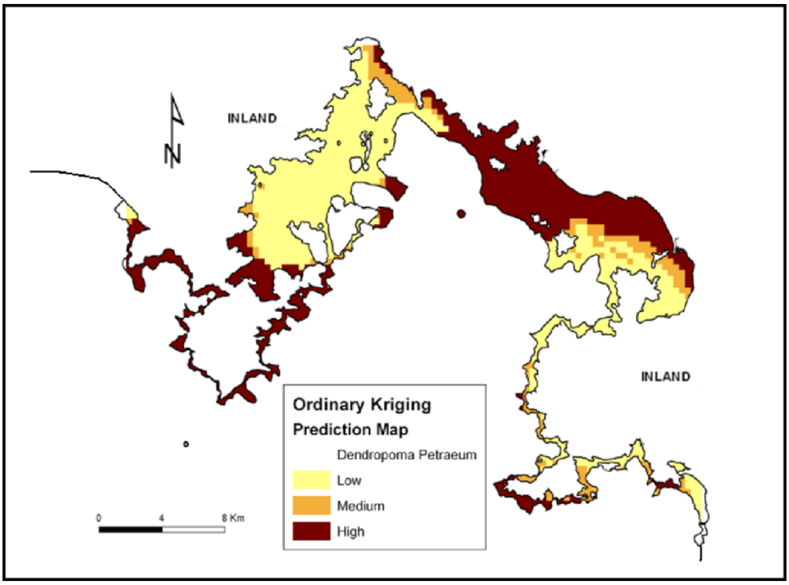

Figure 6. Predicted Dendropoma petraeum density map generated by kriging.

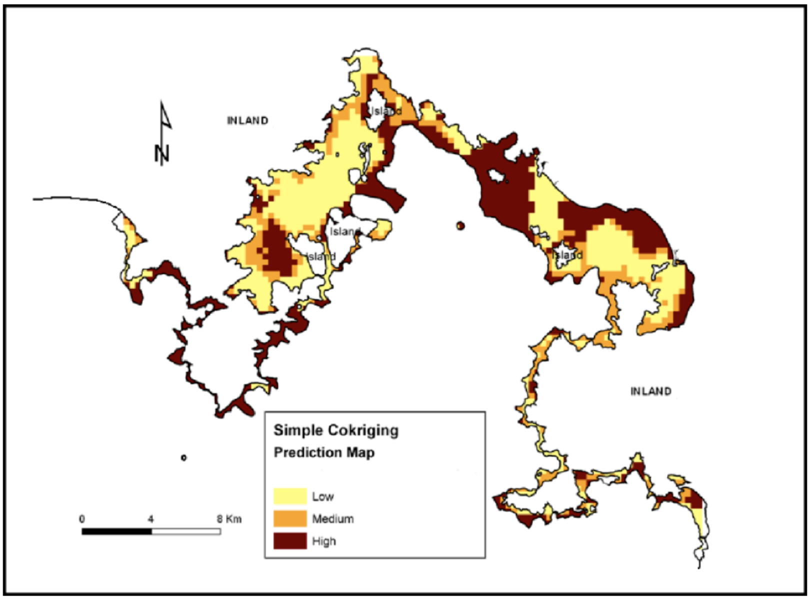

Figure 7. Predicted Dendropoma petraeum density map generated by cokriging.

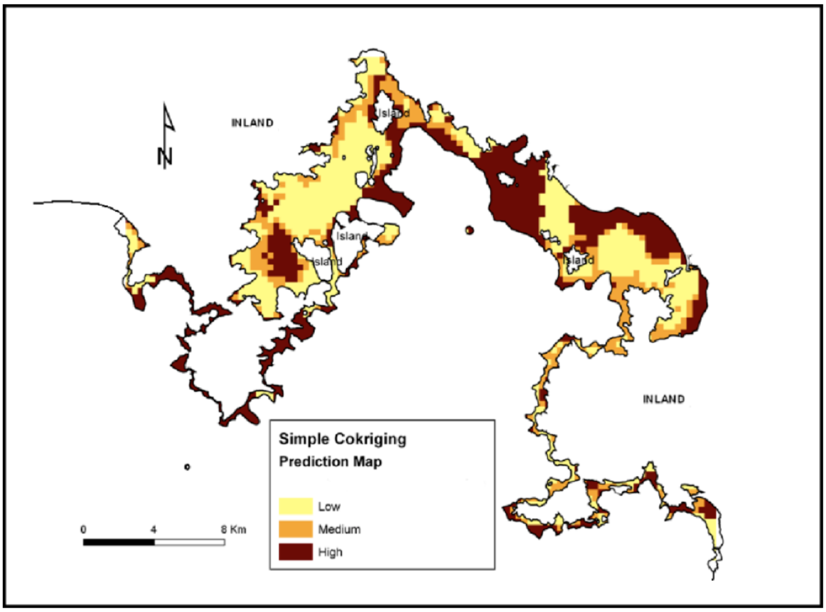

Figure 8. The prediction standard error map of ordinary kriging.

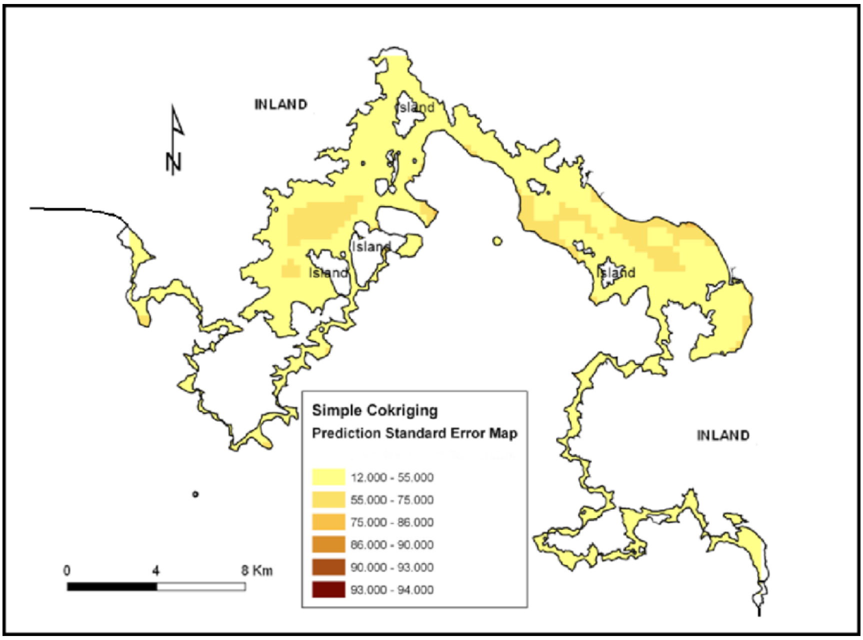

Figure 9. The prediction standard error map of simple cokriging.

In recent years, the coastal areas of Turkey have been exposed to pressure and change processes. Some of these changes include rapid population growth, urbanization, industrialization, tourism development on the land resources and ecosystems, legal forest clearing, overgrazing, plowing of pastureland, and the unsustainable harvesting of threatened plant species. The area has also witnessed the construction of dams, wetland drainage, rerouting of surface waters, poor irrigation practices and civil unrest in the east and southeast, ineffective governmental policies regulating land use (especially of pasturelands and forests), and ineffective natural resource management (fisheries, hunting, and gathering of wild animals, birds, plants, and fish). Pricing policies also exert pressure on biodiversity through excessive irrigation and fertilizer use. Rapid (and sometimes uncontrolled) tourism development and the associated coastal habitat degradation caused by land speculation (especially along the Mediterranean, Aegean and Marmara coast) and the introduction of foreign crops, cultivators, and livestock all had an impact on the coast (UNEP 2005). Therefore, it has become crucial to conserve coastal areas because these are crucial for natural habitats. Recently, management and planning of coastal and seaside areas have become unique tools. Turkey signed the "Convention on Biological Diversity" in Rio. Thus, it committed to act responsibly for the conservation of the biodiversity of plants, animals, and microbiological life within the limits of its national jurisdiction, use biological resources in a sustainable manner, and seek ways to equitably share the benefits arising from the utilization of biodiversity (Ministry of Environment 2002). With very little knowledge about the system, distribution models of marine species offer detailed baseline information on the spatial ecology of a species. This information can be incorporated into species management strategies to enable more effective monitoring and protection of individual species and communities (Maravelias 1999, Maravelias et al. 2000). Therefore, the aim of this study was to predict spatial patterns of *Dendropoma petraeum* species that can be used with some confidence for decision making in marine management and sustainable ecology around Fethiye-Gocek.

Geostatistics employs a broad range of tools and modeling techniques that can be applied to several spatial problems including prediction, determination of the spatial variation scale, design of sampling for primary data collection, smoothing of noisy maps, region identification, multivariate analysis, probability mapping, and change of support (Haining et al. 2010). In recent years, several scientists (González-Gurriarán et al. 1993, Maynou et al. 1998, Roa and Tapia 2000, Petitgas 2001, Rueda 2001, P´erez-Casta˜neda and Defeo 2004, Maxwell et al. 2009) have emphasized the need to incorporate spatial analysis into marine species assessment in order to understand the spatial variation of the species. This paper investigated the spatial analysis of *Dendropoma petraeum* in a protected area by using two analytical techniques to predict the distribution patterns of this species. It is expected that the results can contribute to an improved understanding of the dynamics of this species in a protected region and aid decisions in conservation planning. Moreover, they illustrate the advantages of the employed approaches to incorporate spatial analysis in the evaluation of marine species.

The geostatistical techniques used in this study for visualizing, exploring, and modeling spatially continuous data provide a basic set of tools. The proportional symbol map, spatial moving averages, and Voronoi maps help provide better estimates of the distribution of *Dendropoma petraeum*. Then, the modeling of variograms was used to fit a model. After the model fitting procedure, kriging and cokriging techniques were used to model the spatial structure of the most suitable areas for *Dendropoma petraeum.* To obtain better interpolation, RMS values of three kriging and cokriging methods comprising the ordinary, simple, and universal variants were compared. Next, kriging interpolation was applied for *Dentropoma petraeum* to determine whether this method was successful for modeling its spatial variation. Ordinary kriging was chosen because it had the lowest RMS value.

In addition, the cokriging method was used to improve the prediction of the primary variable value for *Dendropoma petraeum* in a special environmental protection region, where it has not been sampled. Then, the secondary variables P, N, and temperature are correlated with the primary variable. It is known that these variables are influential parameters that affect *Dendropoma petraeum*. Thus, these three parameters were used to apply cokriging. The other groups selected from the result of correlation analysis, including some chemicals such as Cd and Hg, were used to examine the possible effects of these chemicals on the modeling of the variation. Comparison of the cokriging results revealed that the RMS values were high for all interpolation methods. However, the cokriging result including the parameters of P, N, and temperature provided a better explanation for the spatial variation of the *Dendropoma petraeum* species prediction. Then, the prediction map of this result was designed according to RMS values in order to verify whether the model predicted the variation well. Cokriging yielded lower interpolation errors compared with ordinary kriging. Comparison of the results of cokriging with those of kriging revealed that the kriging method shows a rough interpolation. This might be because only one primary variable can be used in the kriging method. Furthermore, the comparison of *Dendropoma petraeum* species distribution models incorporating two different techniques indicated that the approach involving the cokriging technique is more accurate for predicting species distribution with secondary variables.

The results indicate that geostatistics is a useful technique for both analysis and mapping of the spatial structure of marine populations and for improving estimates of their densities. The predicted distributions provide a solid baseline against which future changes in species distributions and management practices may be monitored and compared. This information may facilitate more effective planning and monitoring of this unique biologically important but relatively unknown marine protected area.

ACKNOWLEDGEMENT

Authors would like to thank Professor H. Şebnem DÜZGÜN for providing expertise that greatly assisted and improved the research.

REFERENCES

1. Antonioli F, Chemello R, Improta S, Riggio S (1999) Dendropoma lower intertidal reef formations and their palaeoclimatological significance, NW Sicily. Marine Geology 161: 155-170.
2. Bailey TC, Gatrell AC (1995) Interactive Spatial Data Analysis. Addison Wesley Longman Limited, Harlow, UK.
3. Bianchi CN, Morri C (2000) Marine biodiversity of the Mediterranean Sea: situation, problem and prospects for future research. Marine Pollution Bulletin 40: 367-376.
4. Borrough PA (2001) GIS and geostatistics: essential partners for spatial analysis. Environmental Ecological Statistics 8: 361-377.
5. Boudouresque CF (2004) Marine biodiversity in the Mediterranean: status of species, populations and communities. Scientific Reports of Port-Cros National Park, France 20: 97-146.
6. Calvo M, Templodo J, Oliverio M, Machordom A (2009) Hidden mediterranean biodiversity: molecular evidence for a cryptic species complex within the reef building vermetid gastropod *Dendropoma Petraeum* (Mollusca: Caenogastropoda). Biological Journal of the Linnean Society 96: 898-912.
7. Diodato N (2005) The influence of topographic co-variables on the spatial variability of precipitation over small regions of complex terrain. International Journal of Climatology 25: 351-363.
8. Elith J, Leathwick JR (2009) Species distribution models: ecological explanation and prediction across space and time. Annual Review of Ecology, Evolution, and Systematics 40: 677–697.

9. González-Gurriarán E, Freire J, Fernández L (1993) Geostatistical analysis of spatial distribution of liocarcinus depurator, macropipus tuberculatus and polybius henslowii (Crustacea: Brachyura) over the Galician continental shelf (NW Spain). Marine Biology 115: 453-461.

10. Haining RP, Kerry R, Oliver MA (2010) Geography, spatial data analysis, and geostatistics: an overview. Geographical Analysis 42: 7-31.

11. Hassan MM, Atkins PJ (2007). Arsenic risk mapping in Bangladesh: a simulation technique of cokriging estimation from regional count data. Journal of Environmental Science and Health 42: 1719-1728.

12. Hernandez-Stefanoni JL, Ponce-Hernandez R (2006) Mapping the spatial variability of plant diversity in a tropical forest: comparison of spatial interpolation methods. Environmental Monitoring and Assessment 117: 307-334.

13. Heywood VH (1995) Global Biodiversity Assessment. Cambridge University Press, Cambridge, UK.

14. Isaaks EH, Srivastava RM (1989) An Introduction to Applied Geostatistics. Oxford University Press, New York.

15. Laborel J (1986) Vermetids. In: Van De Plaasche O. (ed), Sea Level Research, A Manual for the Collection and Evaluation of Data, Geo Books, Norwich, 281-310.

16. Laborel J, Laborel-Deguen F (1996) Biological indicators of Holocene sea-level and climatic variations on rocky coasts of tropical and subtropical regions. Quaternaria International 31: 53-60.

17. Lambeck K, Antonioli F, Purcell A, Silenzi S (2004) Sea-level change along the Italian coast for the past 10,000 yr. Quternary Science Reviews 23: 1567-1598.

18. Lawton JH, Woodroffe GL (1991) Habitat and the distribution of water voles-why are there gaps in a species range. Journal of Animal Ecology 60: 79-91.

19. Leathwick JR, Rowe D, Richardson J, Elith J, Hastie T (2005) Using multivariate adaptive regression splines to predict the distributions of New Zealand's freshwater diadromous fish. Freshwater Biology 50: 2034–2052.

20. Leathwick JR, Elith J, Francis MP, Hastie T, Taylor P (2006) Variation in demersal fish species richness in the oceans surrounding New Zealand: an analysis using boosted regression trees. Marine Ecology Progress Series 321: 267–281.

21. Lunetta GDA, Damiani F (2002) Spermiogenesis in the vermetid gastropod Dendropoma petraeum (Gastropoda, Prosobranchia). European Journal of Histochemistry 46: 75-86.

22. Maravelias CD (1999) Habitat selection and clustering of a pelagic fish: effects of topography and bathymetry on species dynamics. Canadian Journal of Fisheries and Aquatic Sciences 56: 437-450.

23. Maravelias CD, Reid DG, Swartzman G (2000) Modelling spatio-temporal effects of environment on Atlantic herring Clupea harengus. Environmental Biology of Fishes 58: 157-172.

24. Maynou FX, Sarda F, Conan GY (1998) Assessment of the spatial structure and biomass evaluation of Nephrops norvegicus (L.) populations in the northwestern Mediterranean by geostatistics. ICES Journal of Marine Science 55: 102-120.

25. Maxwell DL, Stelzenmüller V, Eastwood PD, Rogers SI (2009) Modelling the spatial distribution of plaice (Pleuronectes platessa), sole (Solea solea) and thornback ray (Raja clavata) in UK waters for marine management and planning. Journal of Sea Research 61(4): 258-267.

26. Ministry of Environment (2002) National report on sustainable development 2002, Ministry of Republic of Turkey.
27. Myers N, Mittermeier RA, Mittermeier CG, da Fonseca GAB, Kent J (2000) Biodiversity hotspots for conservation priorities. Nature 403: 853-858.
28. Pearson DL, Carroll SS (1998) Global patterns of species richness: spatial models for conservation planning using bioindicator and precipitation data. Conservation Biology 12: 809-821.
29. Petitgas P (2001) Geostatistics in fisheries survey design and stock assessment: models, variances and applications. Fish and Fisheries 2: 231-249.
30. P´erez-Casta˜neda R, Defeo O (2004) Spatial distribution and structure along ecological gradients: penaeid shrimps in a tropical estuarine habitat of Mexico. Marine Ecology Progress Series 273: 173-185.
31. Phillips SJ, Anderson RP, Schapire RE (2006) Maximum entropy modelling of species geographic distributions. Ecological Modelling 190: 231–259.
32. Roa R, Tapia F (2000) Cohorts in space: geostatistical mapping of the age structure of the squat lobster Pleuroncodes monodon population off central Chile. Marine Ecology Progress Series 196: 239-251.
33. Rossi RE, Mulla DJ, Journel AG, Franz, EH (1992) Geostatistical tools for modeling and interpreting ecological spatial dependence. Ecological Monographs 62(2): 277-314.
34. Rueda M (2001) Spatial distribution of fish species in a tropical estuarine lagoon: a geostatistical appraisal. Marine Ecology Progress Series 222: 217-226.
35. Sara` M (1985) Ecological factors and their biogeographic consequences in the Mediterranean ecosystem. In: Moraitous-Apostolopoulou M, Kiortsis V (eds) Mediterranean Marine Ecosystems. Plenum Press, New York, 1-17.
36. Silenzia S, Antoniolib F, Chemelloc R (2004) A new marker for sea surface temperature trend during the last centuries in temperate areas: vermetid reef. Global and Planetary Change 40: 105-114.
37. Tortonese E (1985) Distribution and Ecology of Endemic Elements in the Mediterranean Fauna (Fishes and Echinoderms). In: Moraitous-Apostolopoulou M, Kiortsis V (eds) Mediterranean Marine Ecosystems. Plenum Press, New York, 57-83.
38. Underhill LG, Gibbons DW (2002) Mapping and Monitoring Bird Populations: Their Conservation Uses. In: Norris K, Pain DJ (eds) Conserving Bird Biodiversity: General Principles and Their Application. Cambridge University Press,Cambridge, 34-60.
39. Ungerer MJ,Goodchild MF (2002) Integrating spatial data analysis and GIS: a new implementation using the component object model (COM). International Journal of Geographical Information Science 16(1): 41-53.
40. United Nations Environment Programme (UNEP) (2005). Coastal area management programme.
41. UNEP/MAP-Plan Bleu (2009) State of the Environment and Development in the Mediterranean, UNEP/MAP Plan Bleu, Athens, 201.
42. Wu C, Murray AT (2005) A cokriging method for estimating population density in urban areas. Computers Environment and Urban Systems 29(5): 558-579.

Weather Early Warning System by Stream Processing Raınfall and Wind Sensor Data

Özgür YILMAZEL[1]

CHAPTER 2

1 Assoc. Prof., Anadolu Universty, Eskişehir, Turkey

INTRODUCTION

Rainfall and wind speed data are obtained through ground-based weather stations that are geographically distributed around Turkey. These ground-based weather stations in Turkey have communication capability and all sensor data is accumulated at Turkish State Meteorological Service. In this work, a prototype weather early warning system was implemented to process the streaming sensor data using big data technology and produce weather alarm levels according to the meteorological threshold specifications. The scope of the work was to demonstrate the techniques to perform stream processing on rainfall and wind speed sensor data that flows from a distributed climate sensor network. It was confirmed that our prototype had detected the color-coded alarm levels in real-time. It was shown that with a rule engine implemented, the system could deliver insightful and timely information in terms of catching the early warnings.

Until the late twentieth century most weather corresponding data has been kept locally due to the lack of efficient and effective data storage and transfer systems. With the recent dramatic developments in computer and network technologies most meteorological data are now transmitted digitally to centralized collection centers around the world (Frolov et al., 2016). A major step forward in climate database management was taken with the World Climate Data Monitoring Programme Climate Computing project in 1985. The World Climate Data Monitoring Programme (https://public.wmo.int/en) was developed to manage the collection of large climate data. Similarly, World Weather Records' (WWR) (Guide to Climatological Practices, 2011) primary goal is to maintain the huge size of records such as monthly temperature, precipitation and pressure data that are collected from thousands of weather stations around the world. Not only the number of weather stations have been increasing lately but also the stations have started to collect the data in continuous form globally. In that regard, some international organizations and national meteorological offices maintain NoSQL database to store that huge amount of data.

The volume, the velocity and the variety of data have been increasing continuallyin the last decade. Not only capturing and storing the streaming data is a challenge but analyzing and visualizing the streaming data is also a big challenge for organizations. As the value in the data can quickly degrade, the value in the data needs to be captured in real time. Stream data processing is the in-memory analysis of machine data that is in motion. The main purpose of the stream processing is to react to operational data analysis in real time. Apache Spark, which is used in this work, is a general purpose distributed computational framework providing more flexibility compared to MapReduce (Shoro & Soomro, 2015).

Turkish State Meteorological Service needed a weather early warning system based on the sensor data submitted real-time by distributed climate sensor network around Turkey. In this work, a prototype system was implemented to process the streaming sensor data using big data technology, mainly Apache Spark, and produce weather alarm levels according to the meteorological specifications that would support Turkish State Meteorological Service's goal.

BACKGROUND

Until now a number of information systems have been developed to serve for the purpose of early warnings. GIS Amur (Frolov et al., 2016) system was developed in Russian Federation to monitor, forecast and serve as an early warning mechanism. This system was used to collect, visualize and analyze the hydrometeorology data. GIS Amur system delivered real-time information by merging the ground-based, satellite and model information for the Amur River basin's hydrological data. The United States' WaterWatch (Jian et al., 2008) is a U.S. Geological Survey website that displays and processes hydrological data maps, graphs and tables that are served real-time. The European Flood

Awareness System is a distributed hydrological model under development at the European Commission Joint Research Centre (Bartholmes, 2009). This system was designed specifically for large European river basins by using GIS technologies. A new concept of automated evaluation of local wind maximum speed in mountain regions is considered in (Refice et al., 2017). This study allows estimating both the speed and the origination time of the expected wind in different areas and with different weather conditions.

In this study, we developed a weather early warning system algorithm that utilizes big data technologies mainly Apache Spark, Flume and Kafka. Apache Spark is designed to perform both batch processing and stream processing on new workloads. Apache Spark can also be used for interactive queries and machine learning. This big data technology provides highly scalable and fault-tolerant stream processing while providing near real time processing. Apache Flume is a distributed and reliable service for effectively collecting and moving large amounts of log data. Apache Flume was used to ingest the sensor data from that server to our server. Apache Kafka is a distributed, partitioned, replicated commit log service. In this project, Apache Kafka was used to store the data, service the data to the stream processor and maintain the stream data scalably and reliably between Apache Kafka and other systems.

The scope of the work was to demonstrate the tools and techniques to perform stream processing on rainfall and wind speed sensor data of Turkish State Meteorological Service and produce weather alarm levels in real-time accordingly.

For the study, winds and rainfalls data from 18 ground-based stations in Antalya southern region of Turkey over the period of 2010 and 2014 was used. Sensor data for rainfall and wind speed were processed using Apache Spark and the data was classified into color coded alarm levels of yellow, orange and red. The color-coded alarm levels were determined by the already used rules set. The success criteria of the work was to demonstrate real-time data processing on meteorological sensor data and produce alarm levels accordingly and accurately. The system was required to be fault tolerant (none of the sensor data should be left unprocessed), low latency (with a latency of less than 2 minutes in the 99th percentile), and scalable (10000+ sensor data should be able to be processed).

MATERIALS AND METHODS

Current Data Structure

There are 1.800 Automatic Weather Stations (AWS) in the climate sensor network around Turkey. The sensors observe and send meteorological data every 1 to 10 minutes intervals. In the near future, a total of 3.000 AWS are being planned within the system. The main communication method of the AWS is GPRS (General Packet Radio Service) and ADSL (Asymmetric Digital Subscriber Line) technologies are also being used. About two hundred stations are managed by operators and the rest of them are unmanned. Data is collected by a TCP based socket software and archived in the Oracle database. At the end of each day, approximately three and a half million data rows are inserted into the database. The database used for archiving is different from the database used for retrieving. The archiving database Oracle 12c is for fast transactions, especially for "insert" operation. Sybase IQ 16 data warehouse is being used for fast data retrieval process. While transferring data from Oracle to Sybase IQ with ETL, some fundamental quality control processes are being followed.

Structure of Data

The rainfall and wind speed data used in our prototype were supplied by Turkish

State Meteorological Service. The data included 18 different sensors located in Antalya –a southern region city in Turkey- for the period of 2010 and 2014. Although the data included the rainfall and wind speed sensor outputs the data schema consisted of other climate sensor types as well for us to use in our future projects. The data fields of 'AVERAGE_WIND_SPEED' and 'TOTAL_RAIN_PRECIPITATION' were used in the processing and analysis of wind speed and rainfall data correspondingly. The size of the dataset was about 4GB and it included a total of 38 million records.

Weather Early Warning System Business Rules

- The weather warning system in Turkey uses color-coded symbols indicating different levels of severity and each level is associated with different criteria as shown below:
- **Yellow**: This color means potential danger. The weather is unlikely to be extreme but care is called for in activities that are dependent on the weather.
- **Orange**: This color means danger. There is severe weather that may cause damage or accidents. The weather brings risks. It is wise to be careful and keep abreast of the latest developments in the weather. Take heed of advice given by the authorities.
- **Red**: Great danger from extremely severe weather. Major damage and accidents are likely, in many cases with threat to life and limb, over a wide area.

In this work, two weather sensor data criteria for rainfall and wind speed were processed. The color codes and the corresponding criteria are shown below in Table 1 and 2.

Grade	Rainfall Criteria
Yellow	Precipitation would be between 20-60 mm within 12 hours period
Orange	Precipitation would be between 61-100 mm within 12 hours period
Red	Precipitation would be above 100 mm within 12 hours period

Table 1. The color codes for rainfall

Grade	Wind Speed Criteria
Yellow	The average wind speed would be between 50-80 km/h
Orange	The average wind speed would be between 81-110 km/h
Red	The average wind speed would be above 110 km/h

Table 2. The color codes for windspeed

It was required that the system must be reliable as every log has the potential to be the critical one and system cannot afford to drop a single line in the dataset. Also it was required that the system should process each and every sensor data only once. It was also required that the system must be scalable so that it should be able to process 10.000+ sensor data with a latency of less than 2 minutes in the 99th percentile.

METHODOLOGY AND DESIGN

In this work, we propose a weather early warning system algorithm that uses Apache Spark, Flume and Kafka. Apache Spark is an open source cluster computing system designed to perform both batch processing and new workloads like streaming, interactive queries and machine learning. This big data technology provides highly scalable and fault-tolerant streaming processing while providing real time processing. Apache Spark significantly outperforms Hadoop MapReduce by providing primitives for in-memory cluster computing. As a result it does avoid the I/O bottleneck between the individual jobs of an iterative MapReduce workflow (Liu et al.,2014).

Apache Spark leverages distributed memory, full directed graph expressions for data parallel computations, and improves developer experience and does still retain linear scalability, fault-tolerance and data locality based computations (Shreedharan, 2015). It is being used across different industries such as identification of fraudulent transactions as soon as they occur, dynamic re-routing of traffic or vehicle fleet, dynamic inventory management, real-time retail offers, user engagement optimization based on user's current behavior and personalization of content based on real-time data (Shreedharan, 2015). Many companies use big data to make user's decisions in the form of such as recommendation systems, predictive analysis. One of the key properties of any decision is latency which is the time it takes to make the decision from the moment the input data is available. Reducing latency can significantly increase the effectiveness of the analysis. Especially when these decisions are based on complex computational algorithms, Apache Spark is an ideal fit to speed up the critical decision-making process. Turkish State Meteorological Service's sensor network data frequency and the corresponding requirement of processing that sensor data in real time fit well into the streaming data processing scenario.

All the rainfall and wind speed data were accumulated at one server. The data was gathered in folders of which name represented the date and time that the sensor data arrived on. Mainly three different technologies were used in the system: Apache Flume to ingest sensor data to our server; Apache Kafka to store the data and service the data to the stream processor and maintain the stream data scalably and reliably between Apache Kafka and other systems; and Apache Spark to process the streaming sensor data and produce alarm levels according to the business rules.

Apache Flume was used to ingest the sensor data from that server to our server. Flume is a distributed and reliable service for effectively collecting and moving large amounts of log data. It has a simple and flexible architecture based on streaming data flows (Vohra, 2016) as shown in Figure 1.

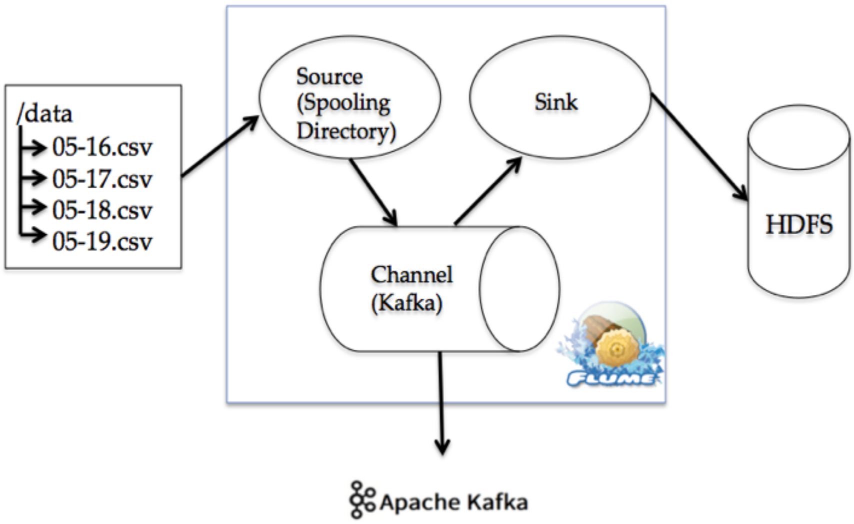

Figure 1. Flume Topology

The Flume source consumes events delivered to it by an external source. When a Flume source receives an event, it stores it into one or more channels. The channel is a passive store that keeps the event until it is consumed by a Flume sink. The sink removes the event from the channel and puts it into an external repository, in our case HDFS. The spooling directory in our architecture above waits for the folders that contain timely sensor data. It parses each file in a folder and sends it over to Channel. When it reaches the end of the file it changes the file name so it indicates that it was processed.

Apache Kafka is a distributed, partitioned, replicated commit log service. It provides the functionality of a messaging system with a unique design (Kreps et al., 2011). In this project Apache Kafka was used to store the data, service the data to the stream processor and maintain the stream data scalably and reliably between Apache Kafka and other systems.

Apache Kafka maintains feeds of messages in categories called topics. The processes that publish messages to a Kafka topic are called producers. The producers that subscribe to topics and process the feed of published messages are called consumers. Apache Kafka is run as a cluster comprised of one or more servers each of which is called a broker. A topic is a category or feed name to which messages are published. For each topic the Kafka cluster maintains a partitioned log. The messages in the partitions are assigned a sequential id number which is called offset and the offset uniquely identifies each message with the partition. The Kafka cluster keeps track of all published messages whether or not they have been consumed for a configurable period of time (Kreps et al., 2011).

The following features of Apache Kafka met the system requirements of the project and therefore this motivated us to include the technology in our system:

Reliable and Fault Tolerant- The partitions of the log are distributed over the servers in the Kafka cluster and each partition is replicated across a configurable number of servers for fault tolerance. Each partition has leader and followers where the leader handles all read and write requests for the partition. The followers replicate the leader. If the leader fails, the follower will automatically become the new leader.

Scalable- The structure for the fault tolerance feature also provides the scalability for the system. Its ability to increase the partition count per topic provides flexibility to increase the throughput when desired.

Low Latency- Apache Kafka has a latency of about 3 milliseconds in the 99-th percentile which meets and exceeds the system requirements.

The experiment design included a Spark Streaming application. Spark Streaming is an extension of the core Spark API that enables scalable, high-throughput, fault-tolerant stream processing of live data streams. Data can be ingested from many sources such as Kafka, Flume, Twitter or TCP sockets and can be processed using complex algorithms. Finally, processed data can be pushed out to filesystems. The Figure 2 shows the principle of how Spark works. The Spark Streaming provides a high-level abstraction called discretized stream (DStream) representing a continuous stream of data. Internally DStream is represented as a sequence of RDDs. Each RDD was pushed into the queue are treated as a batch of data in DStream. The Spark Streaming program in our prototype was written in Scala (Karau et al., 2015).

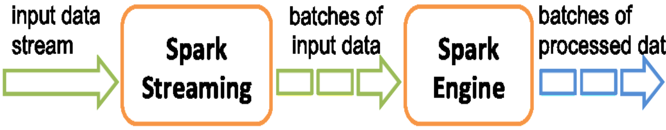

Figure 2. Spark Streaming Process

Spark Streaming provides windows computations which allows us to apply transformations over a sliding window of data. The Figure 3 below shows this sliding window feature of Apache Spark. Every time the windows slides over a source Dstream the source RDDs that fall within the window are combined and operated in order to produce the RDDs of the windowed DStream. In our case the system design accumulated the rain fall sensor data for windows of 12 hours period and decided on whether or not it produced an alarm level based on the business rules shown in Table 1. Therefore, with the windowed computation of Dstream the system was able to handle the aggregation of data so that each window length and duration could be configured.

For the wind speed sensor data no data accumulation process was needed according the business rules in Table 2. Therefore, the wind speed data was processed as the data was acquired.

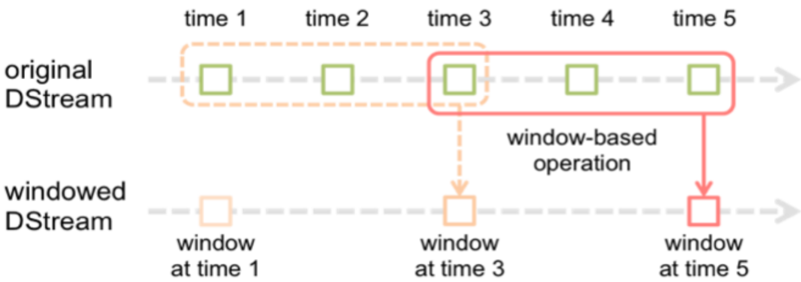

Figure 3. Spark Streaming Internal Process

The pseudo-code that was written for stream processing rainfall data is shown below:

```
// Data has the structure of { stationId: Int, totalRain: Double }
  streamingData
  // Construct a tuple from it by making the stationId key
    .map(x => (x.stationId,x.totalRain))
  // Calculate the total rain in a sliding (1min slide duration)window (720min window
duration)
    .reduceByKeyAndWindow((y, z) =>
(y.stationId, y.totalRain + z.totalRain))
  // Generate alert levels from the aggregated data
.map(t => (t, if(t.totalRain >= 100) RedAlert
  else if(t.totalRain => 60) OrangeAlert
  else if(t.totalRain => 20) YellowAlert
         else NoAlert))
  // Filter out no alert actions
    .filter(u => u._2 != NoAlert
```

RESULTS AND CONCLUSION

A prototype weather early warning system was developed to process the streaming sensor data using big data technology and produce weather alarm levels according to the meteorological threshold specifications. The scope of the work was to demonstrate the techniques to perform stream processing on rainfall and wind speed sensor data that flows from a distributed climate sensor network.

The proof of concept system resulted in total of 8594 alarms for rainfall and wind sensor data. For rainfall data all three levels of alarms – yellow, orange, red- were produced whereas for wind speed data only yellow level was produced due to the corresponding data range. The following Table 3 displays the produced alarm level counts for the corresponding data.

Alarm Level	Rainfall	Wind Speed	Grand Total
Yellow	7892	28	7920
Orange	564	0	564
Red	110	0	110
Grand Total	8566	28	8594

Table 3. Alarm level counts for rainfall and wind speed

This work successfully demonstrated the purpose of the big data proof of concept project which was applying streaming data analysis on the meteorological sensor data and producing real time alarm levels according to the threshold levels determined by the department. Since the prototype has served its purpose on the two-sensor data, the streaming processing technology can be applied to the complete set of weather corresponding data to produce further real-time analysis. As a further study, pattern analysis of yellow/red alarms and their accruing sequence can be analyzed in order to improve efficiency of decision support systems more. Also, additional data such as imagery data can be included within the analysis to enhance the detection.

REFERENCES

1. Bartholmes, J. C., Thielen, J., Ramos, M. H., & Gentilini, S. (2009). The european flood alert system EFAS–Part 2: Statistical skill assessment of probabilistic and deterministic operational forecasts. *Hydrology and Earth System Sciences*, *13*(2), 141-153.
2. Frolov, A.V., Asmus, V.V., Zatyagalova, V.V., Krovotyntsev, V.A., Borshch, S.V., Vil'fand, R.M., Zhabina, I.I., Kudryavtseva, O.I., Leont'eva, E.A., Simonov, Y.A., Stepanov, Y.A.:
3. GISAmur system of flood monitoring, forecasting, and early warning. *Russian Meteorol. Hydrol.* 41(3), 157–169 (2016)
4. Guide to Climatological Practices WMO-No. 100 (third edition). (2011). Available at http://www.wmo.int/pages/prog/wcp/ccl/guide/documents/WMO_100_en.pdf.
5. Jian, X., Wolock, D., & Lins, H. (2008). *WaterWatch-Maps, Graphs, and Tables of Current, Recent, and Past Streamflow Conditions* (No. 2008-3031). Geological Survey (US).

6. Karau, H., Konwinski, A., Wendell, P., & Zaharia, M. (2015). *Learning Spark: Lightning-Fast Big Data Analysis*. O'Reilly Media, Inc..
7. Kreps, J., Narkhede, N., & Rao, J. (2011, June). Kafka: A distributed messaging system for log processing. In *Proceedings of the NetDB* (pp. 1-7).
8. Liu, X., Iftikhar, N., & Xie, X. (2014, July). Survey of real-time processing systems for big data. *In Proceedings of the 18th International Database Engineering & Applications Symposium* (pp. 356-361). ACM.
9. Refice, A., D'Addabbo, A., & Capolongo, D. (Eds.). (2017). *Flood Monitoring Through Remote Sensing*. Springer.
10. Shoro, A. G., & Soomro, T. R. (2015). Big data analysis: Apache spark perspective. *Global Journal of Computer Science and Technology*.
11. Vohra, D. (2016). Apache Flume. In *Practical Hadoop Ecosystem* (pp. 287-300). Apress, Berkeley, CA.

General Screening of Propolis Around The World: Chemical Composition and Its Polyphenol Concentration

Merve KESKİN[1]

Şaban KESKİN[2]

Sevgi KOLAYLI[3]

CHAPTER 3

[1] Karadeniz Technical University, Faculty of Science, Department of Chemistry, Trabzon, Turkey
[2] Bilecik Şeyh Edebali University, Faculty of Science, Department of Chemistry, Bilecik, Turkey
[3] Karadeniz Technical University, Faculty of Science, Department of Chemistry, Trabzon, Turkey

INTRODUCTION

Propolis, is a resinous mixture, collected by honeybees from tree bud and exudates of the plants. Propolis is collected by bees to coat their hive cracks and also to protect hives against microorganisms. Propolis contains flavonoids, aromatic acids, diterpenic acids and phenolic compounds and these components provide its antitumor, anticancer, antiviral and antifungal effects. Propolis was widely used in ancient cultures as folk medicine in some cultures and nowadays it is used in different forms and formulations as food additive, complementary medicine, cosmetic products, etc. Main aim of this review is to discuss and collect current knowledge on the chemical composition of propolis samples all around the world.

History of Propolis Usage

The use of propolis goes back to ancient times, at least to 300 BC, and it has been used as a medicine in local and popular medicine around the world. Arabs, Romans and Egyptians used it as a medicine or embalming agent, etc.

In the 12th century propolis was used as medicinal preparations for treating mouth and throat infections as well as dental caries. It was documented as a medication in the 1600s in London (Walgrave, 2005). It was often used to treat skin wounds and to protect raw skin before bandages were available. Nowadays, in 21th century, propolis is used as complementary medicine, food additive for preserver or enhancer in food formulations and cosmetic product’s formulation.

Physical properties of propolis

The color of propolis changes from yellow to dark brown depending on the origin of the resins. Transparent propolis has also been reported by Coggshall and Morse (1984). Propolis is a soft, pliable and very viscous at temperatures of 25 to 45 °C. It becomes rigid and millable at less than 15 °C and particularly when frozen or at near freezing. It becomes increasingly sticky and gummy above 45 °C. Propolis could be liquefied at 60 to 70 °C, but for some samples the melting point may be as high as 100 °C (Alfahdawi, 2017).

Because of its resinous nature consumption of raw propolis is a bit difficult. In order to make propolis beneficial for either medical treatment or food additive it should be extracted by using suitable solvent. The most commonly used solvents for commercial extraction are ethyl alcohol, diethyl ether, glycerol and water. For chemical analysis a large variety of solvents may be used in order to extract the various fractions. Many of the components are soluble in water or alcohol.

Chemical Composition of Propolis

The chemical composition of all propolis samples alters depending on many factors such as the flora, the time of the year, bee species and collection method. Up to now, over 300 substances have been determined in propolis samples (**Organic acids**, Gallic acids, caffeic, cinnamic, ferulic, isoferulic, p-coumaric, vanilic, isovanilic, coumaric, esculetol, scopoletol, **Flavonoids**, flavones, acacetine, chrysine, pectolinarigenine, pinocembrine, tectochrysine, **Flavonols**, galangine, izalpinine, kaempferidae, querestine, rhamnocitrine, **Flavonones**, pinostrobine, sakuranetine, flavononols and pinobanksine etc.). In general, a propolis mainly consists of 50–80% resin, 8–30% beeswax, 6% plant wax, 10–14% essential oils, 5% pollen, 10% tannin and 5% mechanical impurities (Alfahdawi, 2017; Kumar , 2017; Burdock, 1998). Out of its valuable polyphenolic composition, propolis also contains numerous beneficial constituents including:

- Elements: Manganese, tin, zinc, calcium, copper, etc.
- Vitamins: Vitamin B1, pro vitamin A, B2, etc.
- Aromatic esters: caffeic acid and ethyl esters of cinnamic, etc.
- Flavanoids: Chrysin, tectochrysin, etc. (Kumar, 2017).

Other compounds present in the European propolis are geraniol, aromatic compounds, hydrocarbons, triterpene alcohols, and enzymes (amylase and esterase). In low concentrations, volatile compounds are found in propolis which contribute to its aroma and significant biological activity (Kumar, 2017).

It is obvious that the antioxidant activity correlates well with the total concentration of polyphenols of propolis from different geographical and botanical origin (Göçer and Gülçin, 2011). The antioxidant activity differs according to the type of polyphenols. CAPE, a typical constituent of poplar propolis, seems to be one of the most powerful antioxidant substances of propolis (Kumar, 2017; Tolba, 2016).

For poplar type propolis, the chemical constituents responsible for its beneficial biological activities and especially for its antibacterial and antifungal properties are flavonoids and other (poly) phenolic compounds, mainly substituted cinnamic acids and their esters. In Brazilian propolis, such activities are due to prenylated p-coumaric acids (also substituted cinnamic acids) and diterpenes (Lotfy, 2006).

As mentioned before chemical composition of propolis depends on many factors (Bankova and Popova, 2007). As a result of this situation there are some problems of propolis medicinal use. Standardization of propolis extracts and products containing propolis may be a solution for this situation. This creates the necessity of more thorough investigations on the chemical composition, plant origin and biological activity of propolis from different regions of the world, especially from places not to be investigated yet (Bankova, 2005).

With the development of separation and purification techniques such as high performance liquid chromatography (HPLC), thin layer chromatography (Alencar, 2007), gas chromatography (GC), as well as identification techniques, such as mass spectroscopy (MS) (Fernandes, 2008), nuclear magnetic resonance (NMR), gas chromatography and mass spectroscopy (GC-MS) (Maciejewicz, 2001), more compounds have been identified in propolis for the first time; including flavonoids, terpenes, phenolic acids and their esters, sugars, hydrocarbons and mineral elements. In contrast, relatively common phytochemicals such as alkaloids, and iridoids have not been reported. Two hundred and forty one (241) compounds have been reported for the first time from propolis between 2000 and 2012 (Huang, 2014). Some compounds detected in different propolis samples are summarized in Table 1.

The major constituents of propolis from most of the sources are flavonoids. Some of the principal phenolic esters and flavonoids like caffeic acid phenyl ester, quercetin, baicalin, pinocembrin, naringin, galangin, and chrysin have been found to be responsible for antimicrobial, antioxidant, and anti-inflammatory activities of propolis (Savickas, 2005; Andrzej, 2013).

The amount of balsam extracted from crude propolis is an important characteristic, because high percentage of balsam means the propolis contains relatively higher content of biologically active components and a low percentage of wax and insoluble matter. It was reported that amount of total polyphenols changes between 120 µg GAE/g propolis to 600 mg GAE/g propolis and amount of total flavanoids changes between 100 µg QE/g propolis to 350 mg QE/g propolis. Table 2 shows propolis polyphenol and flavanoid contents from different regions.

Types of Propolis

Propolis composition changes according to geographical region. It's reported that propolis composition is directly related to that of bud exudates collected by bees from various trees. It could be possible to type a propolis by its main sources. Table 3 shows different types of propolis. This types of propolis have found significance on the basis of their botanical origin and chemical composition.

Preparation of Propolis Extract

There is increasing interest on propolis. Commercial formulations like tablets, capsules, ampoules, and syrups are produced. Propolis has a complex structure so different solvents are used for extracting propolis. The solvent should be carefully chosen. Ethyl ether, ethanol, olive oil, DMSO, water, methanol and chloroform can be used for extraction of propolis but the best solvent for propolis is ethanol.

Propolis Usage

Propolis has a very wide usage area because of its composition. It has antioxidant, antiaging, antibacterial, antifungal, antiviral, antitumor effects. Because of these effects it is used in lots of area like cosmetic, medicine, food industry, etc.

Propolis is an antioxidant mixture. Free radical causes oxidative damage and for aging it is primary factor. An antioxidant is a molecule capable of slowing or preventing the oxidation of other molecules and so to prevent such changes. The antioxidant effect correlates roughly with the anti-inflammatory and hepatoprotective activity (Bogdavov, 2015).

The antimicrobial activity of propolis is by far the most important biological property which has deserved the highest scientific interest, considering the high number of performed studies. A number of papers deal with this aspect. In spite of the big compositional differences of the different propolis types, they all have antimicrobial activity (Kujumgiev, 1999). Propolis has antibacterial, fungicide, antiviral and antiparisitic effects of against harmful and pathogen organisms. These properties make it a good candidate for its application in therapy (Bogdavov, 2015).

Recently, propolis has received the special interest in the areas of oncology research as a source for either prevention or treatment of cancer. Accordingly, a large number of compounds possessing the anticancer activity such as CAPE, artepillin C, and propolin A-C have been reported from propolis (Ahuja & Ahuja, 2011; Li, 2009). It was reported that propolis prevented and mitigated diabetes and hypertension (Koya-Miyata, 2009). It was stated that propolis could be used in dentistry as a pulp therapy in primary and permanent teeth and inhibits plaques (Ahuja & Ahuja, 2011).

CONCLUSION

Propolis a golden bee product has been attracted notice recently as an alternative and complementary medicine. In modern therapy, doctors have the consensus on the usage of natural products as dose and composition controlled manner. In this respect, we tried to gather the current knowledge on chemical composition of propolis samples studied all around the world. Although total poly phenol concentration ranges from 0.2 mg GAE/g to 617 mg GAE/g, all propolis samples possessed antimicrobial activity. The possibility of propolis usage in the cancer therapy and identification of the active ingredient(s) has revealed much attentions recently. It was reported that some polyphenols and flavonoids were responsible for the anticancer activity of the propolis. In this respect, the types of propolis and their main constituents were represented. Although many papers reported anticancer activity of the propolis extract but scientists have not been able to create a standard drug from propolis to cure different cancer lines. In future direction, the necessity of more thorough investigations is obvious to establish a correlation between biological activity like anticancer and the chemical composition of propolis samples.

REFERENCES

1. Walgrave, S.E., Warshaw, E.M. & Glesne, L.A. Allergic contact dermatitis from propolis, *Dermatitis*. **16(4),** 209-15 (2005).
2. Coggshall, W. L. & Morse, Roger A. *Beeswax; Productıon, Harvestıng, Processıng And Products.* Published by Wicwas Press, Ithaca, New York, U.S.A. (1984).
3. Alfahdawi, I. *Propolis In Medicine & Dentistry* (Wolfgang, P.M.) Edition: 1, (LAMBERT, 2017).
4. Kumar, R. et. al. Propolis: Nature's boon - A review, *J Indian Acad Oral Med Radiol.* **29**, 119-121 (2017).
5. Burdock, G.A. Review of the biological properties and toxicity of bee propolis (propolis), *Food and Chemical Toxicology.* **36**, 347–363 (1998).
6. Göçer, H. & Gülçin, İ. Caffeic acid phenethyl ester (CAPE): correlation of structure and antioxidant properties, *International Journal of Food Sciences and Nutrition*. 62(8), 821–825 (2011).
7. Tolba, M. F. et. al. Caffeic Acid Phenethyl Ester: A Review of Its Antioxidant Activity, Protective Effects against Ischemiareperfusion Injury and Drug Adverse Reactions, *Critical Reviews in Food Science and Nutrition*. **56**, 2183–2190 (2016).
8. Lotfy, M. Biological Activity of Bee Propolis in Health and Disease, *Asian Pacific Journal of Cancer Prevention*. 7 (2006).
9. 9. Bankova V, Popova M: Propolis of stingless bees: a promising source of biologically active compounds. *Pharmacogn Rev*, **1**, 88–92 (2007).
10. Bankova, V. Recent trends and important developments in propolis research**,** *eCAM,* **2(1)**, 29–32 (2005).
11. Alencar, S.M. et. al. Chemical Composition and Biological Activity of a New Type of Brazilian Propolis: Red Propolis, *Journal of Ethnopharmacology*. **113**, 278–283 (2007).
12. Campo Fernandez, M.; Cuesta-Rubio, O. & Rosado Perez, A. GC-MS determination of isoflavonoids in seven red Cuban propolis samples. *J. Agric. Food Chem.* **56**, 9927–9932 (2008).
13. Maciejewicz, W. Isolation of flavonoid aglycones from propolis by a column chromatography method and their identification by GC-MS and TLC methods. *J. Liq. Chromatogr. Relat. Technol.* **24**, 1171–1179 (2001).
14. Huang, S., Zhang C. P., Wang, K., George Q. Li, G.Q. & Hu, F.L. Recent Advances in the Chemical Composition of Propolis. *Molecules,* **19**, 19610-19632 (2014).
15. Aliyazıcıoglu, R. et. al. Propertıes of Phenolıc Composition And Bıologıcal Activity of Propolıs From Turkey, *International Journal of Food Properties*. **16**, 277–287 (2013).
16. Pellati, F. et. al. An efficient chemical analysis of phenolic acids and flavonoids in raw propolis by microwave-assisted extraction combined with high-performance liquid chromatography using the fused-core technology, *Journal of Pharmaceutical and Biomedical Analysis.* 81– 82, (2013).
17. Saleh, O.M., Soliman, M.M., Mansour, A. A. & Abdel-Hamid, O.M. Protective Effects of Propolis on GammaIrradiated Nigella sativa Extract Induced Blood and Immune Changes in Wistar Rats American Journal of Biochemistry and Biotechnology, 9 (2): 162-171 (2013)

18. Toreti, V.C. et. al. Recent Progress of Propolis for Its Biological and Chemical Compositions and Its Botanical Origin, *Complementary and Alternative Medicine.* (2013).
19. Savickas, A. et. al. Chemical composition and antimicrobial activity of Lithuanian and Czech Propolis, *Biologija*. **4**, 59–63 (2005).
20. Andrzej, K. et. al. Historical Aspects of Propolis Research in Modern Times, *Complementary and Alternative Medicine.* (2013).
21. Bonvehf J. S. & Coll, F. V. Phenolic Composition of Propolis From China and From South America, *Z. Naturforsch.* **49**, 712 -718 (1994).
22. Wolsky, R. G. & Salatıno, A. Analysis of Propolis: Some Parameters and Procedures For Chemical Quality Control *Journal of Apicultural Research,* **37(2)**, 99-105 (1998).
23. Ildenize, B. et. al. Factors That Influence the Yield And Composition of Brazilian Propolis Extracts, *J. Braz. Chem. Soc.* **15**, 6, 964-970 (2004).
24. Kumazawa, S., Hamasaka, T. & Nakayama, T. Antioxidant Activity of Propolis of Various Geographic Origins, *Food Chemistry.* **84**, 329–339 (2004).
25. Hamasaka,T. et. al. Antioxidant Activity and Constituents of Propolis Collected in Various Areas of Japan, *Food Sci. Technol. Res.* **10 (1)**, 86–92 (2004).
26. Yaghoubi S.M.J., et.al. Antimicrobial Activity of Iranian Propolis and its Chemical Composition, *Daru.* **15** (2007).
27. Trusheva, B., Trunkova, D. & Bankova, V. Different extraction methods of biologically active components from propolis: a preliminary study. *Chemistry Central Journal*, **1**, 13 (2007).
28. Leandro Moreira, Luís G. Dias, José Alberto Pereira, Leticia Estevinho Antioxidant Properties, Total Phenols And Pollen Analysis of Propolis Samples From Portugal, *Food And Chemical Toxicology.* **46**, 3482–3485 (2008).
29. Kalogeropoulos, N. et. al. Chemical composition, antioxidant activity and antimicrobial properties of propolis extracts from Greece and Cyprus, *Food Chemistry.* **116**, 452–461 (2009).
30. Beatriz, C.B.S. et. al. Concentration of Flavonoids and Phenolic Compounds in Aqueous and Ethanolic Propolis Extracts Through Nanofiltration, *Journal of Food Engineering.* **96**, 533–539 (2010).
31. Moreno, M.N., Isla, M. I, Sampietro, A.R. & Vattuone, M.A. Comparison of the free radical-scavenging activity of propolis from several regions of Argentina. *Journal of Ethnopharmacology,* **71**, 109–114 (2000).
32. Laskar, R. A. et. al. Antioxidant Activity of Indian Propolis and its Chemical Constituents, *Food Chemistry.* **122**, 233–237 (2010).
33. Miguel, M.G. et. al. Phenols And Antioxidant Activity of Hydro-Alcoholic Extracts of Propolis From Algarve, South of Portugal, *Food And Chemical Toxicology.* **48**, 3418–3423 (2010).
34. Naama, J. H. et. al. Effects of Active Materials in Alcoholic Extract of Iraqi Propolis on Growth of Some Cancer Lines in The Laboratory And Cancer of Mammary Gland in Mice, *Report And Opinion.***2(5)** (2010).
35. Bonvehı´, J.S. & Gutie´rrez, A. L. Antioxidant Activity and Total Phenolics of Propolis from the Basque Country (Northeastern Spain), *J Am Oil Chem Soc*. **88**, 1387–1395 (2011).
36. Lagouri, V., Prasianaki, D. & Krysta, F. Antıoxıdant Propertıes And Phenolıc Composıtıon of Greek Propolıs Extracts. *International Journal of Food Properties*, **17**,

511–522 (2014).

37. Stan, L. Mărghitaş, L. & Dezmirean, D. Quality Criteria for Propolis Standardization, *Scientific Papers: Animal Science and Biotechnologies*. **44 (2)** (2011).
38. Cabral, I. S. R. et. al. The Correlation Between The Phenolic Composition And Biological Activities of Two Varieties Of Brazilian Propolis (G6 And G12), *Brazilian Journal of Pharmaceutical Sciences.* **48** (2012).
39. Dias, L. G., Pereira, A. P. & Estevinho, L.M. Comparative study of different Portuguese samples of propolis: Pollinic, sensorial, physicochemical, microbiological characterization and antibacterial activity, *Food and Chemical Toxicology*. **50**, 4246–4253 (2012).
40. Musa, T., Salih, M. N. & Ulaiwi, W.S., Detection of Some Active Compounds in Aqueous and Ethanolic Extracts of Iraqi Propolis and Examine Their Antibacterial Effects, *Pakistan Journal of Nutrion*, **11 (1)**, 83-87 (2012).
41. Valencia, D. et.al. Seasonal Effect on Chemical Composition And Biological Activities of Sonoran Propolis, *Food Chemistry*. **131**, 645–651 (2012).
42. Al-Jumaily, E., Al-Obaidiand , R.S. & Abdulla, J.M. Hepatoprotective Activity of Flavonoids Purified and Ethanolic Extract from Iraqi Propolis Against Carbon tetrachlorideInduced Liver Damage In Male Mice, *IOSR Journal of Pharmacy*, **4**, 22-27 (2014).
43. Righi, A. A., Negri, G. & Salatino, A. Comparative Chemistry of Propolis from Eight Brazilian Localities, *Complementary and Alternative Medicine.* (2013).
44. Choi, S.J., Shimomura2, K., Kumazawa2, S. & Ahn, M.R. Antioxidant Properties and Phenolic Composition of Propolis from Diverse Geographic Regions in Korea. *Food Sci. Technol. Res.*, **19** (2), 211 – 222 (2013).
45. Soraia, I. et. al. Phenolic Quantification and Botanical Origin of Portuguese Propolis, *Industrial Crops and Products.* **49**, 805– 812 (2013).
46. Feás, X , Pacheco, L. , Iglesias, A. & Estevinho, L. M. Use of Propolis in the Sanitization of Lettuce. *Int. J. Mol. Sci*., **15**, 12243-12257 (2014).
47. Talla, E., Dabole, B., Taiwe, G.S., Ngo Bum, T. & Mbafor, J.T. Antinociceptive pentacyclic triterpenoids from the Cameroonian brown propolis. *Pharmacologia*, **4**, 218-227 (2013).
48. El Sohaimy, S.A. & Masry, S.H.D. Phenolic Content, Antioxidant and Antimicrobial Activities of Egyptian and Chinese Propolis American-Eurasian. *J. Agric. & Environ. Sci*., **14 (10)**, 1116-1124 (2014).
49. Rebiai, A. Lanez, T. & Belfar, M. L. Total Polyphenol Contents, Radıcal Scavengıng and Cyclıc Voltammetry of Algerıan Propolıs. *International Journal of Pharmacy and Pharmaceutical* Sciences, **6** (2014).
50. Can, Z., Yıldız, O., Şahin, H., Asadov, A. & Kolaylı, S. Phenolic Profile and Antioxidant Potential of Propolis from Azerbaijan. *Mellifera,***15(1)**, 16–28 (2015).
51. Sime, D. et. al. Phenols and Antıoxıdant Actıvıtıes of Natural Honeys And Propolıs Collected From Dıfferent Geographıcal Regıons of Ethıopıa, *Bull. Chem. Soc. Ethiop*. **29(2)**, 163-172 (2015).
52. Socha, R. et. al. Phenolic Composition and Antioxidant Activity of Propolis From Various Regions of Poland, *Natural Product Research*. **29**, 5, 416–422 (2015).
53. Marquiafável, F.S. et. al. Development and characterization of a novel standardized propolis dry extract obtained by factorial design with high artepillin C content. *Journal of Pharmaceutical Technology & Drug Research*, 4 (2015).

54. Belfar, M.L. , Lanez, T. , Rebiai, A. & Ghiaba, Z. Evaluation of Antioxidant Capacity of Propolis Collected in Various Areas of Algeria Using Electrochemical Techniques. *Int. J. Electrochem. Sci*., **10**, 9641 – 9651 (2015).
55. Wali, A. F. et. al. *In Vitro* Antioxidant and Antimicrobial Activities of Propolis From Kashmir Himalaya Region, *Free Radicals And Antioxidants*. **6** (2016).
56. Bankova, V. et. al. Standard methods for Apis mellifera propolis research. *Journal of Apicultural Research*, **56** (2016).
57. Popova, M., Trusheva, B. & Bankova, V. Content of biologically active compounds in Bulgarian propolis: a basis for its standardization. *Bulgarian Chemical Communications,* **49**, 115 – 120 (2017).
58. Narimane, S. et. al. Correlation Between Antioxidant Activity and Phenolic Acids Profile and Content of Algerian Propolis: Influence of Solvent, *Pak. J. Pharm. Sci*. **30**, 1417-1423 (2017).
59. Boulanouar, B., et. al. Total Phenolic, Flavonoid Contents and Antioxidant Activities of Honey and Propolis Collected From The Region of Laghouat (South Of Algeria), *Int J Pharmacogn Chinese Med*. **1(2)** (2017).
60. C. de Groot, A. Propolis: A Review of Properties, Applications, Chemical Composition, Contact Allergy, and Other Adverse Effects. *Dermatıtıs*, **24**, 6 (2013).
61. Bogdanov, S., Propolis: composition, health, medicine. Bee Product Science, **1**, 40 (2015)
62. Kujumgiev, A. et. al. Antibacterial, antifungal and antiviral activity of propolis of different geographic origin. *Journal of Ethnopharmacology.* **64 (3)**, 235-240 (1999).
63. Ahuja, V. & Ahuja, A. Apitherapy - A sweet approach to dental diseases. Part II: Propolis, *Journal of Academy of Advanced Dental Research*. **2** (2011).
64. Li, F. et. al. Cytotoxic constituents of propolis from Myanmar and their structure–activity relationship, *Biol. Pharm. Bull.* **32(12)**, 2075—2078 (2009).
65. Koya-Miyata, S. et. al. Propolis Prevents Diet-Induced hyperlipidemia and mitigates weight gain in Diet-Induced obesity in mice, *Biol. Pharm. Bull*. **32(12)**, 2022—2028 (2009).

Sample	**Compounds identified**
Bulgarian propolis	3,7-Dihydroxy-5-methoxyflavanone 2,5-dihydroxy-7-methoxyflavanone Dihydrocaffeic acid Dihydroferulic acid Dihydroxyacetophenone hydroxymethoxyacetophenone β-Phenethyl alcohol Benzyl alcohol pinobanksin Pinostrobin Dimethyl kaempferol

Brazil/S˜ao Paulo state	3-Prenyl-4-dihydrocinnamoloxynnamic acid Dehydroabietic acid Abietic acid β-Amyrine Triterpenic alcohol of amyrine Lanosterol isomer with 9(11) double bond
Brazil/S˜ao Paulo state/Botucatu city	9-E and 9-Z 2,2-Dimethyl-6-carboxyethenyl-8-prenyl-2H-benzopyran
Japan/Okinawa	Prokinawan
Brazilian propolis type 6	Hyperibone A
Mexico/Champoton	1-(3',4'-Dihydroxy-2'-methoxyphenyl)-3-(phenyl)propane (z)-1-(2'-Methoxy-4',5'-dihydroxyphenyl)-2-(3-phenyl)propene 3-Hydroxy-5,6-dimethoxyflavan (−)-7-Hidroxyflavanone (−)-Mucronulatol (−)-Arizonicanol a (+)-Vestitol (−)-Melilotocarpan a, d (+)-Pinocembrin
Greece (six regions)	18-Hydroxyabieta-8, 11,13-triene Dihydroxyabieta-8,11,13-triene; hydroxydehydroabietic acid 18-Succinyloxyabietadiene 18-Succinyloxyabietadiene (isomer) 18-Succinyloxyhydroxyabietatriene
Greece	Palmitoyl isocupressic acid 18-Hydroxyabieta-8,11,13-triene Pimaric acid 3,4-seco-Cycloart-12-hydroxy-4(28),24-dien-3-oicacid

Kenyan propolis	Tetrahydrojusticidin B 6-Methoxydiphyllin Phyllamyricin C Macarangin Schweinfurthin A, B
Indonesia/East Java province/Batu city	5-Pentadecylresorcinol 5-(8'z, 11'z Heptadecadienyl)-resorcional 5-(11'z-Heptadecenyl)-resorcinol 5-Heptadecylresorcional Propolin d, c, f, g
Indonesia	1,3-Bis(trimethylsilylloxy)-5,5-proylbenzene Dofuranuronic acid
Jordanian propolis	24(z)-1β-3β-Dihydroxyeupha-7,24-dien-26-oic acid
Honduras	(E, Z)-Cinnamyl cinnamate
Solomon island	Solophenol (A)
Turkey	9,12-Octadecadienoic acid Caffeic acid t-cinnamic acid 4,8 Diphenyl-1-thieno-2-benzazol-1,3-dione Pinobanksin L-proline
Australia	3,5,4'-Trihydroxy-3'-methoxy-2-prenyl-*E*-stilbene 4-Prenyldihydroresveratrol
Iran	Tschimganin Ferutinol *p*-hydroxybenzoate Bornyl vanillate

Italy	Caffeic acid Pinobanksin-5-methyl-ether Pinocembrin Caffeic acid phenylethyl ester (CAPE) p-Coumaric benzyl ester
United Kingdom	Pinobanksin Caffeic acid pentenyl ester Chrysin Kaempferol methyl ether Hydroxypropionate ethyl ester Acetylcaffeoyl coumaryl glycerol

Table 1. Compounds in propolis (The table is design by some modifications of Huang, 2014; Aliyazıcıoglu, 2013; Pellati, 2013; Saleh, 2013; Toreti, 2013).

Country/Region/Type	Total Polyphenol (mg GAE/g)	Total Flavanoid (mg QE/g)	Reference
Uruguay	0.2	0.1	Bonvehf, 1994
Brazil	43.7	42.5	Wolsky & Salatino, 1998
Brazil	120	-	Ildenize, 2004
Argentina	212		
Australia	269		
Hungary	242	-	Kumazawa, 2004
United State	256		
Uzbekistan	174		
Japan	120	70	Hamasaka, 2004

Iranian	360	-	Yaghoubi, 2007
Red propolis	232	43	Alencar, 2007
Italy	440	86	Trusheva et. al. 2007
Portugal	329 151	-	Moriera, 2008
Greece	200	20	Kalogeropoulos, 2009
Cyprus	250	7	
Brazil	98.74	69.35	Beatriz, 2010
Argentina	-	13-40	Moreno, 2000
Indian	159	57	Laskar, 2010
Portugal	6.27	3.0	Miguel, 2010
Iraq	21.90	-	Naama, 2010
Spain	0,25	0,12	Bonvehi, 2011
Turkey	180	-	Aliyazıcıoglu, 2013
Greek	80	30	Lagouri, 2014
Romania	280	90	Stan, 2011
Brazil	14.8 169	3.2 61.5	Cabral, 2012

Portugal	190	70	Dias, 2012
Iraq	248	136.5	Musa, 2012
Mexico	601	300	Valencia, 2012
Iraq	0.2	0,6	Al-Jumaily, 2014
Brazil	150	20	Righi, 2013
Korea	230	90	Choi, 2013
Portugal	220	350	Soraia, 2013
Portugal	29.5	10.3	Feas, 2014
Cameron	45.1	15.2	Talla, 2013
Egypt **China**	0.14 0.12	-	El Sohaimy, 2014
Algeria	4.93	1.94	Rebiai, 2014
Azerbaijan	47.1	-	Can, 2015
Ethiopian	617	224	Sime, 2015
Poland	170	50	Socha, 2015
Green	23.19	5.5	Marquiafavel, 2015

Algeria	2.62	2.2	Belfar, 2015
Kashmir	260	105	Wali, 2016
Poplar type	210 50	80 5	Bankova, 2016
Bulgaria	307	70	Popova, 2017
Algeria	9.97	3.53	Narimane, 2017
South Algeria	23.85	2.79	Boulanouar, 2017

Table 2. Amount of total polyphenol and total flavanoid content of different propolis samples.

Type	Region	Plant Sources	Major (Typical) Constituents
Poplar	Europe, North America, nontropical regions of Asia, New Zealand, China	Populus species of section Aigeiros, most often P. nigra L.	Flavones and flavanones (pinocembrin, pinobanksin, pinobanksin-3-O-acetate, chrysin, galangin), cinnamic acids (notably caffeic acid) and their benzyl-, phenethyl-, and prenyl esters
Green (alecrim) Brazilian	Brazil	Baccharis species, predominantly B. dracunculifolia DC	Prenylated p-coumaric acids, diterpenic acids, prenylated acetophenones
Birch	Russia	Betula verrucosa Ehrh.	Flavones and flavonols (not the same as in poplar type): acacetin, apigenin, ermanin,
Red propolis	Cuba, Brazil, Mexico	D. ecastophyllum and other Dalbergia species	Isoflavonoids (isoflavans, terocarpans)

Mediterranean	Sicily, Greece, Crete, Malta	Cupressaceae (species unidentified, possibly C. sempervirens) and Pinaceae	Diterpenes (mainly acids of labdane type), anthraquinones
Clusia	Cuba, Venezuela	Clusia species including C. major, C. minor	Polyprenylated benzophenones
Pacific	Pacific region (Okinawa, Taiwan, Indonesia)	Macaranga tanarius	C-prenyl-flavanones

Table 3. Types of propolis and its major chemical composition (Groot, 2013).

Getting Information From Human-Based Signals

Özgür AFŞAR[1]

CHAPTER 4

[1] Ege University, Faculty of Science, Department of Physics, Izmir-Turkey

INTRODUCTION

Human-based signals are time series that store some useful information about life characteristics of person. Beat-to-beat fluctuations of cardiovascular system, stride time variabialities of a gait and fluctuations of electric activity of the neurons are some typical examples. It is needed to apply some analysis on the signals to expose hidden structures of such systems. Various complexity measure from informatics or heuristic approaches can be used to reveal the dynamics and to define the degree of order (or disorder) of the systems.

The stride intervals (or time) from one stride to the next in time constitutes stride-to-stride fluctuations as a gait variability when a person is walking. They are generally called stride time variability (STV) of gait. It is well known that pathologies in some neurological diseases such as ALS, Huntington or Parkinson effect human movement and coordination. Thereby, fluctuation dynamics of gait for a patient with such diseases represent distinct behavior from healthy one (Hausdorff et al., 1997). For example, stride intervals in time are completely random that means statistically independent for a patient with Parkinson disease (PD) although they are correlated variables for a healthy person. Also, stride intervals possess some memory effect and temporal structures for healthy person. These self-similar structures disappear for the patient one. Diffusion fluctuation analysis (DFA) shows that gait signal from healthy subject posses fractal indices of around 0.8-1. It is close to 0.5 for a patient with PD (Hausdorff et al., 1995).

As an another human-based signal, heart rate variability (HRV) comes from beat-to-beat fluctuations of cardiovascular system. HRV has common and uncommon properties with STV (Goldberger 1991). For a healthy person, complex fluctuations and self-similar fractal structures emerge and destroye with aging as the common properties. However, for a pathological case the magnitude of fluctuations increases in STV whereas it decreases in HRV. Generally, beat-to-beat fluctuations of cardiovascular system for a healthy person are similar to the fluctuations of chaotic dynamical systems which is forced to go away from an equilibrium state (Glass, 1987). There is a huge effort to mimic such signals with model systems. This enable us to make a detailed investigation on the systems under non-equilibrium conditions.

Electroencephalography (EEG) is an another important exploited signals recorded from humans. It has a recording of electrical activity along the scalp generated by the cerebral cortex nerve cells of the brain. The states of a person (in sleep, awake or anaesthetized) can be determined by following characteristic patterns in recordings of the electrical potentials. They represent different dynamics in an EEG for the states. Analysis of EEG patterns is also of great importance for clinicians in diagnosis and treatment of neuro-degenerative diseases and abnormalities. The major application of EEG recording is in epilepsy. Epileptic activity of a patient shows some abnormalities such as sudden changes in electrical functioning of the brain, that is called seizures, according to a standard EEG from healthy person. An abnormal activity that can be emerged in EEG signal is in two different phases. They are ictal phase that is during an epileptic seizure and inter-ictal phase between seizures. The detection of the phases clearly is an important factor for diagnosis and treatment (Niedemeyer and Silva, 2005).

A quantiative determination or comparison of different regimes (or phases, or stages, or systems) can be done with a complexity analysis using entropy-based measures that come from informatics approaches (Afsar, 2016). Shannon entropy (S) is a standard measure of disorder of a system. It is also well known that entropy production for a transition between two states is related to the changes of the Shannon entropy of the system as $\Delta S = S_2 - S_1$. This quantity requires the second law of thermodynamics as $\Delta S \geq 0$ for an isolated transition between the states. Another most famous entropy-based measure is relative or Kullback-Leibler entropy ΔS_{KL} that may be a useful measure to make a comparison between an equilibrium state and an arbitrary state. The third one is renormalized entropy ΔS_{RE} that enable us to compare two states with different mean energies combaining a renormalization procedure and Kullback Leibler entropy. The method also enable us to mimic an open system to closed one and to apply Boltzmann's H-theorem on open systems. All of these entropic measures have some advantages (or disadvantages) according to the each others. For example, The second law has a strong limitation since it is only valid for isolated transitions. The Kullback-Leibler measure can not explain spatial patterns that emerge in a self-organized evaulation since it satisfies a condition as $\Delta S_{KL} \geq 0$ such as the usual second law. Moreover, it should be noted that the most used method in literature for a distinction of the regimes is analysis of Lyapunov exponent that is also related to the Kolmogorov-Sinai entropy (or metric entropy) from the information theoretic approach. However, it is also known that it is not sensitive for transitions between periodic oscilations of a system. Thereby, it is of great importance to make a comparision of distinct phases also considering such advantages (or disadvantages) (Afsar, 2018).

Using heuristic measures from Recurrence plot (RP) and its quantification analysis, recurrence quantification analysis (RQA), is an alternative method to understand dynamics under human-based signals (Marwan et al., 2007). The measures provide a quantification of the system using heuristic measures such as divergence, determinizm, laminarity, etc. Recurrence is an important property of dynamical system. The recurrence theorem, that is introduced by Poincare in 1980, states that all trajectories of dynamical systems will return very close (in the very small range of ε) to their previous position in the phase space after a sufficientlty long but finite time. As an example, in the phase space of a flow that has a bounded value, the recurrence theorem is always valid. The heuristic measures that are derived from point density and line structures in the RP, has been obtained for various human-based signals in neurology (Ouyang, 2008), cardiology (Marwan et al., 2002) and physiology (Afsar et al., 2018).

In the following sections, informatics and heuristic approaches are introduced. In the next step, some applications of the approaches on the human-based signals in the literature are presented. As a sample application, entropy and recurrence-based calculations are applied on heart rate variability data seperately.

Informatics Approaches

Let us now consider a time series $X(t, a_k)$ over time t that comes from a specific subject or a segment (a_k) of whole trajectory under investigation, which belongs to the state k. The corresponding probability distribution $P(\omega, a_k)$ can be callculated from a spectral intensity as $P(\omega, a_k) = F(\omega, a_k) \cdot F^*(\omega, a_k)$ using the Fourier transformation of the time series $X(t, a_k)$ instead of the residence time distribution.

First, we need to estimate normalized spectral intensities $p(\omega, a_k)$ for every state, satisfying $p(\omega, a_k) = CP(\omega, a_k)$ where C is a normalization constant that enables us to normalize the spectral intensity to unit in the frequency range of $\Delta\omega \in \left(0, \frac{1}{2\Delta t}\right)$.

After we estimate the spectral intensities as the distributions for the subjects $\{a_k\}_{k=0}^{N_{per}-1}$ where N_{per} is the total number of the subjects (or segments) under investigation, the Shannon entropy (Shannon, 1948) of the state k reads

$$S\big(p(\omega, a_k)\big) = -\int p(\omega, a_k) \ln p(\omega, a_k)\, d\omega\,. \tag{1}$$

Suppose first that the state '0' is reference state and the state '1' an arbitrary state. The entropy change ΔS from the state '0' to the state '1' reads

$$\Delta S = S_2 - S_1 = \int (p_0 \ln p_0 - p_1 \ln p_1)\, d\omega\,. \tag{2}$$

where $p_0 = p(\omega, a_0)$ and $p_1 = p(\omega, a_1)$. It should be noted that ΔS as an entropy production would require $\Delta S \geq 0$ according to the second law of thermodynamics if this equation indicated an isolated transition from the state '0' to the state '1'.

Another informatics measure is the Kullback-Leibler entropy or relative entropy (Kullback and Leibler, 1951) or information gain defined as

$$\Delta S_{KL} = \int p_1 \ln \frac{p_1}{p_0} d\omega\,. \tag{3}$$

The relative entropy states the information of p_1 relative to p_0. It is also a divergence, mathematically. It satisfies $\Delta S_{KL} \geq 0$, and $\Delta S_{KL} = 0$ if $p_1 = p_0$. However, it does not provide the conditions which are symetry and triangle inequality for a distance function.

Klimontovich introduced another entropy-based measure, the renormalized entropy ΔS_{RE} (Klimontovich, 1987), that is related to the Kullback-Leibler entropy. It satisfies $\Delta S_{RE} = -\Delta S_{KL}(p_1, \tilde{p}_0) < 0$ as the quantitative measure for the relative degree of order. It gives us the powerful results that are able to explain self-organized spatial patterns that emerge through successive bifurcations in evolution processes. In the method, the reference state p_0 is renormalized as $\tilde{p}_0 = K(T_{eff}) {p_0}^{1/T_{eff}}$, where T_{eff} is an effective temperature, so that mean energies $\langle E \rangle$ of the states requires the equality condition which is defined by

$$\langle E \rangle = \int \tilde{p}_0 \ln \tilde{p}_0\, d\omega = \int p_1 \ln \tilde{p}_0\, d\omega\,. \tag{4}$$

The effective temperature T_{eff} is defined from the equality of mean energies of the state '0' and '1' in Eq. (4). This condition enable us to find whether reference state is more disordered. If $T_{eff} > 1$, then it is true that the state '0' is more disordered. Thereby, the renormalized entropy

$$\Delta S_{RE} = S_1 - \tilde{S}_0 = -\int p_1 \ln \frac{p_1}{\tilde{p}_0} \, d\omega = -\Delta S_{KL} < 0 \,. \tag{5}$$

If $T_{eff} < 1$, then it is not true and one has to interchange the states, i.e. to take the state '1' as more disordered and to repeat all procedure.

Heuristic approaches

Suppose that $\boldsymbol{x}_i$ is the i-th point on the trajectory that in d-dimensional phase space, for $i = 1, \dots, N$, $\boldsymbol{x} \in \mathbb{R}^d$. Poincare recurrence theorem states that the trajectory point will return to the ε neighborhood of a previous state (Poincare, 1980). The recurrence plot (RP) is a visualisation as an array of dots in a $N \; x \; N$ (time vs time) matrix (Marwan et al., 2007).

First, if only a one dimensional time series is given, time-delay embedding can be used to reconstruct the phase space trajectory for a time series $(\{X(t, a_k)\} = \{u_i\}_{i=1}^{N})$ with length N as $\boldsymbol{x}_i = \left(u_i, u_{i+\tau}, \dots, u_{i+(m-1)\tau}\right)$ where m is the embedding dimension and τ is the embedding delay. For the trajectory $\{\boldsymbol{x}_i\}$, the RP is defined as

$$R_{i,j}(\varepsilon) = \Theta\left(\varepsilon - \left\|x_i - x_j\right\|\right), \quad i,j = 1, \dots, N, \tag{6}$$

where $\Theta(\cdot)$ is the Heaviside function and $\|\cdot\|$ is a norm. For a visualisation of RP in a white background, a block dot is placed at (i,j) whenever $\boldsymbol{x}_j$ is sufficiently (in the range of the threshold ε) close to $\boldsymbol{x}_i$.

In order to quantify distinct regimes such as healthy or patient and to define dynamics of the systems, some heuristic measures can be calculated from point densities on RP (Afsar et al., 2018). This procedure is called recurrence quantification analysis (RQA). Recurrence rate (RR) as the measure of the density of recurrence points in the plot is defined by

$$RR = \frac{1}{N^2} \sum_{i,j=1}^{N} R_{i,j} \,. \tag{7}$$

The probability $p(l)$ to find a diagonal line of an exact length l in RP is given by

$$p(l) = \frac{P(l)}{N_l} \tag{8}$$

where $N_l = \sum_{l \geq 2} P(l)$ is the total number of diagonal lines and $P(l)$ is the histogram of diagonal lines of length l. Thereby, recurrence-based Shannon entropy measure is given as

$$ENT = -\sum_{l=2}^{N} p(l) \ln p(l) \,. \tag{9}$$

The maximum length L_{max} of the diagonal lines in the RP is defined by $L_{max} = max(\{l_i; i = 1, \dots, N_l\})$. The measure of divergence of the points is called divergence (DIV) and related to the largest positive Lyapunov exponent:

$$DIV = \frac{1}{L_{max}}. \tag{10}$$

The ratio of recurrence points on the diagonal structures to all recurrence points

$$DET = \frac{\sum_{l=2}^{N} lP(l)}{\sum_{i,j}^{N} R_{i,j}} \tag{11}$$

is a measure of predictability and is called determinism (DET). The avarage diagonal line length is defined by

$$\langle L \rangle = \frac{\sum_{l=2}^{N} lP(l)}{\sum_{l=2}^{N} P(l)} \tag{12}$$

as average time that two segments of the trajectory are close to each other. It means prediction time in average.

Applications to the Human-Based Signals

In the context of informatics-theoretical approaches, the entropy-based measures were applied to the human-based signals by several researchers. Invasive EEG recordings of patients suffering from focal epilepsy were analyzed using the method of the Shannon and the renormalized entropies by Kopitzki et al. They showed the renormalized entropy decreases within ictal phase of seizure and suggested that the method of the renormalized entropy is a useful method for seizure detection and localization of epileptic foci. They also showed that the Shannon entropy does not serve as a feature characterizing the ictal phase. Moreover, they investigated the spatial behavior of the renormalized entropy corresponding to recording locations of different distance to the epileptic focus. They showed that magnitude of the renormalized entropy has the highest absulute value for the location of smallest distance to the epileptic focus (Kopitzki et al., 1998). In another study, Wessel et al. investigated complex properties of HRV in terms of nonlinear measure of the renormalized entropy using different spectral estimation methods based on fast fourier transformation and autoregressive model. They showed that the method of the renormalized entropy within autoregressive model is an independent parameter in HRV assessment that seems to be potent for risk stratification of patients after myocardial infraction. In the study, it was shown that the renormalized entropies possess negative values for normal HRV as they have positive values for pathological cases of heart rate (Wessel et al., 2000). In our one of recent works, we have shown that the renormalized entropy that is calculated from gait variables is a better measure than the Shannon or the Kullback Leibler measures for determination of disease stages of patients with Parkinson disease. It has been also shown that successive rate of the determination increases with pathology in terms of Hoehn-Yahr stage (Afsar et al., 2016).

Now, we apply a complexity analysis within the informatics approaches on HRV as an sample application. The entropy production, Kullback-Leibler and renormalized entropies were calculated from filtered and interpolated 24 h tachogram of a healthy subject and a high-risk patient in the study. We here use two pilot data that belong to the subjects which were already used in a work (Wessel et al., 2000). However, we calculate and compare the entropy-based measures according to their advantages (or disadvantages) here. As can be seen in Fig. (1), for the healthy person higher values of the entropies than the patient one is a common properties for all measures. Moreover, negative values of the renormalized entropy implies a healthy state as the cardiac patient possesses a renormalized entropy of only positive values in all periodograms. However, the Shannon and Kullback-Leibler entropies can not do this kind of distinction since they have only positive values both the healthy person and the patient one through the periodograms.

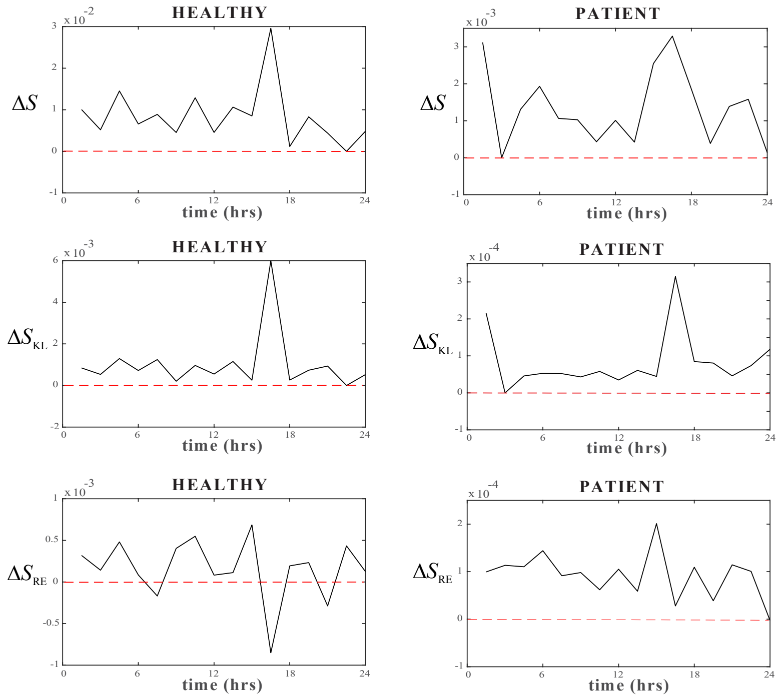

Figure 1. From top to bottom, results of the entropy production, the KL entropy and the renormalised entropy of a healthy person (left) and a patient person (right) over 24 hrs. Holter analysis.

As a new visualisation technique, the recurrence plot was applied on various human-based signals in the literatüre in order to show behaviours in the phase space of the signals. This technique has an advantage since it's heuristic measures coming from recurrence quantification analysis enable us to evaluate dynamics of the systems quantitively. Acharya et al. used the EEG recordings in recurrence plot and managed to classify the EEG signals into normal, ictal and interictal classes extracting RQA measures from the RPs (Acharya et al., 2011). Moreover, Marwan et al. applied the recurrence technique on HRV data. They showed differences between a healthy state and the state before a life-threatening cardiac arrhythmia in terms of the RP visualisation. Quantifying a laminar state before the arrhythmia enabled them to proposed a prediction of such an event (Marwan et al., 2002). Recently, we have applied the recurrence plot method on the gait variables of healthy adults and patients with Parkinson disease in order to quantify quasi-periodic character of gait. Using the RQA measures, we have also shown that pathology in Parkinson disease alters the degree of quasiperiodiciy of gait (Afsar et al., 2018).

Here, we present an application of RP method and calculate the heuristic measures from RQA using the HRV data for both the healthy person and the cardiac patient.

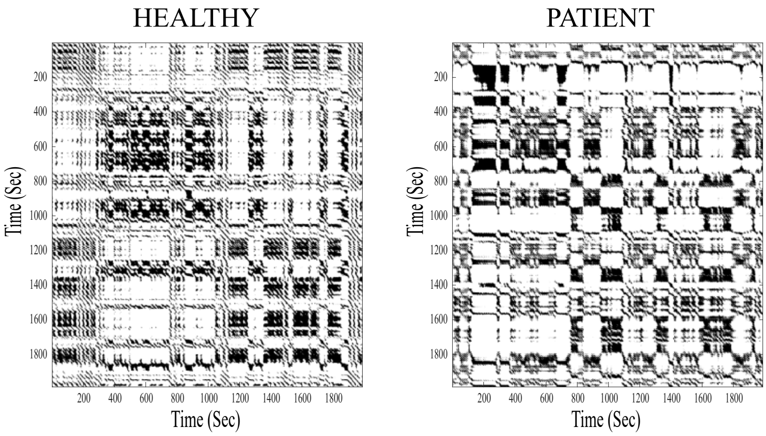

Figure 2. Recurrence plots of the HRV signals of the healthy person and the cardiac patient.

In Figure 2, we plot the recurrence visualisations of the interpolated signals from the subjects. As can be seen from the figure, the RP from the healthy person shows the smaller rectangles as the big black rectangles emerge in the RP that belongs to the cardiac patient. Also, for the quantification analysis, we calculate the heuristic measures using point densities on the RPs, which are recurrence-based Shannon entropy, divergence, determinism and avarage diagonal line length that are given in the Eqs. (9-12).

Subject	**RQA measures**			
	$\boldsymbol{ENT}$	$\boldsymbol{DIV}$	$\boldsymbol{DET}$	$\langle \boldsymbol{L} \rangle$
Healthy	3.34	0.0005	0.98	12.30
Patient	2.82	0.0008	0.94	9.47

Table 1. The heuristic measures from RQA for the healthy person and the cardiac patient.

We summarize the results in Tablo 1. As can be seen from the table, the measures differ from the healthy subject to the patient one. Such results are of great importance so that they enable us to reveal evaluation in dynamics of a person from healthy state to patient one quantitatively.

REFERENCES

1. Acharya UR, Sree SV, Chattopadhyay S, Yu W and Ang PC, (2011). Application of recurrence quantification analysis fort he automated of epileptic EEG signals, *International Journal of Neural Systems*, 21(3), 199-211.
2. Afsar O, Tirnakli U and Kurths J, 2016. Entropy-based complexity measures for gait data of patients with Parkinson's disease, *Chaos: An Interdisciplinary Journal of Nonlinear Science*, 26, 023115-6.
3. Afsar O, 2018. A comparison of Shannon, Kullback-Leibler and renormalized entropies within successive bifurcations, *Physica D (in Press*), https://doi.org/10.1016/j.physd.2018.11.002
4. Afsar O, Tirnakli U and Marwan N, 2018. Recurrence quantification analysis at work: Quasi-periodicity based interpretation of gait force profiles for patients with Parkinson disease. *Nature-Scientific Reports*, 8:9102, 1-12.
5. Glass L, 1987. Complex cardiac rhythms, *Nature* 330, 695-696.
6. Goldberger AL, 1991. Is the normal heartbeat chaotic or homeostatic? *News in physiological sciences* 6, 87-91.
7. Hausdorff JM, Peng CK, Ladin Z, Wei JY and Goldberger AL, 1995. *Journal of Applied Physiology*, 78, 349-358.
8. Hausdorff JM, Mitchell SL, Firtion R, Peng CK, Cudkowicz ME, Wei JY and Goldberger AL, 1997. Altered fractal dynamics of gait: reduced stride-interval correlations with aging and Huntington's disease, *Journal of Applied Physiology*, 82, 262-269.
9. Klimontovich YL, 1987. Entropy evolution in self-organization processes: H-theorem and S-theorem, Physica A, 142, 390-404.
10. Kopitzki K, Warnke PC and Timmer J, 1998. Quantitative analysis by renormalized entropy of invasive electroencephalograph recordings in focal epilepsy. *Physical Review E*, 58(4), 4859-4864.
11. Kullback S and Leibler RA, 1951. On information and sufficiency, *The Annals of Mathematical Statistics*, 22(1), 79-86.
12. Marwan N, Romano MC, Thiel M and Kurths J, (2007). Recurrence Plots For The Analysis of Complex Systems, *Physics Report*, 438, 237-329.
13. Marwan N, Wessel N, Meyerfeldt U, Schirdewan A and Kurths J, (2002). Recurrence Plot Based Measures of Complexity and its Application to Heart Rate Variability Data, *Physical Review E*, 66 (2), 026702-8.
14. Niedermeyer E. and Lopes da Silva F, (2005). *Electroencephalography: basic principles, clinical applications, and related fields*, Lippincott Williams & Wilkins, ISBN 0781751268, 5th edition.
15. Ouyang G, Li X, Dang C and Richards DA, 2008. Using recurrence plot for determinism analysis of EEG recordings in genetic absence epilepsy rats, *Clinical neurophysiology*, 119, 1747-1755.
16. Poincare H, 1890. Sur le probleme des trois corps et les equations de la dynamique, *Acta mathematica*, 13, 1-270.
17. Shannon CE, 1948. A mathematical theory of communication, *The Bell System Technical Journal*, 27(3), 379-423.
18. Wessel N, Voss A, Kurths J, Schirdewan A, Hnatkova K and Malik M, (2000). Evaluation of renormalised entropy for risk stratification using heart rate variability data, *Medical & Biological Engineering & Computing*, 38, 680-685.

Importance of Algae as Biomass Energy

Betül KUT GÜROY[1]

Sibel BAYIL OĞUZKAN[2]

CHAPTER 5

[1] Central Research Laboratory, University of Yalova, Turkey

[2] Department of Medical Services and Techniques, Health Services, University of Gaziantep, Turkey

1. INTRODUCTION

Among the algae are species that are easy to produce, produce little pressure on agricultural areas and water resources, and are efficient in terms of lipid content, making biomass handling possible. High-lipid plants such as sugar cane, canola, soybeans and sunflower, which are used as the main food source, are produced in recent years to obtain biomass energy.For these plants that grow on fertile soil, extensive agricultural land and irrigation volume are required. The most important advantage that the fuels obtained from the algal must be underlined is that the fertile soil and irrigation needs are much less than the amount required for the productionof terrestrial energy plants. Many articles emphasize that algal energy production is an expensive option. However, geothermal water and algae production is an option that can help reduce the cost of nutrients needed for the culture medium and improve the getting dry product phase.Algae has the potential to convert CO_2 emissions into bioenergy during the energy production phase. CO_2 emitted from flue gas can be used to produce algae biomass. Costs can be reduced by using flue gas heat during drying of the biomass. Flue gases and geothermal waters should be taken into consideration while reducing algae production costs.

In order to control the release of carbon released into the environment, the Kyoto Protocol has set the widespread application of edible and environmentally friendly energy production processes among the world's energy policies. The use ofalternative energy sources with features that protect the environmentally friendly, local and global carbon balance is encouraged by the International Energy Agency (IEA) [1].

2. ALGAL ENERGY

Algal energy studies began to accelerate in the middle of the 20th century [2], [3]. The ability of algal energy to produce at competitive prices with fossil fuels has been an important research topic. It was reported that methane gas was produced by carbohydrate fermentation in algae cells in the late 1950s [4]. Comprehensive investigations of fuels obtained from microalgae have been carried out from 1978 to 1996 under the Renewable Energy Program [5]. When first started working in algal energy production, it was seen as the main target to obtain hydrogen gas. But in the 1980s, liquid fuel production from biomass became more attractive.Once the potential microalgae that could be obtained from the fuel were detected, the ability of the algae to accumulate lipids was investigated when many strains were stimulated under nutrient stress conditions. Information on the change in the overall rate of oil production in algae exposed to nutrient deficiency in culture was obtained. Some algal strains have been found to produce triacylglycerol (TAG) at a dry cell weight of 20 to 50%, which is important for biomass therapy [5, 6].

Algal oil; when combined with alcohol and the H + or OH - group, it is used in the production of fatty acid methyl esters by the transesterification process to form biodiesel. The esters formed as a result of transesterification are called "algal biodiesel" [7]. Algal biomass has three important stages. 1st biomass production is the 2nd lipid extraction and 3rd conversion stages. Cost reduction methods and technological commercialization are important at all stages in order to spread the algae energy.

From the mid-20th century to the present, algae have been identified as a fuel source, and it has been an important research topic to identify the biological mechanisms of algae and determine a viable method for algal energy optimization. For the sustainability of algal energy studies, the expansion of the "biosystem engineering" profession will provide innovative and cost-effective approaches for oil production with algal culture.

2.1. Types of Algae Used in Biomass Energy Generation

Biogas and biodiesel produced from lipid or carbohydrate components in microalgae, cyanobacteria and macro algae are defined as "algae energy". Algal energy production can be achieved successfully by choosing a suitable type and efficient biomass production system. The conversion of the main raw material to fuels and products depends on these bases. Among the subjects to be considered in selection of algal species for biomass production for algal energy production, the type of fuel and by-product types to be produced are considered. Fuel types that can be obtained in algae include hydrogen gas, carbohydrates, lipids, isoprenoids, methane (via anaerobic digestion) or ethylenealcohols (either directly or through biomass conversion). By-products include food and feed supplements, pharmaceuticals, nanotechnology materials or petrochemicals.Algal biogas production is an alternative and renewable energy source. Some species of the cyanobacteria class are produced for this purpose. Cyanobacteria are valuable in terms of carbohydrate and secondary metabolite products even in high amounts of lipid deposits. Some algal species are used as algae biogases in the production of hydrogen. By changing the genetics it can be transformed into attractive organisms in biofuel production [7].

Carbon metabolism for the production of hydrocarbon fuels and intermediates of *Synechocystis* has been investigated[8], [9].

The *Synechococcus* strain has been found to secrete cellulose, sucrose [10], ethanol [11] and isobutanol [12] and have a specialized cellular structure and metabolism important for the production of hydrogen.

Cyanothece sp. ATCC 51142 [13] and Osilatoria [14], nitrogenase as a catalyst, Gloeocapsaalpicola species hydrogenase and *Cyanothece* sp. PCC 7822 is used in the production of H_2 in the dark by the hydrogenase enzyme.

Chlamydomonasreinhardtii, a microalga species of the class Chlorophyta (green algae), is used as a "model species" to understand the bases of cellular lipid synthesis and regulation, and foreign genes are synthesized steadily and successfully [15, 16].

*Chlorella*protothecoides is a kind of Chlorophyta class that can produce abundant lipid. Addition of carbon source has been reported to induce heterotrophic growth by increasing both growth rate and lipid production and producing lipid over 50% of its dry weight [17].

Dunaliellasalina produces abundant amounts of lipids in large-scale biofuel production, and it is reported to be one of the important species in the purest culture category because of its high salt production [18].

Diatoms have a high lipid accumulation potential and use 20% of total global carbon [19]. Silicon is an important nutrient requirement for diatoms because the cell wall contains silica. The presence of silicone has been reported to be a trigger for lipid accumulation in diatoms [19], [20].

Macro algaes are aquatic plants rich in carbohydrates that have low lipid content but can be converted into a variety of fuels. Kelp-like macroalgae (Phaeophyta), *Ulva* sp. green algae (Chlorophyta) and *Porphyra* sp. red algae (Rhodophyta) species are commercially produced in the world.

2.2. Algae Production Methods

For the growth of the algal biomass; Sunlight or sugar, water, CO_2 and several nutrients are required. Algal for obtaining biofuel and bio products; Algae production can be achieved under phototrophic, mixotrophic or heterotrophic conditions. This method is called heterotrophic if algae are fed to produce biomass in a non-light environment and with a carbon source such as sugar. Heterotrophic and photoototrophic conditions are used together in the mixotrophic growth. [21]. In the dark phase, biomass losses can affect the net efficiency of photosynthetic cultures. When cells are grown in a mixotrophic source of carbon in the dark phase, high cell densities can be achieved in the dark phase as well as in the light phase [13]. For low cost biofuel production; Long-term culture stability and high-yield metabolite production of the algae produced are important. Knowing the physiology and metabolic processes of the algae that are intended for production, knowing when and how the carbon used in culture turns into lipids or carbohydrates, plays a key role in the development of biofuels and in the design of planting strategies. Rapid growth or the ability to effectively retain nutrients is important both in terms of overall productivity and competition with the development of undesirable microorganisms in culture water.

Algal biomass yield depends on the biochemical, thermo-chemical and chemical processes that occur during the cultivation process. Algal energy efficiency depends on the technology of the conversion of organic matter in the final product. High volume but low-value products can also result in the risk of obtaining results. Harvesting and drying of the algae is a process that brings high energy cost.

Harvesting by flocculation [22] or removal of lipid droplets from cells is an efficient but costly step. For this reason algal biomass is used the type and conditions of algae produced, harvesting time and shape, the technology applied to the raw material should be considered as a whole.

Inadequate nutrient mediums and temperature changes in the environment may be stimulating factors in the storage of carbon in fat form in some algae cells. How these conditions can be manipulated in favor of biofuel production is not yet clear. Three different decision points are envisaged for the determination of the process of converting the algae to fuels and products. First; it is the conversion of all algae biomass into fuel. The second one; the extraction of algal metabolites and the processing of direct algal secretions as the third. If all algal biomass is to be produced for use as fuel, it is necessary to know how and when carbon is used in the production of lipids or carbohydrates in a cell. Biofuel efficiency depends on how sowing and harvesting strategies are designed. The basic understanding of the cellular system that controls and regulates carbon flow in algae is an important research topic for metabolic and biosystem engineering. Research should be increased for better understanding of fatty acid synthesis in the algae. This lack of information can cause lipid yields from algal biomass culture efforts to fall behind the high values observed in the laboratory (50% - 60%) [6]. Understanding the lipid order will help to maximize the algal biofuel handhold.

The basic objective of bio-fuel or bio-product producing technologies is algal biomass cleansing of water and separation of lipids. There are three main components of algal biomass, lipids, carbohydrates and proteins. Lipids and carbohydrates can be used for gasoline and jet fuel production, while proteins can be used for animal / fish feed [23].

Algal cultures are predominantly grown in water and are harvested and dewatered to extract the harvested algae biomass before extraction and conversion.Algae are dried before degreasing. Algal lipids are separated by solvent after filtration and drying. These steps increase energy costs. Geothermal water sources, which are used for many purposes, are a valuable alternate for algae production and drying. Geothermal water [24] and heat are potential sources of algal production. While the minerals contained in the nutrient medium show the characteristics of the nutrient medium, the possibility of drying by utilizing the heat energy can be a factor to decrease the cost. It is important to reduce the cost due to drying in order to produce biomass production from algae economically.

3. USING ALGAL ENERGY

The most important added value of using micro algae for biomass production is that they can effectively use CO_2 emitted from waste flue gas. During the production of 1 kg dry micro algae mass, 1.83 kg CO_2 is absorbed from the air. In the photoautotrophic system biomass production has been reported to theoretically yield an average of 46 L unrefined algal oil at 1 m ^{2} [1]. In 1998, the cost of algae oil obtained by CO_2 reduction was between $ 59- $ 186 per barrel [25] and the cost is still a problem nowadays. In 2019, oil is trading at 54 dollars per barrel (42 gallon). Given the International Energy Agency and the Kyoto Protocol, algal fuels are environmentally friendly, renewable and have a high energy density and potential to be an alternative additive for liquid fuels.

In 1991, the European Community (EC) applied a 90% tax reduction on biofuel use, including algae biomass. Today, 21 countries worldwide produce biomass fuel. Since microalgae have a high photosynthetic yield, biomass production has been suggested to be a sustainable candidate for fuel production compared to other energy plants [26], [27].

In algal energy production, less water is used than is used in the production of terrestrial energy plants.Furthermore, algae produced at the beginning of the unit area produce higher volumes of oil compared to terrestrial-based energy plants.In the year, 12 gallons of fuel are produced with soybean filed growing on 1 acre of land, which is determined as 25 for sunflower, 50 for jatropha plant and 155 gallon for palm oil. The amount of algae produced per year in 1 acre of land varies from 350 to 1250 gallons [1]. For this reason, algae; it can provide high biomass yield per acre.

For the direct use of algal biomass fuels, there are nowadays options such as transesterification, thermal cracking (pyrolysis) blending and microemulsions. Biocompatible oils can be used directly by blending them with diesel fuel in transesterification or diesel engines [28], [29]. Rapeseed and methyl ester, an important biomass source, are widely available and commercially available as alternative fuels since 1988 in many European countries [30]. While biomass oil costs $ 0.50 per liter, normal diesel is priced at $ 0.35 per liter [25].

It is an alternative liquid fuel obtained from oils and oils of plants such as micro algae, soybeans, sunflowers, canola or jatropha which can be used in diesel engines and can provide similar power to conventional diesel fuel which helps to reduce oil import dependency. There are two important stages in the production of Algal energy, such as the production phase and the final production of dry matter. The high cost of algal energy is the production of fat after dry matter production. Each phase is energy dependent. If geothermal heat and geothermal water are integrated into these phases, the costs of algal energy production may be reduced.

4. DISCUSSION

Biomass fuel obtained in plants is sustainable because it is a biodegradable, renewable and non-toxic fuel. It does not make a net carbon dioxide or sulfur additive to the atmosphere, but produces less gas pollutants than normal diesel. Moreover, the fact that the transportation sector is dependent on imported oil reveals the importance of biomass production in the name of national energy security.Cleaner and renewable energy solutions have come to the forefront with a growing awareness of the effects of climate change. Algae are a sustainable resource for reducing CO_2 emissions levels due to biomass to CO_2 conversion capacities [31]. Increasing use of modern biomass energy based on agriculture of energy plants is important for the country’s economy and environmental pollution.

Algal energy is one of the environmentally sensitive options among sustainable energy sources. However, production costs of fuel obtained from algae are higher than market energy prices. Alternative solutions can be used to overcome this problem. When selecting strategic alternatives, technological and commercial aspects are also considered. Integrated solutions with algae production from wastewater can be considered as the development of more efficient production technologies, the use of cheaper nutrient media with geothermal waters and the preferential cost of integrated production to benefit from geothermal heat in the drying phase. In addition, since high-value products or by-products are obtained from algae produced for oil, the profit of the production can be increased[1], [21], [30].

State support is very important to support the development of the energy of the algae. The major sources of emissions include energy, electricity, transportation, housing, agriculture and waste. Private or public enterprises with high wastewater and CO_2 emissions can be encouraged to encourage algae production.

Biological production of algal biomass using geothermal water and heat, domestic waste water and flue gas can positively affect the cost and it is suggested to expand the integrated production facilities in the enterprises operating in these areas.

Although algae have significant potential for serving as renewable transport fuels, the physiology and oil accumulation mechanisms of algae need to be understood for commercial scale production.

5. CONCLUSION

The academic community should increase its efforts to optimize algae biomass production as a renewable energy source and to ensure that it is open for commercialization. The development and implementation of next-generation biofuels is seen as a necessity to limit dependence on fossil fuels and to reduce the adverse effects of greenhouse gases on the climate.

REFERENCES

1. International Energy Agency. "World Energy Outlook 2009 Fact Sheet". 6 p.Website: http://www.worldenergyoutlook.org/docs/weo2009/fact_sheets_WE O_2009.pdf [Access date: 05.10.2010]
2. Meier RL. Biological cycles in the transformation of solar energy into useful fuels. Solar Energy Research 1955; 179-183.
3. Oswald WJ,Golueke CG. Biological transformation of solar energy. Adv. Appl. Microbiol 1960; 11: 223–242.
4. Benemann JR, Pursoff P, Oswald WJ. Engineering Design and Cost Analysis of a Large-Scale Microalgae Biomass System. Final Report to the US Energy Department, NTIS# H CP/ T 1978; 1605(UC-61), 91p.
5. Fishman D, Majumdar R, Morello J, Pate R, Yang J. National Algal Biofuels Technology Roadmap. U.S. Department of Energy, Office of Energy Efficiency and Renewable Energy, Biomass Program. National Algal Biofuels WorkshopDecember 9-10, 2008. College Park, Maryland.
6. Hu Q, Sommerfeld M, Jarvis E, Ghirardi M, Posewitz M, Seibert M, Darzins A.Microalgaltriacylglycerols as feedstocks for biofuel production: Perspectives and advances. Plant Journal 2008; 54(4): 621-639.

7. Majid M, Shafqat S, Inam H, Hashmi U,Kazi AG. Production of Algal Biomass. In book: Biomass and Bioenergy 2014; Chapter(13): 209-210. DOI: 10.1007/978-3-319-07641-6_13.
8. Kaneko T, Sato S, Kotani H, Tanaka A, Asamizu E, Nakamura Y, Miyajima N, Hirosawa M, Sugiura M, Sasamoto S, Kimura T, Hosouchi T, Matsuno A, Muraki A, Nakazaki N, Naruo K, Okumura S, Shimpo S, Takeuchi C, Wada T, Watanabe A, Yamada M, Yasuda M, Tabata S. Sequence analysis of the genome of the unicellular cyanobacteriumSynechocystis sp. strain PCC6803. II. Sequence determination of the entire genome and assignment of potential protein-coding regions. DNA Research 1996; 3(3): 109-136.
9. Kamrava D, Herwig C, Lackner M, Slouka C,Limbeck A. Increased carbohydrate production from carbon dioxide in randomly mutated cells of cyanobacterial strain Synechocystis sp. PCC 6714: Bioprocess understanding and evaluation of productivities. Bioresource Technology 2019; 273:277-278. DOI: 10.1016/j.biortech.2018.11.02
10. Nobles DR, BrownRM. Transgenic expression of gluconacetobacterxylinus strain ATCC 53582 cellulose synthase genes in the cyanobacterium*Synechococcusleopoliensis* strain UTCC 100. Cellulose 2008;15(5): 691-701.
11. Deng MD, Coleman JR. Ethanol synthesis by genetic engineering in cyanobacteria. Applied and Environmental Microbiology 1999; 65(2); 523-528.
12. Atsumi S, Higashide W, Liao JC. Direct photosynthetic recycling of carbon dioxide to isobutyraldehyde. Nature Biotechnology 2009; 27(12): 1177-1180.
13. Toepel J, Welsh E, Summerfield TC, Pakrasi HB, Sherman LA. Differential transcriptional analysis of the cyanobacterium*Cyanothece* sp. strain ATCC 51142 during light-dark and continuous-light growth. Journal of Bacteriology 2008; 190(11): 3904-3913.
14. Stal LJ, Krumbein WE. Temporal separation of nitrogen fixation and photosynthesis in the filamentous, non-heterocystouscyanobacteriumOscillatoria sp. Archives of Microbiology 1987; 149(1): 76–80.
15. Neupert J, Karcher D, Bock R. Generation of Chlamydomonas strains that efficiently express nuclear transgenes. The Plant Journal: For Cell and Molecular Biology2009; 57(6): 1140-1150.
16. Ferrante P, Catalanotti C, Bonente G, Giuliano G. An optimized, chemically regulated gene expression system for *Chlamydomonas*. PloS One.2008; 12: 3(9):e3200. doi: 10.1371/journal.pone.0003200.
17. Xu H, Miao X, Wu Q. High quality biodiesel production from a microalga chlorella protothecoides by heterotrophic growth in fermenters. Journal of Biotechnology 2006;126; 499-507.
18. Weldy CS, Huesemann M. Lipid production by dunaliellasalina in batch culture effects of nitrogen limitation and light intensity. U.S. Department of Energy Journal of Undergraduate Research 2007; 115-122 p.
19. Armbrust EV, Berges JA, Bowler C, Green BR, Martinez D, Putnam NH, Zhou S, Allen AE, Apt KE, Bechner M, Brzezinski MA, Chaal BK, Chiovitti A, Davis AK, Demarest MS, Detter JC, Glavina T, Goodstein D, Hadi MZ, Hellsten U, Hildebrand M, Jenkins BD, Jurka J, Kapitonov VV, Kröger N, Lau WW, Lane TW, Larimer FW, Lippmeier JC, Lucas S, Medina M, Montsant A, Obornik M, Parker MS, Palenik B, Pazour GJ, Richardson PM, Rynearson TA, Saito MA, Schwartz DC, Thamatrakoln K, Valentin K, Vardi A, Wilkerson FP, Rokhsar DS. The Genome of the diatom thalassiosirapseudonana: Ecology, evolution, and metabolism. Science2004; 306(5693): 79-86 p.

20. Bowler C, Allen AE, Badger JH, Grimwood J, Jabbari K, Kuo A, Maheswari U, Martens C, Maumus F, Otillar RP, Rayko E, Salamov A, Vandepoele K, Beszteri B, Gruber A, Heijde M, Katinka M, Mock T, Valentin K, Verret F, Berges JA, Brownlee C, Cadoret JP, Chiovitti A, Choi CJ, Coesel S, De Martino A, Detter JC, Durkin C, Falciatore A, Fournet J, Haruta M, Huysman MJ, Jenkins BD, Jiroutova K, Jorgensen RE, Joubert Y, Kaplan A, Kröger N, Kroth PG, La Roche J, Lindquist E, Lommer M, Martin-Jézéquel V, Lopez PJ, Lucas S, Mangogna M, McGinnis K, Medlin LK, Montsant A, Oudot-Le Secq MP, Napoli C, Obornik M, Parker MS, Petit JL, Porcel BM, Poulsen N, Robison M, Rychlewski L, Rynearson TA, Schmutz J, Shapiro H, Siaut M, Stanley M, Sussman MR, Taylor AR, Vardi A, von Dassow P, Vyverman W, Willis A, Wyrwicz LS, Rokhsar DS, Weissenbach J, Armbrust EV, Green BR, Van de Peer Y, Grigoriev IV. The Phaeodactylum genome reveals the evolutionary history of diatom genomes. Nature 2008; 456(7219): 239-244.

21. Zhang Ning. Mixotrophic Cultivation of Microalgae for Biomass Production Optimization Using Statistical Methods 2016, AllTheses 2425.

22. Sheehan J, Dunahay T, Benemann J, Roessler P. Look Back at the U.S. Department of Energy’s Aquatic Species Program: Biodiesel from Algae; Close-Out Report. United States: N. p., 1998. Web. doi:10.2172/15003040.

23. Gendy TS, El-Temtamy SA.Commercialization potential aspects of microalgae for biofuel production: An overview. Egyptian Journal of Petroleum2013;22 (1): 43-51. https://doi.org/10.1016/j.ejpe.2012.07.001

24. Güroy B. *Arthrospira* (*Spirulina*) *platensis* production with Şanlıurfa (Karaali) geothermal water. 1. International GAP Agriculturleand Livestock Congress. 2018. http://ziraat.harran.edu.tr/assets/uploads/other/files/ziraat/files/Dekanl%C4%B1k/KONGRELER/UGAP-2018-DRAFT-compressed.pdf. 783-787.

25. Weyer K, Bush M, Darzins DRA,Willson BD. Theoretical Maximum Algal Oil Production. BioEnergy Research 2010; 3 (2); 204-213.

26. Sawayama S, Inoue S, Dote Y, Yokoyama SY. CO2 fixation and oil production through microalga. Energy Conversion and Management 1995; 36: 729-731.

27. Miao X, Wu Q. High yield bio-oil production from fast pyrolysis by metabolic controlling of *Chlorella protothecoides*. Journal of Biotechnology 2004; 110(1): 85-93.

28. Peterson, A. A., F. Vogel, R. P. Lachance, M. Froling, M. J. Antal, and J. W. Tester. (2008). Thermochemical biofuel production in hydrothermal media: A review of sub- and supercritical water technologies. Energy & Environmental Science. 1, 32-65 p.

29. Zhang, B., Wu, Q.Y., Sheng, G.Y., and Fu, J.M. (1994). Influences of bacterial degradation on gases generated by pyrolysis of heterotrophically yellowing algae. Chinese Science Bulletin. 39(23), 2018-2022 p.

30. Iverson, S.J., Lang, S.L. & Cooper, M.H., 2001. Comparison of the Bligh and Dyer and Folch methods for total lipid determination in a broad range of marine tissue. Lipids, 36(11), 1283–1287 p.

31. Lackner M (2018). 3rd-Generation Biofuels: Bacteria and Algae as Sustainable Producers andConverters. Handbook of Climate Change Mitigation and Adaptation. Pages 1-32. DOI 10.1007/978-1-4614-6431-0_90-1.

Null Curve Evolution and Geometric Phase

Nevin GÜRBÜZ[1]

CHAPTER 6

[1] Prof. Dr., Eskişehir Osmangazi University, Faculty of Arts and Sciences, Department of Mathematics, Eskişehir, Turkey

Motion of space curves have many applications in modern physics such as thin vortex filament in a fluid and spin chains.

Hasimoto discovered a connection between the motion of space curves and isolated very thin vortex filament (Hasimoto, 1972). Later Lamb generalized fascinating result of Hasimoto (Lamb, 1977). Nakayama, Segur, Wadati studied integrability and the motion of curves (Nakayama et al., 1992). Lakshmanan, Myrzakulov and Danlybaeva studied motion of curves and surfaces and nonlinear evolution equations in (2+1) dimensions (Lakshmanan, 1998).

Chou and Qu studied the KdV equation and motion of plane curves (Chou & Qu, 2001). Gürses studied motion of curves on two dimensional surfaces and soliton equations (Gürses, 1998). Gürbüz investigated null and non-null curve evolution (Gürbüz, 2009, 2013-2019) .

Bonnor studied null curves in a Minkowski space-time (Bonnor, 1969). A connection between the local motion of a null curve and the celebrated KdV equation has been studied by Nersessian and Ramos (Nersessian & Ramos, 1998). Musso and Nicolodi showed that special motions are constructed whose induced evolution equations are the members of the KdV hierarchy (Musso & Nicolodi, 2009). Li studied motions of Cartan curves in n-dimensional Minkowski space (Li, 2013). Terrones, Giménez and Lucas investigated Hamiltonian structure for null curve evolution (Terrones et al., 2014). Grbovic and Nesovic presented Backlund transformation and vortex filament equation for null Cartan curve in Minkowski 3-space (Grbovic & Nesovic, 2016).

The angle of rotation of linearly polarized light is expressed with Berry phase. Berry introduced the quantum geometric phase (Berry, 1984). Aharonov and Anandan presented phase change during a cylic quantum evolution (Aharonov & Anandan, 1987).

Balakrishnan, Bishop, and Dandoloff showed time evolution of the space curve is associated with a geometric phase (Balakrishnan et al., 1990). Murugesh and Balakrishnan showed that there is exist two other formulation of curve evolution except of formulation of Lamb in Euclidean 3-space (Murugesh & Balakrishnan, 2001). Gürbüz denoted three classes of curve evolution and studied three geometric phases according to Frenet frame in Minkowski 3-space (Gürbüz, 2017). Later Gürbüz presented three classes of curve evolution associated three geometric phases according to Darboux and Bishop frame (Gürbüz, 2018-2019).

Let β (s) a unit speed curve in Minkowski 3-space R_1^3 (O' Neill, 1983), s being the arclength parameter . Let Y be a three dimensional vector field in in Minkowski 3- space. If $\langle Y,Y\rangle = 0$ and $Y \neq 0$, Y is called as null vector. A null curve β : [a, b] → R_1^3 has a causal structure if all its tangent vectors are null.

A null curve β, $\{t=\beta', n, w\}$ is called as Minkowski Cartan frame (Duggal & Jin , 2007): satisfying

$$\langle t,t\rangle = 0, \langle n,n\rangle = 0 , \langle t,w\rangle = 0,$$
$$\langle w,n\rangle = 0, \langle t,n\rangle = 1, \langle w,w\rangle = 1.$$

Cross product for null curves is given as

$$t \times n = w, \quad w \times t = t, \; n \times w = n.$$

Intrinsic derivatives of the Null Frenet type orthonormal triad are given as (Duggal & Jin , 2007):

$$\begin{aligned} t_s &= \kappa w, \\ n_s &= \tau w \\ w_s &= -\tau t - \kappa n. \end{aligned} \qquad (1)$$

Here κ and τ are the curvature and torsion functions of β, respectively.

In this work, a null curve evolution associated with the coupled modified Korteweg de Vries like (mKdV-like) equation will studied. Later geometric phase formula for null curve evolution associated with the coupled mKdV-like equation will presented.

MOVING NULL CURVES

Time evolution according to u time of Minkowski Cartan frame $\{t,n,w\}$ is given as following:

$$t_u = D\times t = -Bw + (\kappa_0 + \tilde{\tau}_0)t = u_0 t + gw \tag{2}$$
$$n_u = D\times n = Aw - (\kappa_0 + \tilde{\tau}_0)n = -u_0 n + fw \tag{3}$$
$$w_u = D\times w = -At + Bn = -ft - gn \quad . \tag{4}$$

Darboux vector for null curves is given by as following

$$D = (At + Bn + (\kappa_0 + \tau_0)w) \tag{5}$$

From compatibility conditions

$$\begin{aligned} t_{us} &= t_{su} \\ n_{us} &= n_{su} \\ w_{su} &= w_{us}, \end{aligned} \tag{6}$$

time evolution of curvature and torsion according to null Frenet frame,

$$\begin{aligned} \kappa_u &= g_s + \kappa u_0 \\ \tau_u &= f_s - \tau u_0 . \end{aligned} \tag{7}$$

and

$$u_{0s} = -f\kappa + g\tau \tag{8}$$

are obtained. Set new frame as $\{I, J, J^*\}$

$$I = w \tag{9}$$

$$J = \frac{t+in}{\sqrt{2}} \tag{10}$$

$$J^* = \frac{t-in}{\sqrt{2}} \tag{11}$$

and introduce transformation

$$\psi = \frac{\kappa + i\tau}{\sqrt{2}} . \tag{12}$$

Using equations (4) and (5), it can be written by

$$\begin{bmatrix} I_s \\ J_s \\ J_s^* \end{bmatrix} = \begin{bmatrix} 0 & i\psi & -i\psi \\ \psi & 0 & 0 \\ \psi^* & 0 & 0 \end{bmatrix} \begin{bmatrix} I \\ J \\ J^* \end{bmatrix} . \tag{13}$$

The derivatives of I and J with respect to u time can be written by

$$I_u = \eta J + \delta J^* + \varsigma I \tag{14}$$
$$J_u = \phi J + \varphi J^* + \xi I \quad . \tag{15}$$

Using equations (14) and (15),

$$\eta = i\xi \tag{16}$$
$$\delta = -i\xi^* \tag{17}$$
$$\varsigma = 0 \tag{18}$$

are obtained. From Equations (14), (15), (16), (17) and (18), the followings are obtained:

$$I_u = i\xi J - i\xi^* J^* \tag{19}$$
$$J^*_u = iRJ + \xi^* I \quad . \tag{20}$$

Using the compatibility conditions

$$I_{su} = I_{us} \tag{21}$$

$$J_{su} = J_{us} \tag{22}$$

$$J^*_{su} = J^*_{us}, \tag{23}$$

the followings are obtained:

$$\psi_u = iR\psi^* - \xi_s \tag{24}$$

$$\psi^*_u = iR\psi + \xi_s^* \tag{25}$$

$$R_s = -\xi^*\psi + \xi\psi^* \quad . \tag{26}$$

Consider

$$\xi = \frac{g+if}{\sqrt{2}} \quad . \tag{27}$$

Equation (26) satisfies equation (19). With aid of equations (2) and (3), the followings are obtained:

$$\begin{aligned} \frac{t_u + in_u}{\sqrt{2}} &= w\frac{(if+g)}{\sqrt{2}} + u_0\frac{(t-in)}{\sqrt{2}} \\ &= \xi I + u_0 J^*. \end{aligned} \tag{28}$$

Equations (8), (26) and (28) imply

$$R_s = -u_{0s} = f\kappa - g\tau \quad . \tag{29}$$

The anholonomy density $H(s,u)$ according to null Frenet frame is defined as following:

$$H(s,u) = -R_s = g\tau - f\kappa \tag{30}$$

The total phase Φ is given by

$$\begin{aligned} \Phi &= -\iint R_s dsdu \\ &= -\iint (f\kappa - g\tau)dsdu \\ &= \iint \langle w, w_s \times w_u \rangle dsdu \quad . \end{aligned} \tag{31}$$

APPLICATION

The coupled modified KdV-like equation according to three dimensional Minkowski null Frenet frame is given by

$$w_u = w \times (w \times w_{ss})_s \quad . \tag{32}$$

Using (1) and (32),

$$w_u = -\tau_{ss} t - \kappa_{ss} n \quad . \tag{33}$$

is obtained. From equations (4) and (32), it can be written by

$$f = \tau_{ss}, \quad g = \kappa_{ss} \tag{34}$$

$$\xi = \frac{\kappa_{ss} + i\tau_{ss}}{\sqrt{2}} = \psi_{ss} \tag{35}$$

$$R_s = (\tau_s\kappa - \kappa_s\tau)_s \quad . \tag{36}$$

With aid of equations (24), (34), (35) and (36), the coupled modified KdV-like equation

$$\psi_u + \psi_{sss} + 2i\psi\psi^*\psi^*_s - i\psi^*|\psi|_s^2 = 0$$

is obtained. From Equation (30), anholonomy density associated with the coupled modified KdV-like equation of null curve evolution is obtained as following

$$H(s,u) = \kappa_{ss}\tau - \tau_{ss}\kappa \,.$$

Acknowledgements. The author is supported by ESOGU BAP Project Number: 2017-19029

REFERENCES

1. A. Nersessian, E. Ramos, " Massive spinning particles and the geometry of null curves", *Physics Letters B* 445 (1998) 123-128.
2. Duggal, K.L., Jin, D.H., Null Curves and Hypersurfaces of Semi-Riemannian Manifolds. World Scientific, Singapore (2007).
3. E.Musso, L. Nicolodi ,"Hamiltonian flows on null curves", *Nonlinearity* 23 (2010) 2117–29 .
4. G. L. Lamb, "Solitons on moving space curves", *J. Math. Phys* 18 (1977) 1654-1661.
5. J. Del Amor Terrones, A. Gimenez, P. Lucas, " Hamiltonian structure for null curve evolution", *Nonlinearity* 27 (2014)) 2627–2641.
6. H. Hasimoto, "A soliton on a vortex filament", *J. Fluid Mech.* 51(1972) 477-485.
7. K. Nakayama, H. Segur, M. Wadati, "Integrability and the motion of curves", Phys. Rev. Lett. 69 (1992) 2603-2606.
8. K-S Chou, C. Qu , "The KdV equation and motion of plane curves", *J. Phys. Soc. Japan* 70 (2001) 1912–16.
9. M. Lakshmanan, R. Myrzakulov, S. Danlybaeva, " Motion of curves and surfaces and nonlinear evolution equations in (2+1) dimensions", J. Math. Phys. 39 (1998) 3765-3771.
10. M. Gürses, "Motion of curves on two dimensional surfaces and soliton equations", *Phys. Lett. A* 241(1998), 329-334.
11. M. Grbovic, E. Nesovic, "On Backlund transformation and vortex filament equation for null Cartan curve in Minkowski 3-space"., *Mathematical Physics, Analysis and Geometry* , 19 (2016) 1-15.
12. M.V. Berry, "Quantal phase factors accompanying adiabatic changes", *Proceedings of the Royal Society of London Series A, Mathematical and Physical Sciences*, 392 (1984) 45-57.
13. N. Gürbüz, "Inextensible flows of spacelike, timelike and null curves", *Int, J. Contemp. Math. Sciences* 4 (2009) 1599 – 1604.
14. N. Gürbüz, "Inextensible flows of non-null curves an pseudo-Eucldean hypersurface in pseudo-Euclidean space", *Life Science Journal* 10 (2013) 1084-1087.
15. N. Gürbüz, " The geometry of vortex filaments for MHD in Minkowski 3-space", *International Journal of Pure and Applied Mathematics* 91 (2014) 2019-2029.
16. N. Gürbüz, "Moving non-null curves according to Bishop frame in Minkowski 3-space", *International Journal of Geometric Methods in Modern Physics* 12 (2015) 1550052.
17. N. Gürbüz, E. Işık, "Intrinsic Geometry of the Nonlinear Heat Equation for Spacelike Curves with Timelike Normal According to Bishop 2-Type Frame in Minkowski 3-Space", *International Mathematical Forum* 11 (2016) 1109 – 1116.
18. N. Gürbüz, "Inextensible curve flows according to Bishop 2-type frame in Minkowski 3-space", *International Mathematical Forum* , 11 (2016) 1167-1174. *Mathematical Forum* 12, (2017) 879 – 889.
19. N.Gürbüz, "Anholonomy according to three formulations of non-null curve evolution", *Int. J. Geom. Methods Mod. Phys.*, 14 (2017)1750175.
20. N. Gürbüz, "Three class of non-lightlike curve evolution according to Darboux frame and geometric phase", *International Journal of Geometric Methods in Modern Physics* 15 (2018) 1850023 16 page.

21. N. Gürbüz, "Three anholonomy densities according to Bishop frame in Euclidean 3-space", *Journal of Mathematical Physics, Analysis, Geometry* 3 (2019).
22. O'Neill, B. Semi-Riemannian Geometry with Applications to Relativity (Academic, New York, 1983).
23. R. Balakrishnan, R. Bishop, R. Dandoloff, "Geometric Phase in the Classical Continuous Antiferromagnetic Heisenberg Spin Chain", *Phys Rev Lett.* 64 (1990) 2107-2110.
24. S.Murugesh, R.Balakrishnan, "New connections between moving curves and soliton equations". *Physics Letters A* 290 (2001) 81-87.
25. W. B. Bonnor, "Null curves in a Minkowski space-time", *Tensor.* **20** (1969). 229–242.
26. Y. Aharonov and J. Anandan, "Phase change during a cylic quantum evolution", *Physical Review Letters* 58 (1987) 1593-1596.
27. Y. Y. Li, "Motions of Cartan curves in n-dimensional Minkowski space", *Modern Physics Letters* A 28 (2013) 1350110.

Usage of Pleurotus Ostreatus Fungal Biomass as A Biosorbent for Removal of Cr(VI) İons

Aslı GÖÇENOĞLU SARIKAYA[1]

CHAPTER 7

[1] Bursa Uludağ University, Faculty of Arts and Sciences, Department of Chemistry, Bursa, Turkey

INTRODUCTION

During the industrial development one of the important environmental problem is toxic heavy metal contamination. Electroplating, metal finishing, automotive, tannery, textile and steel industries are main sources of the various concentrations of heavy metals such as copper, zinc, nickel, lead, chromium and cadmium (Kocaoba, & Arısoy, 2011). Some heavy metals are necessary for plants and animals at low concentration. However, heavy metals are not biodegradable, they can accumulate the living tissues and can affect the living organisms in higher doses.

There are several methods to remove the heavy metals from wastewater such as chemical treatment, membrane seperation, electro dialysis, ion-exchange, etc. (Bai, & Abraham, 2002; Ertugay, & Bayhan, 2010). Biosorption is one of the metal treatment from wastewater and based on the passive metal binding onto biological materials. Fungi, bacteria, yeast, algae are the most common biosorbents for removal of various pollutants (Ramanaiah, Ventaka Mohan, & Sarma, 2007).

In aqueous solution $HCrO_4^-$, H_2CrO_4, $Cr_4O_{13}^{2-}$, $Cr_3O_{10}^{2-}$, CrO_4^{2-} and CrO_7^{2-} are the most common forms of Cr(VI) and depends on pH. In the pH range 2-6, $HCrO_4^-$ and CrO_7^{2-} ions are in equilibrium, nearly pH 8, CrO_4^{2-} ions and at lower pH (pH<2), $Cr_3O_{10}^{2-}$ and $Cr_4O_{13}^{2-}$ ions are formed. Because of the carcinogenic and toxic effects the permitted concentration of Cr(VI) is 0.05 mg/L (Bai, & Abraham, 2001, Bai, Abraham, 2002, Barrera-Diaz, Lugo-Lugo, & Bilyeu, 2012).

The goal of this study was to investigate the usage of *Pleurotus ostreatus* biomass as a biosorbent to remove Cr(VI) from aqueous solutions. The effects of contact time, initial metal ion concentration, temperature and biosorbent dosage on the removal of Cr(VI) were evaluated.

MATERIALS AND METHODS

P. ostreatus which was obtained from Müpa Tarım ve Gıda Sanayi A.Ş., was washed with deionized water three times, then dried in an oven at 323 K. The dried *P. ostreatus* biomass were cut into small pieces and homogenized in a blender into smaller fragments of 50-100 μm diameter. The dried biomass was preserved in glass jar to be used biosorption tests.

FTIR spectrophotometer was used to obtain the FTIR spectrum of *P. ostreatus* biomass (Perkin Elmer Spectrum BX FTIR System). FTIR spectra were plotted of biosorbent before and after Cr(VI) biosorption to study the functional groups and binding sites. Scanning electron microscopy (SEM) was used to examine the surface morphology of the biosorbent system (ZEISS EVO 40).

Stock solution of Cr(VI) (1000 mg/L) was prepared by dissolving unhydrated potassium dichromate in distillate water. The stock solution was diluted with distilled water in the range 10-100 mg/L for biosorption studies. 0.025 g of *P. ostreatus* biomass was used to perform batch biosorption experiments with 25 mL of known Cr(VI) ion solutions in 50 mL Erlenmeyer flasks. The pH was adjusted to pH 2.0 using 0.1 N HCl and 0.1 N NaOH before addition the fungal biomass to the Cr(VI) solution. The effect of temperature was studied in the range 4-45 ºC. The flasks were shaken on a magnetic shaker at 200 rpm. Biomass was removed from solution by centrifugation at 5000 rpm for 10 min before analysing the remaining Cr(VI) solution and Cr(VI) concentration of the supernatant was determined by using an UV-vis spectrophotometer (Perkin Elmer Lambda 35 UV/Vis Spektrometer). 1,5-diphenylcarbazide in an acid medium was used to measure the concentrations of Cr(VI) in the solution at 540 nm (Kara, A., Osman, B., Göçenoğlu, A., & Beşirli, N., 2014).

The amount of percentage removal (% R) of Cr(VI) was calculated using Eq. 1:

$$\% \, Removal = \frac{(C_0 - C_e)}{C_0} \times 100 \qquad (1)$$

RESULTS AND DISCUSION

The FTIR spectroscopy was used to determine the functional groups which are responsible for the biosorption of Cr(VI). The FTIR spectra of before and after biosorption from range of 600-4000 cm^{-1} is given in Fig. 1. Identified functional groups are listed in Table 1.

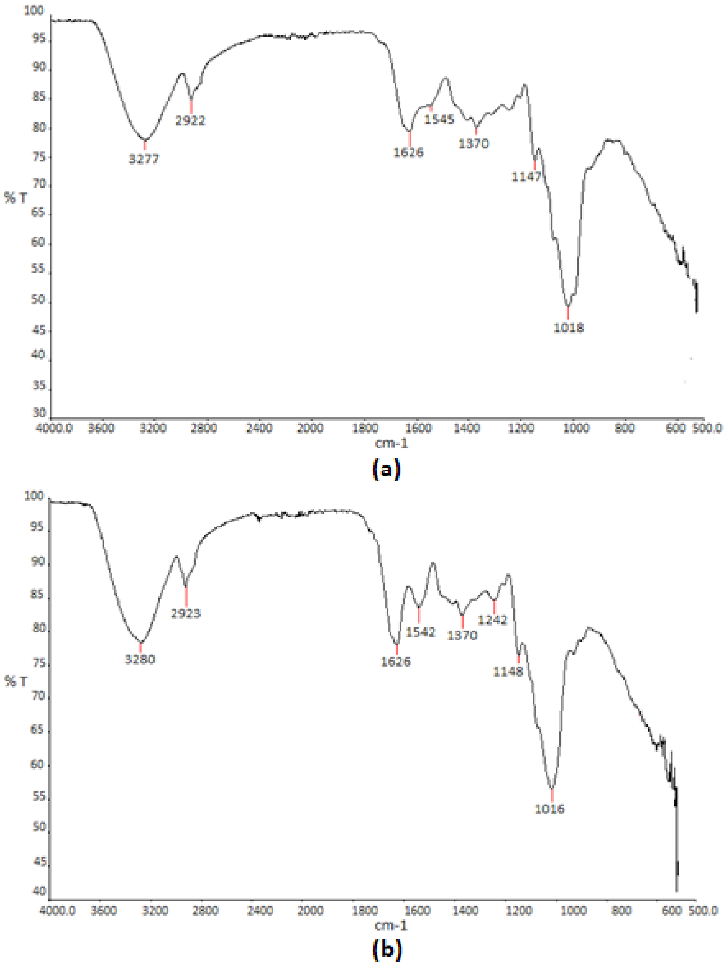

Figure 1. FTIR spectra of *P. ostreatus* (a) before and (b) after biosorption of Cr(VI)

Wavenumber (cm^{-1})			
Before biosorption	**After biosorption**	**Identified groups**	**Reference(s)**
3277	3280	-OH groups and -NH groups	Bayramoğlu, G., & Arıca, M. Y., 2008
2922	2923	C-H stretching, -CH, $-CH_2$, $-CH_3$	Bueno, B. Y. M., Torem, M. L., Molina, F., & de mesquita, L. M. S., 2008; Akar, T., Kaynak, Z., Ulusoy, S., Yuvacı, D., Ozsari, G., & Akar, S.T., 2009
1626	1626	Carboxylate functional groups, carboxyl groups	Chen, G., Zeng, G., Tang, L., Du, C., Jiang, X., Huang, G., Liu, H., & Shen, G., 2008
1546	1542	N-H deformation	Bhanoori, M., & Venkateswerlu, G., 2000
1370	1370	Stretching of -COO	Pavia, D. L., Lampman, G. M., & Kriz, G. S., 1996
1147	1148	-C-O, carboxylic acid	Fereidouni, M., Daneshi, A., & Younesi, H., 2009
1018	1016	-C-O- or -C-N- groups	Bueno, B. Y. M., Torem, M. L., Molina, F., & de mesquita, L. M. S., 2008; Akar, T., Kaynak, Z., Ulusoy, S., Yuvacı, D., Ozsari, G., & Akar, S.T., 2009

Table 1. Functional groups of *P. ostreatus* biomass before and after biosorption of Cr(VI)

Scanning electron microscopy (SEM) images were taken before and after biosorption of Cr(VI) to determine the surface texture and morphology of the biosorbent. The results show that the surface area is large and has some heterogeneity so the Cr(VI) ions can easly interact with acitive sites. After Cr(VI) biosorption the surface of the fungal biosorbent is flattened (Fig. 2).

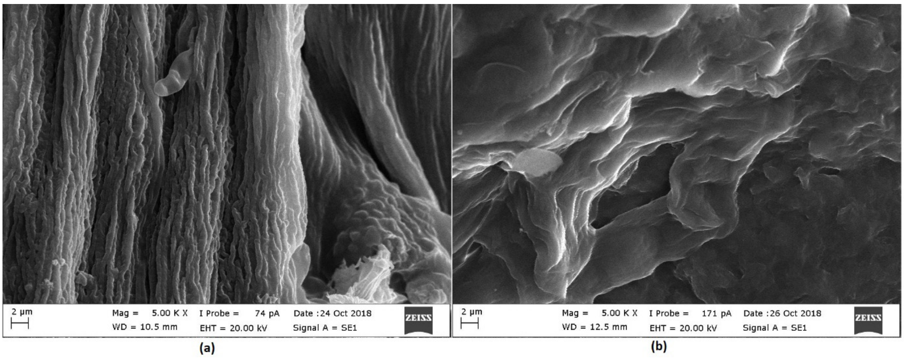

Figure 2. SEM images of *P. ostreatus* **(a)** before and **(b)** after biosorption of Cr(VI)

To determine the effect of temperature the experiments were performed the range 4-45 ºC. Due to biosorption is an energy-independent process, it could be affected by temperature (Javaid, A., Bajwa, R., Shafique, U., & Anwar, J., 2011). As seen in Fig. 3, when temperature was increased from 4 ºC to 45 ºC, % removal was also increased from %

16.24 to % 30.07. The adsorbed amounts of Cr(VI) ions increased with an increase in both temperature and contact time. Biosorption process was efficient during the first 90 minutes and slow biosorption was continued till 180 minutes.

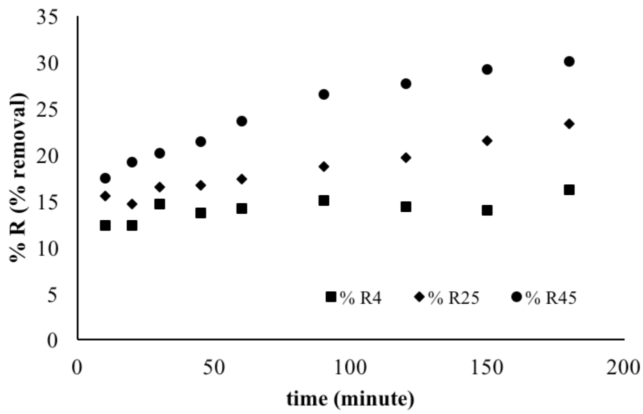

Figure 3. Effect of temperature onto % removal for biosorption of Cr(VI) onto *P. ostreatus*

The biosorption of Cr(VI) onto fungal biomass was carried out at different initial ion concentrations the range 10 mg/L to 1000 mg/L at pH 2.0 during 180 minutes. The results showed that removal efficiency decreased when the metal ion concentration increased (Fig. 4). The reason of the decrease was due to the saturation of the sorption sites of the fungal biomass. Thus, the higher removal yields were observed at lower initial concentrations (Ertugay, N., Bayhan, Y. K., 2010).

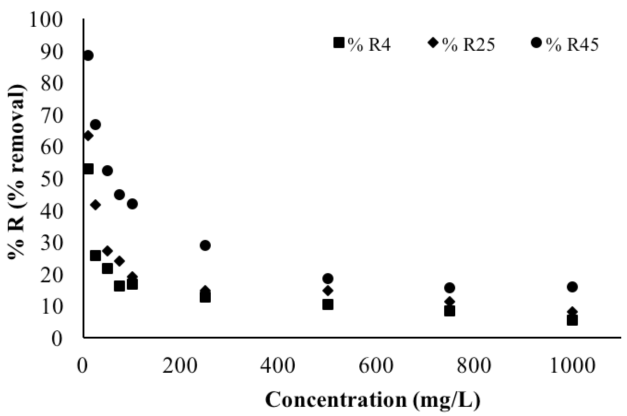

Figure 4. Effect of initial concentration onto % removal for biosorption of Cr(VI) onto *P. ostreatus*

To determined the optimum amount of *P. ostreatus* biomass as a biosorbent, different amount of biomass were investigated ranging from 0.025 g to 0.2 g. % removal of Cr(VI) from aqueous solutions was increased from 20.78 % to 92.42 % with increasing the amount of biomass from 0.025 g to 0.2 g (Fig. 5).

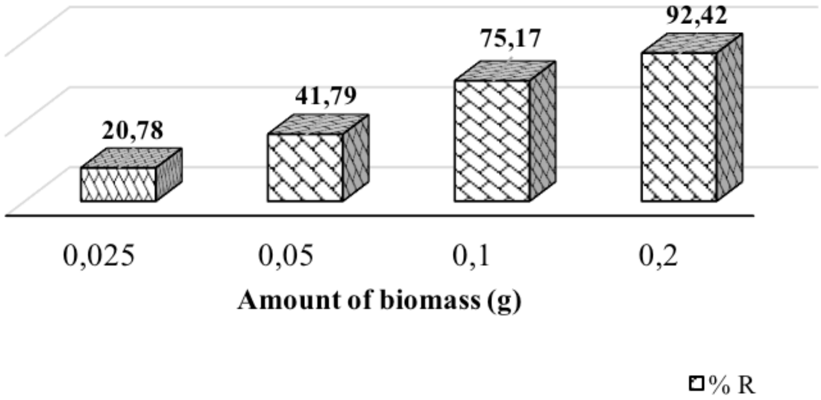

Figure 5. Effect of biosorbent dosage

Biosorption-desorption studies are important to determine the usability of the biosorbent in a more economic manner. 0.1 M HNO_3 and 0.1 M HCl were used as a desorption agent to remove the Cr(VI) from the biosorbent. To investigate the reusability of biosorbent, 5 biosorption-desorption process cycle was studied and the biosorption capacity of the biosorbent was decreased only 9 % during the cycle. The desorption efficiency of a HNO_3 (0.1 M) and HCl (0.1 M) was calculated as 96.15 % and 56.25 %, respectively.

CONCLUSION

The aim of this study was to investigate the usability of biomass of P. ostreatus as a biosorbent for removal of Cr(VI) ions from an aqueous solutions. The influence of various process parameters such as temperature, contact time, biosorbent dosage and desorption was studied. All experiments were achieved at pH 2.0. Increasing the temperature from 4 ºC to 45 ºC, the % removal of Cr(VI) ions were also increased from % 16.24 to % 30.07. Also the biosorbent dosage was investigated. % removal of Cr(VI) ions was increased form 20.78 % to 92.42 % with increasing the amount of biosorbent dosage from 0.025 g to 0.2 g.

REFERENCES

1. Kocaoba, S., & Arısoy, M. (2011), ''The use of a white rot fungi (Pleurotus ostreatus) immobilized on Amberlite XAD-4 as a new biosorbent in trace metal determination'', Bioresource Technology, Vol. 102, pp. 8035-8039.
2. Bai, R. S., Abraham, T. E. (2002), ''Studies on enhancement of Cr(VI) biosorption by chemically modified biomass of Rhizopus nigricans'', Water Research, Vol. 36, pp. 1224-1236.
3. Ertugay, N., Bayhan, Y. K. (2010), ''The removal of copper (II) ion by using mushroom biomass (Agaricus bisporus) and kinetic modelling'', Desalination, Vol. 255, pp. 137-142.

4. Ramanaiah, S. V., Ventaka Mohan, S., & Sarma, P. N. (2007), ''Adsorptive removal of fluoride from aqueous phase using waste fungus (Pleurotus ostreatus 1804) biosorbent: Kinetics evaluation'', Ecological Engineering, Vol. 31, pp. 47-56.
5. Bai, R. S., & Abraham, T. E. (2001), ''Biosorption of Cr(VI) from aqueous solution by Rhizopus nigricans'', Bioresource Technology, Vol. 79, pp. 73-81.
6. Barrera-Diaz, C. E., Lugo-Lugo, V., & Bilyeu, B. (2012), ''A review of chemical, electrochemical and biological methods for aqueous Cr(VI) reduction'', Journal of Hazardous Materials, Vol. 223-224, pp. 1-12.
7. Javaid, A., Bajwa, R., Shafique, U., & Anwar, J. (2011), ''Removal of heavy metals by adsorption on *Pleurotus ostreatus*'', Biomass and Bioenergy, Vol. 35, pp. 1675-1682.
8. Kara, A., Osman, B., Göçenoğlu, A., & Beşirli, N. (2014), ''Kinetic, isothermal, and thermodynamic studies of Cr(VI) adsorption on L-Tryptophan-containing microspheres'', Environmental Engineering Science, Vol. 31(6), pp. 261-271.
9. Bayramoğlu, G., & Arıca, M. Y. (2008), ''Removal of heavy mercury (II), cadmium (II) and zinc (II) metal ions by live and heat inactivated *Lentinus edodes* pellets'', Chemical Engineering Journal, Vol. 143 (1-3), pp. 133-140.
10. Bueno, B. Y. M., Torem, M. L., Molina, F., & de mesquita, L. M. S. (2008), ''Biosorption of lead (II), chromium (III) and copper (II) by *R. opacus*: Equilibrium and kinetic studies'', Minerals Engineering, Vol. 21, pp. 65-75.
11. Akar, T., Kaynak, Z., Ulusoy, S., Yuvacı, D., Ozsari, G., & Akar, S.T. (2009), ''Enhanced biosorption of nickel (II) ions by silica-gel-immobilized waste biomass:biosorption characteristics in batch and dynamic flow mode'', Journal of Hazardeous Materials, Vol. 163(2-3), pp. 1134-1141.
12. Chen, G., Zeng, G., Tang, L., Du, C., Jiang, X., Huang, G., Liu, H., & Shen, G. (2008), ''Cadmium removal from simulated wastewater to biomass byproduct of *Lentinus edodes*'', Bioresource Technology, Vol. 99(15), pp. 7034-7040.
13. Bhanoori, M., & Venkateswerlu, G. (2000), ''In vivo chitin-cadmium complexation in cell wall of *Neurospora crassa*'', Biochimica et Biophysica Acta, Vol. 1523(1), pp. 21-28.
14. Pavia, D. L., Lampman, G. M., & Kriz, G. S. (1996), Introduction to spectroscopy: a guide for students of organic chemistry, Saunders, New York.
15. Fereidouni, M., Daneshi, A., & Younesi, H. (2009), ''Biosorption equilibria of binary Cd (II) and Ni (II) systems onto *Saccharomyces cerevisiae* and *Ralstonia eutropha* cells: Application of response surface methodology'', Journal of Hazardeous Materials, Vol. 168, pp. 1437–1448.

A Survey on The Historical Perspective of Soft Set Theory

Güzide ŞENEL[1]

CHAPTER 8

[1] Dr. Öğr. Üyesi, Amasya University, Amasya, Turkey

1. INTRODUCTION

Vague concepts have been used in different areas in recent years such as medical applications, pharmacology, economics and engineering since the classical mathematics methods are inadequate to solve many complex problems in these areas with classical mathematical tools. To overcome these difficulties, the concept of fuzzy sets is introduced by Zadeh. But, there are some boundaries of usage of the fuzzy sets. We can give an easy example to see one of the limitations of the formulation of vagueness in the standard theory of fuzzy sets: consider a specific vague concept; the concept of redness. Clearly, the set of red objects is can not defined exactly. That is, we may not be able to say definitely, for pink or orange objects could cause difficulties. Ordinary fuzzy sets seek to capture this vagueness by attaching a number between zero and one to each object (K. Basu et al., 1992). In 1999, Molodtsov showed that the soft set theory can be applied to several areas successfully; for example, the smoothness of functions, game theory, Riemann-integration, Perron-integration, etc. He also showed that soft set theory is free from the parametrization inadequacy syndrome of other theories developed for vagueness (Yuksel et al., 2013). This work gives the definition of soft sets which emphasis on a series of applications especially in decision making problems. Also this work presents comprehensive study, development and survey of its existing literature.

2. CONCEPT OF SOFT SET

A pair (F, E) is called a soft set (over U) if and only if F is a mapping of E into the set of all subsets of the set U. In other words, the soft set is a parameterized family of subsets of the set U. Every set $F(e)$, $e \in E$, from this family may be considered as the set of e -approximate elements of the soft set (Molodtsov, 1999). Let us consider the following example is given in [Pal & Mondal, 2011].

Example 2.1: A soft set (F, E) describes the attractiveness of the bikes which Mr. X is going to buy. U is the set of bikes under consideration. E is the set of parameters. Each parameter is a word or a sentence. E = (e_1= stylish; e_2 =heavy duty; e_3= light; e_4 =steel body; e_5 = cheap; e_6 = good mileage; e_7 =easily Started; e_8 = long driven; e_9=costly; e_{10} = fibre body).

In this case, to define a soft set means to point out stylish bikes, heavy duty bikes, and so on (Pal & Mondal, 2011).

Soft set is a parametrized general mathematical tool which deal with a collection of approximate descriptions of objects. Each approximate description has two parts; a predicate and an approximate value set. In classical mathematics, a mathematical model of an object is constructed and define the notion of exact solution of this model. Usually the mathematical model is too complicated and the exact solution is not easily obtained. So, the notion of approximate solution is introduced and the solution is calculated. In the soft set theory, we have the opposite approach to this problem. The initial description of the object has an approximate nature, and we do not need to introduce the notion of exact solution. The absence of any restrictions on the approximate description in soft set theory makes this theory very convenient and easily applicable in practice. Any parameterization we prefer can be used with the help of words and sentences, real numbers, functions, mappings and so on (Ibrahim&Yusuf, 2012).

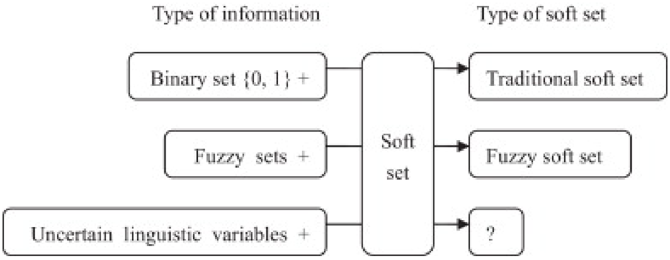

This table explains the transformation of the information to the soft sets.

Suppose a binary operation denoted by *, is defined for all subsets of the set U. Let (F, A) and (G, B) be two soft sets over U. Then the operation * for the soft sets is defined in the following way:

$(F, A) * (G, B) = (H, A \times B)$, where $H(\alpha, \beta) = F(\alpha) * G(\beta)$, $\alpha \in A$, $\beta \in B$ and $A \times B$ is the Cartesian product of the sets A and B (Saraf, 2013).

$$
\begin{array}{lcccccc}
\text{central soft sets:} & (f_A, A) & \sqcup & (g_B, B) & = & (h_C, C) \\
 & \upharpoonleft\downharpoonright & & \upharpoonleft\downharpoonright & & \upharpoonleft\downharpoonright \\
\text{soft sets:} & F_A & \tilde{\cup} & G_B & = & H_C
\end{array}
$$

3. APPLICATIONS OF SOFT SETS

Applications of soft set theory in other disciplines and real life problems are now on fast track development in the decision making area. In 1999 Molodtsov showed that soft set theory has potential applications in many different fields which include the smoothness of functions, game theory, operations research, Riemann integration, Perron integration, probability theory, and measurement theory. Applications of soft set to stability and regularization, game theory and operational research are discussed in Molodtsov in details. Applications of soft set theory in other disciplines and real life problems are now on development in the decision making area that is started with Maji et al., in year 2002. Maji et al. gave first practical application of soft sets in decision making problems. It is based on the knowledge of reduction in rough set theory. Nagarajan & Meenambigai (2011) initiated the study of application of soft set to lattices, soft lattices, soft distributive lattices, soft modular lattices, soft lattice ideals, soft lattice homomorphism etc and several related properties are investigated. Fuzzy parameterized fuzzy soft set theory and its applications were discussed in Cagman et al., (2010). Soft set theory based classification algorithm was proposed in Mushrif et al. (2006) which can be applied to texture classification, proposed computational complexity when compared with Bayes classification technique. In Feng et al., (2008) soft set theory is used to initiate the study of semi-rings, soft semi-rings, soft sub semi-rings, soft ideals, idealistic soft semi-rings and soft semi-ring homomorphism are introduced. Xiao et al., (2012) presented a new method of evaluation based on D–S generalized fuzzy soft sets and apply it into a medical diagnosis problem. With these notions and operations mentioned above an application of soft set in decision-making problems is revealed deeply.

4. HISTORICAL PERSPECTIVE OF SOFT SET THEORY

The derivation of soft set theory could be scent out the work of Pawlak in 1993 titled "Hard and Soft Set "in Proceeding of the International EWorkshop on rough sets and knowledge discovery at Banff. His notion of soft sets is a unified view of classical, rough and fuzzy sets. This motivated Molodtsov's work in 1999 titled "Soft set theory: first result". In this work the basic notions of the theory of soft sets and some of its possible applications were presented. For positive motivation, the work discusses some problems of the future with regards to the theory (Ibrahim&Yusuf, 2012). In 1996 Lin have present a set theory for soft computing and presenting unified view of fuzzy sets via neighborhoods. This paper proposed fuzzy sets should be abstractly defined by such structures and are termed soft sets (sofsets) (Saraf, 2013). P. K. Majiet al., [24] in 2002, defined some basic terms of the theory such as equality of two soft sets, subset and super set of a soft set, complement of a soft set, null soft set, and absolute soft set with examples. Binary operations like AND, OR, union and intersection were also defined. De Morgan's laws and a number of results are verified in soft set theory context. Pei & Miao (2005) have discussed the relationship between soft sets and information systems. It is showed that soft sets are a class of special information systems. Roy & Maji (2007) presented a novel method of object recognition from an imprecise multi observer data in decision making problem. In the same year, Aktas & Cagman (2007) have introduces the basic properties of soft sets and compare soft sets to the related concepts of fuzzy sets and rough sets. Feng et al., (2008) extended the study of soft set to soft semirings. Jun (2008) have presented a new algebra method is Soft BCK/BCI-algebras and in Jun et al., (2008) apply the notion of soft sets by Molodtsov to commutative ideals of BCK-algebras, commutative soft ideals and commutative idealistic soft BCK-algebras are introduced, and their basic properties are investigated. Herawan et al., (2009) proposed an approach for visualizing soft maximal association rules which contains four main steps, including discovering, visualizing maximal supported sets, capturing and finally visualizing the maximal rules under soft set theory (Saraf, 2013). Jun & Park (2009) introduced the concept of soft Hilbert algebra, soft Hilbert abysmal algebra and soft Hilbert deductive algebra and investigated their properties. In 2010, the concept of soft set relations as a sub soft set of the cartesian product of the soft sets are introduced and many related concepts such as equivalent soft set relation, partition,composition and function are discussed in the work of K. V. Babitha and J.J Sunil. An important novel is published by Cagman & Enginoglu (2010). In this work soft matrices and their operations which are more functional to make theoretical studies in the soft set theory are defined. The aim of Feng et al., (2010) is providing a framework to combine fuzzy sets, rough sets, and soft sets all together, which gives rise to several interesting new concepts such as rough soft sets, soft rough sets, and soft–rough fuzzy sets (Saraf, 2013). In 2011, N. Cagman *et al*. also extended soft set to fuzzy parameterized (fp) soft sets and proposed a decision making method based on FP-soft set theory. With examples, they showed that the method can be successfully applied to the problems that contain uncertainties (Ibrahim&Yusuf, 2012). After the introduction of soft groups by Aktas and Cagman in 2007, many researchers have studied the properties of soft groups and fuzzy soft groups. But in the discussion of soft homomorphic image and preimage of these groups under soft mappings introduced by A. Kharal and B. Ahmad, they have considered a special type of soft mapping calles "mappings on soft classes". In a new manuscript constant soft mapping is redefined, generalized soft elements, constant and pseudo constant soft elements are defined and the behaviour of functional image and preimage of soft sets under soft mappings are discussed by Sk. Nazmul in 2019.

5. CONCLUSION

In this paper, I presented the historical development of the fundamentals of soft set theory in detail. The main acquisition of this paper is to show that observed some properties on classical sets do not hold for soft set operations. For the future works it can be presented the invariant notions for both disciplines. This work is a literature review research and presents the developments year by year.

6. DECLARATIONS

Acknowledgements: The author gratefully acknowledge the comments of the editorial board which led to the improvement of this paper.

Funding: There is no source of funding for the research.

Availability of data and materials: The datasets used or analyzed during the current study are available from the corresponding author on reasonable request.

REFERENCES

1. A. Kharal and B. Ahmad. Mappings on soft classes, Inf. Sci., INS-D-08-1231 by ESS, pp. 1-11, 2010.
2. A. M. Ibrahim and A. O.Yusuf. Development of Soft Set Theory, American International Journal of Contemporary Research 2(9), 205-210, 2012.
3. D. A. Molodtsov. Soft set theory- First results, Computers Math. Appl. 37 (4/5),19-31, 1999.
4. D. Chen, E. C. C. Tsang, D. S. Yeung and X. Wang. The parameterization reduction of soft sets and its application, Comp. Math. with appl. 45, 757-763(2005).
5. D. K. Sut. An Application of Fuzzy Soft Relation in Decision Making Problems, Int. Journal of Mathematics Trends and Technology, Vol.3 Issue 2 2012.
6. E.K.R. Nagarajan & G. Meenambigai (2011), "An Application of Soft Sets to Lattices", Kragujevac Journal of Mathematics, Vol. 35, No. 1, Pp. 75–87.
7. F.Feng, Y. B. Jun, and X. Zhao. Soft semirings, Computers Math. Applic. 56, 2621-2628 2008.
8. H. Prade and D. Dubois. Fuzzy Sets and Systems: Theory and Applications, Academic Press, London, 1980.
9. H. J. Zimmerman. Fuzzy Set Theory and Its Applications, Kluwer Academic, Boston, MA, 1996.
10. H.Aktas and N. Cagman. Soft sets and Soft groups, Information Sciences 177, 2726-2735 2007.
11. H. Yang and Z. Guo. Kernels and closures of soft set relations, and soft set relation mappings, Comp. Math. Appl. 61, 651-662 2011.
12. I. A. Onyeozili and Gwary T. M. A Study Of The Fundamentals Of Soft Set Theory, Int. Journal of Sci .& Tech. Research 3(4), 132-143, 2014.
13. J.Ghosh, B. Dinda and T. K. Samanta. Fuzzy Soft Rings and Fuzzy Soft Ideals, Int. J. Pure Appl. SCI. Technol., 2(2), pp. 66-74, 2011.
14. J. Zhou, Y. Li and Y. Yin. Intuitionistic fuzzy soft set semigroups, MathematicaAeterna, vol. 1, No. 03, 173-183, 2011.
15. K. Atanassov. Operators over interval valued intuitionistic fuzzy sets, fuzzy sets and systems 64, 159-174, 1994.
16. K.V. Babitha and J.J. Sunil. Soft sets relations and functions, Computers Math. Applic. 60, 1840-1849 2010.
17. K. Basu, et.al. Soft sets: An ordinal formulation of vagueness with some applications to the theory of choice, Fuzzy Sets and Systems 45, 45-58, 1992.
18. K. Gong, Z. Xiao and X.Zhang.Thebijective soft set with its operations, Computers and Math. Appl. 60,2270-2278 2010.
19. K. Qin and Z. Hon.On soft equality, Computers Math. Appl. 234, 1347-1355 2010.

20. M. Irfan Ali, F.Feng, X.Liu, W. K. Min and M. Shabir. On some new operations in soft set theory, Comp. and Math. With appl. 57, 1547-1553 2009.
21. M. A.Ozturk and E.Inan. Soft - rings and idealistic soft – rings, annals of fuzzy Mathematics and informatics volume 1, no. 1, pp. 71-80 2011.
22. M. M. Mushrif, S. Sengupta and A. K. Ray.Texture Classification Using A Novel, Soft Set Theory Based Classification Algorithm, LNCS 3851,pp. 246-254 2006.
23. N.Cagman, F.Citak, and S.Enginog;lu. FP-soft set theory and its applications, annals of fuzzy Math. Inform. Vol. 2, No. 2, pp. 219 – 226 2011.
24. N.Cagman, F. Citakand S.Enginoglu. Fuzzy parameterized fuzzy soft set theory and its applications, an official journal of Turkish fuzzy systems association. Vol.1, no.1, pp. 21-35 2010.
25. P.K. Maji, A.R. Roy and R. Biswas. An application of soft sets in a decision making problem, Computers and Mathematics with applications 44 (8/9), 1077-1083, 2002.
26. Sk. Nazmul. Some properties of soft groups and fuzzy soft groups under soft mappings, Palestine Journal of Mathematics, 8(1), 189–199, 2019.
27. S. V. Manemaran. On fuzzy soft groups, int. Journal of Comp. Applications (0975-8887) vol. 15, No. 7 2011.
28. S.Alkhazaleh, A. Salleh and N. Hassan. Soft multisets theory, applied Mathematical sciences, vol. 5, no.72, 3561-3573, 2011.
29. S. Saraf. Survey or Review on Soft Set Theory and Development, The SIJ Transactions on Computer Science Engineering & its Applications (CSEA), 1 (3), 59-66, 2013.
30. T.Herawan, R.Ghazali and M. M. Deris. Soft set theoretic approach for dimensionality reduction, Information journal of Database Theory and Application Vol. 3, No. 2, 2010.
31. W. Xu. Vague soft sets and their properties, Computers and Mathematics with applications 59, 787-794 2010.
32. X.Ge and S. Yan. Investigations on some operations of soft sets, world academy of science, eng. And tech. 75,1113-1116 2011.
33. Y. B.Jun,H. S. Kim and C. H. Park.Positive implicative ideals of BCK-algebras based on a soft set theory, Bull. Malays. Math. Sci. Soc. (2) 34(2), 345-354 2011.
34. Y. B. Jun, K. J. Lee and C. H. Park. Soft Set Theory Applied To Commutative Ideals In BCK-Algebras, J. Appl.Math. And Informatics Vol. 26, No. 3-4,pp. 707-720 2008.
35. Z. Pawlak, HardAnd Soft Sets, Proceeding Of The International EWorkshop On Rough Sets And Knowledge Discovery, Banff, 1993.
36. Z. Xiao et al., “The Trapezoidal Fuzzy Soft Set and its Application in MCDM”, Applied Mathematical Modelling, DOI doi:10.1016/j.apm.2012.01.036, 2012.

On a New Approximation for Weighted Integral-Type Inequalities in VELS

Lütfi AKIN[1]

CHAPTER
9

[1] Mardin Artuklu University, Department of Business Administration, Mardin, Turkey

1. INTRODUCTION

The variable exponent Lebesgue spaces are of interest for their applications to modeling problems in physics and to the study of variational integrals and partial differential equations with non-standard growth conditions. We refer to [1-7]. This studies also has been stimulated by problems of elasticity, fluid dynamics, calculus of variations and differential equations with non-standard growth conditions. More results for Hardy-type inequalities in variable exponent Lebesgue spaces can be found in F. I. Mamedov et al., [9]; L. Akın [10, 11]; A. Kufner and L. E. Persson [14]; V. Kokilashvili and S. Samko [15] and references therein.

The classical weighted Hardy inequalities says that

$$\left\| x^{k}\int_{x}^{\infty} t^{-k}w(t)\epsilon_t \frac{dt}{t}\right\|_{L_w^q((0,\infty),\frac{dx}{x})} + \left\| x^{-k}\int_{0}^{x} t^{k}w(t)\epsilon_t \frac{dt}{t}\right\|_{L_w^q((0,\infty),\frac{dx}{x})} \lesssim \|\epsilon_t\|_{L_w^q((0,\infty),\frac{dx}{x})}$$

For any $k > 0$ and $1 \le q < \infty$. Let w be a weight function on $(0,\infty)$. The weight function w is a measurable function and finite on $(0,\infty)$. Here under the same assumptions we prove that $\|\epsilon_t\|_{L_w^q((0,\infty),\frac{dx}{x})}$ can be replaced by $\left(\int_0^1 \epsilon_t^{q(0)} w(t)\frac{dt}{t}\right)^{1/q(0)} + \left(\int_1^\infty \epsilon_t^{q_\infty} w(t)\frac{dt}{t}\right)^{1/q_\infty}$.

2. AUXILLARY STATEMENTS AND PRELIMINARIES

We well-known that R is reals. Let $N_0 = N \cup \{0\}$ and Z is the set of all integer numbers. The expression $f \lesssim h$ means that $f \le ch$ for some independent constant c with non-negative functions f and h, and $f \approx h$ means $f \lesssim h \lesssim f$. If $F \subset R$ is measurable set, then χ_F is the characteristic function of the set F. We denote c is generic positive constant. We denote a weight function by w. The weight function w is a positive and measurable function on $(0,\infty)$. We denote the set of such functions by Q(R). We use the following standard notations

$$q^- = \operatorname*{ess\,inf}_{y\in R} q(y)\,,\ q^+ = \operatorname*{ess\,sup}_{y\in R}\ q(y)$$

The variable exponent modular is defined by

$$I_{q(.)}(f) = \int_R I_{q(y)}(|f(y)|)\,dy,$$

where $I_q(x) = x^q$. For some $\lambda > 0$, we define the Luxemburg norm on this space by the formula;

$$\|f\|_{q(.)} = \inf\left\{\lambda > 0: I_{q(.)}\left(\frac{f}{\lambda}\right) \leq 1\right\}.$$

A useful property is that $\|f\|_{q(.)} \leq 1$ if and only if $I_{q(.)}(f) \leq 1$, (see [12], Lemma 3.2.4). Let $p, q \in Q(R)$. The mixed Lebesgue-sequence space $\ell^{p(.)}(L^{q(.)})$ is defined on sequences of $L^{q(.)}$ functions by the modular

$$I_{\ell^{p(.)}(L^{q(.)})}((f_n)_n) = \sum_{n=-\infty}^{\infty} \inf\left\{\lambda_n > 0: I_{q(.)}\left(\frac{f_n}{\lambda_n^{1/p(.)}}\right) \leq 1\right\}.$$

The (quasi)-norm is defined by

$$\|(f_n)_n\|_{\ell^{p(.)}(L^{q(.)})} = \inf\left\{\lambda > 0: I_{\ell^{p(.)}(L^{q(.)})}\left(\frac{1}{\lambda}(f_n)_n\right) \leq 1\right\} \tag{2.1}$$

If $p_+ < \infty$, then we write

$$I_{\ell^{p(.)}(L^{q(.)})}((f_n)_n) = \sum_{n=-\infty}^{\infty} \left\||f_n|^{p(.)}\right\|_{\frac{q(.)}{p(.)}}.$$

We say that a function $h: R \to R$ is log-Hölder continuous at the origin (or has a log decay at the origin), if there exists a constant $c_{log}(h) > 0$ such that

$$|h(y) - h(0)| \leq \frac{c_{log}(h)}{\ln(e + 1/|y|)}$$

for all $y \in R$. If, for some $h_\infty \in R$ and $c_{log} > 0$, there holds

$$|h(y) - h_\infty| \leq \frac{c_{log}}{\ln(e + |y|)}$$

for all $y \in R$, then we say that h is a log decay at infinity. The constants $c_{log}(h)$ and c_{log} are called the locally the log-Hölder decay constant.

Lemma 2.1. Let $0 < b < 1$, $\delta \geq 0$ and $0 < q \leq \infty$, let $\{\epsilon_m\}_m$ a sequences of positive real numbers and we denote by

$$\sigma_m = \sum_{i=-\infty}^{\infty} |m - i|^{\delta} b^{|k-i|} \epsilon_i.$$

Then there exists constant $c > 0$ depending only on b and q such that

$$\left(\sum_{m=-\infty}^{\infty} \sigma_m^q\right)^{1/q} \leq c\left(\sum_{m=-\infty}^{\infty} \epsilon_m^q\right)^{1/q}.$$

We will make use, see ([8], Lemma 3.3) for $v = 1$.

$$v(\Phi) = \int_{\Phi} v(y)dy.$$

Lemma 2.2. Let v be a weight function on R and $q \in Q(R)$. Then putting $\tau_z = e^{-4zc_{\log}(1/q)} \in (0,1)$ for every $z > 0$, and $q_{\Phi}^{-} = \operatorname{ess\,inf}_{y\in\Phi} q(y)$ for a cube $\Phi = (b,d) \subset R$ with $0 < b < d < \infty$, therefore, we write

$$\left(\frac{\tau_z}{v(\Phi)}\int_{\Phi} |f(s)|v(s)ds\right)^{q(y)}$$

$$\leq c\max\left(1, \left(v(\Phi)\right)^{1-\frac{q(y)}{q_-}}\right)\frac{1}{v(\Phi)}\int_{\Phi} \Pi(s)v(s)ds + \frac{cv(z,d)}{v(\Phi)}\int_{\Phi} h(y,s)v(s)ds$$

for some positive constant $c > 0$, all $y \in \Phi$ and all $f \in L^{q(.)}(v)$ with $\|f\|_{L^{q(.)}(v)} \leq 1$, where we put $v(z,d) = \min(d^z, 1)$, $\Pi(s) = |f(s)|^{q(s)}$ and $h(y,s) = \left(e + {}^{1}/_{y}\right)^{-z} + \left(e + {}^{1}/_{s}\right)^{-z}$ or $v(z,d) = \min(d^z,1)$, $\Pi(s) = |f(s)|^{q(0)}$.

And $h(y,s) = \left(e + {}^{1}/_{y}\right)^{-z}\chi_{\{u\in\Phi:q(u)<q(0)\}}(y)$ with $q \in Q(R)$ being log-Hölder continuous at the origin. And also we have the same estimate, while

$$v(z,d) = 1, \qquad \sigma_m = e^{-zc_{\log}}, \qquad \Pi(s) = |f(s)|^{q_\infty}$$

and $h(y,s) = (e+y)^{-z}\chi_{\{u\in\Phi:q(u)<q_\infty\}}(y)$ with $q \in Q(R)$ satisfying log-Hölder decay condition. The proof of this lemma is given in [13].

3. MAIN RESULT

As mentioned in the abstract and introduction we present some new estimate for Hardy operators $\int_x^\infty t^{-k}w(t)\epsilon_t\frac{dt}{t}$ and $\int_0^x t^k w(t)\epsilon_t\frac{dt}{t}$, $x > 0$ in weighted VELS (variable exponent Lebesgue spaces).

Theorem 3.1. Let $k > 0$. Let $q \in Q(R)$ be log-Hölder continuous both at the origin and at infinity with $1 \leq q^- \leq q^+ < \infty$. Let $\{\epsilon_x\}_x$ be a sequence of positive measurable functions and w be a weight function on $(0,\infty)$. And let $\mu_x = x^k\int_x^\infty w(t)t^{-k}\epsilon_t\frac{dt}{t}$ and $\lambda_x = x^{-k}\int_0^x t^k w(t)\epsilon_t\frac{dt}{t}$. Then there exists constant $c > 0$ depending only on $k, q^-, c_{\log}(q)$ and q^+ such that

$$\|\mu_x\|_{L_w^q((0,\infty),\frac{dx}{x})} \approx \left(\int_0^1 {\mu_x}^{q(0)}\frac{dx}{x}\right)^{1/q(0)} + \left(\int_1^\infty {\mu_x}^{q_\infty}\frac{dx}{x}\right)^{1/q_\infty} \tag{3.1}$$

and

$$\| \lambda_x \|_{L_w^q((0,\infty),\frac{dx}{x})} \approx \left(\int_0^1 \lambda_x{}^{q(0)} \frac{dx}{x} \right)^{1/q(0)} + \left(\int_1^\infty \lambda_x{}^{q_\infty} \frac{dx}{x} \right)^{1/q_\infty} \tag{3.2}$$

Moreover,

$$\| \mu_x \|_{L_w^q((0,\infty),\frac{dx}{x})} + \| \lambda_x \|_{L_w^q((0,\infty),\frac{dx}{x}))}$$
$$\lesssim \left(\int_0^1 \epsilon_x{}^{q(0)} w(x) \frac{dx}{x} \right)^{1/q(0)} + \left(\int_1^\infty \epsilon_x{}^{q_\infty} w(x) \frac{dx}{x} \right)^{1/q_\infty}.$$

Proof of Theorem 3.1. A few steps will be followed for the proof of theorem 3.1.

Step 1. We prove that (3.1). We suppose that the right-hand side is less than or equal one. Notice that

$$\| \mu_x \|_{L_w^q((0,\infty),\frac{dx}{x})} \approx \left\| \left(x^{-\frac{1}{q(x)}} \mu_x \chi_{\{2^n,2^{n+1}\}} \right)_n \right\|_{\ell^{p(.)}\left(L_w^{q(.)}\right)}.$$

We see that

$$\mu_x \leq \frac{x^k}{\log 2} \int_{\frac{x}{2}}^{x} t^{-k} \mu_x \frac{dt}{t} \lesssim \frac{x^k}{\log 2} \int_{\frac{x}{2}}^{x} t^{-k} \mu_t \frac{dt}{t} \leq \frac{x^k}{\log 2} \int_{2^{n-1}}^{\infty} t^{-k} \mu_t \frac{dt}{t}$$

for any $n \in Z$ and any $x \in [2^n, 2^{n+1}]$. As a result, for $n \in Z$, we write the following,

$$x^k \int_{2^{n-1}}^{\infty} t^{-k} \mu_t \frac{dt}{t} = \sum_{i=n-1}^{\infty} x^k \int_{2^i}^{2^{i+1}} t^{-k} \mu_t \frac{dt}{t}.$$

<u>For $n \leq 0$.</u> And any $x \in [2^n, 2^{n+1}]$, we can write the following

$$\mu_{x,n} = \sum_{i=n-1}^{\infty} x^k \int_{2^i}^{2^{i+1}} t^{-k} \mu_t \frac{dt}{t} = \sum_{i=n-1}^{-1} x^k \int_{2^i}^{2^{i+1}} t^{-k} \mu_t \frac{dt}{t} + \sum_{i=0}^{\infty} x^k \int_{2^i}^{2^{i+1}} t^{-k} \mu_t \frac{dt}{t}$$
$$= \mu_{x,1,n} + \mu_{x,2,n}.$$

Estimate of $\mu_{x,1,n}$. Let $\delta > 0$ be such that $q_+ < \delta$. We have

$$\left(\sum_{i=n-1}^{-1} x^k \int_{2^i}^{2^{i+1}} t^{-k} \mu_t \frac{dt}{t} \right)^{q(x)/\delta} \leq \sum_{i=n-1}^{-1} x^k \left(\int_{2^i}^{2^{i+1}} t^{-k} \mu_t \frac{dt}{t} \right)^{q(x)/\delta}$$

$$\leq \sum_{i=n-1}^{-1} x^k 2^{-ikq(x)/\delta} \left(\int_{2^i}^{2^{i+1}} \mu_t \frac{dt}{t} \right)^{q(x)/\delta}$$

$$= 2^{-nkq(x)/\delta} \sum_{i=n-1}^{-1} x^k 2^{(n-i)kq(x)/\delta} \left(\int_{2^i}^{2^{i+1}} t^{-k} \mu_t \frac{dt}{t} \right)^{q(x)/\delta}$$

By Hölder's inequality, we estimate this expression by

$$c2^{-nkq(x)/\delta} \left(\sum_{i=n-1}^{-1} x^k 2^{(n-i)kq(x)/\delta} \left(\int_{2^i}^{2^{i+1}} t^{-k} \mu_t \frac{dt}{t} \right)^{q(x)} \right)^{1/\delta},$$

where $c > 0$ is independent of n and i. By Lemma 2.2 we find $z > 0$ such that

$$\left(\frac{1}{(i-n+3)\log 2} \int_{2^{n-1}}^{2^{i+2}} \mu_t \chi_{\{2^i, 2^{i+1}\}}(t) \frac{dt}{t} \right)^{q(x)}$$

$$\lesssim \frac{1}{i-n+3} \int_{2^{n-1}}^{2^{i+2}} \mu_t{}^{q(0)} \chi_{\{2^i, 2^{i+1}\}}(t) \frac{dt}{t} + 2^{iz} \chi_{\{x: q(x) < q(0)\}}(x)$$

$$\lesssim \frac{1}{i-n+3} \int_{2^i}^{2^{i+2}} \mu_t{}^{q(0)} \frac{dt}{t} + 2^{iz} \chi_{\{x: q(x) < q(0)\}}(x)$$

for any $n - 1 \leq i \leq -1$ and any $x \in [2^n, 2^{n+1}] \subset \left[2^{n-1}, 2^{i+2}\right]$. Herewith,

$$\mu_{x,1,n}^{q(x)} \lesssim \sum_{i=n-1}^{-1} x^k 2^{(n-i)kq_-/\delta} (i-n+3)^{q_+-1} \int_{2^i}^{2^{i+1}} \mu_t{}^{q(0)} \frac{dt}{t} + g_n$$

for any $x \in [2^n, 2^{n+1}]$, where $g_n = \sum_{i=n-1}^{-1} x^k 2^{(n-i)kq_-/\delta} (i-n+3)^{q_+} 2^{iz}$. We have

$$\int_{2^n}^{2^{n+1}} \frac{dx}{x} \lesssim 1$$

Herewith,

$$\int_{2^n}^{2^{n+1}} \mu_{x,1,n}^{q(x)} \frac{dx}{x} \lesssim \sum_{i=n-1}^{-1} x^k 2^{(n-i)kq_-/\delta}(i-n+3)^{q_+-1} \int_{2^i}^{2^{i+1}} \mu_t{}^{q(0)} \frac{dt}{t} + g_n.$$

Applying Lemma 2.1 we get

$$\sum_{n=-\infty}^{0} \int_{2^n}^{2^{n+1}} \mu_{x,1,n}^{q(x)} \frac{dx}{x} \lesssim \sum_{i=-\infty}^{-1} \int_{2^i}^{2^{i+1}} \mu_t{}^{q(0)} \frac{dt}{t} + c \lesssim \int_0^1 \mu_t{}^{q(0)} \frac{dt}{t} + c \lesssim 1,$$

by taking z large enough such that $z > 0$.

Estimate of $\mu_{x,2,n}$. Let $\delta > 0$ be such that $q_+ < \delta$, we write

$$\left(\sum_{i=0}^{\infty} \int_{2^i}^{2^{i+1}} t^{-k}\mu_t \frac{dt}{t}\right)^{q(x)/\delta} \leq 2^{-nkq(x)/\delta} \sum_{i=0}^{\infty} 2^{(n-i)kq(x)/\delta} \left(\int_{2^i}^{2^{i+1}} \mu_t \frac{dt}{t}\right)^{q(x)/\delta}.$$

By Hölder's inequality, we estimate this expression by

$$c2^{-nkq(x)/\delta} \left(\sum_{i=0}^{\infty} 2^{(n-i)kq(x)/\delta} \left(\int_{2^i}^{2^{i+1}} \mu_t \frac{dt}{t}\right)^{q(x)}\right)^{1/\delta}.$$

By Lemma 2.2 we find $z > 0$ such that

$$\left(\frac{1}{(i-n+1)\log 2} \int_{2^n}^{2^{i+1}} \mu_t \chi_{\{2^i,2^{i+1}\}}(t) \frac{dt}{t}\right)^{q(x)}$$

$$\lesssim \frac{1}{i-n+1} \int_{2^n}^{2^{i+1}} \mu_t{}^{q_\infty} \chi_{\{2^i,2^{i+1}\}}(t) \frac{dt}{t} + 1 \lesssim \frac{1}{i-n+1} \int_{2^n}^{2^{i+1}} \mu_t{}^{q_\infty} \frac{dt}{t} + 1$$

for any $i \geq 0$ and any $x \in [2^n, 2^{n+1}] \subset \left[2^n, 2^{i+1}\right]$. Herewith

$$\mu_{x,2,n}^{q(x)} \lesssim \sum_{i=0}^{\infty} 2^{(n-i)kq_-/\delta}(i-n+1)^{q_+-1} \int_{2^i}^{2^{i+1}} \mu_t{}^{q_\infty} \frac{dt}{t} + g_n$$

for any $x \in [2^n, 2^{n+1}]$, where $g_n = \sum_{i=0}^{\infty} 2^{(n-i)kq_-/\delta}(i-n+1)^{q_+}$. We have $\int_{2^n}^{2^{n+1}} \frac{dt}{t} \lesssim 1$. Observe that

$$g_n \le 2^{\frac{nkq_-}{2\delta}} \sum_{i=0}^{\infty} 2^{(n-i)kq_-/2\delta}(i-n+1)^{q_+} \lesssim 2^{\frac{nkq_-}{2\delta}}, \quad n \le 0.$$

Therefore,

$$\int_{2^n}^{2^{n+1}} \mu_{x,2,n}^{q(x)} \frac{dt}{t} \lesssim \sum_{i=0}^{\infty} 2^{(n-i)kq_-/2\delta}(i-n+1)^{q_+-1} \int_{2^i}^{2^{i+1}} \mu_t{}^{q_\infty} \frac{dt}{t} + 2^{\frac{n}{2\delta}}.$$

And by Lemma 2.1 we get

$$\sum_{n=-\infty}^{-1} \int_{2^n}^{2^{n+1}} \mu_{x,2,n}^{q(x)} \frac{dt}{t} \lesssim \sum_{i=0}^{\infty} \int_{2^i}^{2^{i+1}} \mu_t{}^{q_\infty} \frac{dt}{t} + c \lesssim \int_1^{\infty} \mu_t{}^{q_\infty} \frac{dt}{t} + c \lesssim 1.$$

<u>For $n > 0$.</u> Let $\delta > 0$ be such that $q_+ < \delta$, we write

$$\left(\sum_{i=n-1}^{\infty} \int_{2^i}^{2^{i+1}} t^{-k} \mu_t \frac{dt}{t} \right)^{q(x)/\delta} \le 2^{-nkq(x)/\delta} \sum_{i=n-1}^{\infty} 2^{(n-i)kq(x)/\delta} \left(\int_{2^i}^{2^{i+1}} \mu_t \frac{dt}{t} \right)^{q(x)/\delta}.$$

By Hölder's inequality, we estimate this expression by

$$c2^{-nkq(x)/\delta} \left(\sum_{i=n-1}^{\infty} 2^{(n-i)kq(x)/\delta} \left(\int_{2^i}^{2^{i+1}} \mu_t \frac{dt}{t} \right)^{q(x)} \right)^{1/\delta}.$$

Applying Lemma 2.2 we find $z > 0$ such that

$$\left(\frac{1}{(i-n+3)\log 2} \int_{2^{n-1}}^{2^{i+2}} \mu_t \chi_{\{2^i,2^{i+1}\}}(t) \frac{dt}{t} \right)^{q(x)}$$

$$\lesssim \frac{1}{i-n+3} \int_{2^{n-1}}^{2^{i+2}} \mu_t{}^{q_\infty} \chi_{\{2^i,2^{i+1}\}}(t) \frac{dt}{t} + 2^{-nz} \lesssim \frac{1}{i-n+3} \int_{2^i}^{2^{i+2}} \mu_t{}^{q_\infty} \frac{dt}{t} + 2^{-nz}$$

for any $i \ge n-1$ and any $x \in [2^n, 2^{n+1}] \subset [2^{n-1}, 2^{i+2}]$. Therefore,

$$\mu_{x,n}^{q(x)} \lesssim \sum_{i=n-1}^{\infty} 2^{(n-i)kq_-/2\delta}(i-n+2)^{q_+-1} \int_{2^i}^{2^{i+1}} \mu_t{}^{q_\infty} \frac{dt}{t} + g_n$$

for any $x \in [2^n, 2^{n+1}]$, where $g_n = \sum_{i=n-1}^{\infty} 2^{(n-i)kq_-/\delta}(i-n+3)^{q_+}2^{-nz}$.

Herewith,

$$\int_{2^n}^{2^{n+1}} \mu_{x,n}^{q(x)} \frac{dt}{t} \lesssim \sum_{i=n-1}^{\infty} 2^{(n-i)kq_-/2\delta}(i-n+3)^{q_+-1} \int_{2^i}^{2^{i+1}} \mu_t{}^{q_\infty} \frac{dt}{t} + g_n.$$

Applying Lemma 2.1 we get,

$$\sum_{n=1}^{\infty} \int_{2^n}^{2^{n+1}} \mu_{x,n}^{q(x)} \frac{dx}{x} \lesssim \sum_{i=0}^{\infty} \int_{2^i}^{2^{i+1}} \mu_t{}^{q_\infty} \frac{dt}{t} + c \lesssim \int_1^{\infty} \mu_t{}^{q_\infty} \frac{dt}{t} + c \lesssim 1,$$

by taking z large enough such that $z > 0$.

Step 2. We prove that

$$\left(\int_0^1 \mu_x{}^{q(0)} \frac{dx}{x}\right)^{1/q(0)} + \left(\int_1^{\infty} \mu_x{}^{q_\infty} \frac{dx}{x}\right)^{1/q_\infty} \lesssim \| \mu_x \|_{L^{q(.)}\left((0,\infty),\frac{dx}{x}\right)} \qquad (3.3)$$

We suppose that the right-hand side is less than or equal one. We prove that

$$\sum_{n=1}^{\infty} \int_{2^{-n}}^{2^{1-n}} \mu_x{}^{q(0)} \frac{dx}{x} \lesssim 1.$$

Clearly follows from the inequality

$$\mu_x{}^{q(0)} \lesssim \int_{2^{-n-1}}^{2^{1-n}} \mu_t{}^{q(t)} \frac{dt}{t} + 2^{-n} = \sigma$$

for any $n \in N$ and any $x \in [2^{-n}, 2^{1-n}]$. Therefore, we can write the following formula

$$\left(\sigma^{-\frac{1}{q(0)}} \mu_x\right)^{q(0)} \leq \left(\frac{1}{\log 2} \int_{2^{-n-1}}^{2^{1-n}} \sigma^{-\frac{1}{q(0)}} \mu_t \frac{dt}{t}\right)^{q(0)} \lesssim 1.$$

By Lemma 2.2,

$$\left(\frac{\tau}{\log 2} \int_{2^{-n-1}}^{2^{1-n}} \sigma^{-\frac{1}{q(0)}} \mu_t \frac{dt}{t}\right)^{q(t)} \lesssim \int_{2^{-n-1}}^{2^{1-n}} \sigma^{-\frac{q(t)}{q(0)}} \mu_t{}^{q(t)} \frac{dt}{t} + 1,$$

where $\tau = e^{-4zc_{\log}(1/q)}$ and $z > 0$. Then we can write

$$\sigma^{-\frac{q(t)}{q(0)}} \approx \sigma^{-1}$$

for any $t \in [2^{-n-1}, 2^{1-n}], n \in N$. Herewith, from the definition of σ, we find that

$$\int_{2^{-n-1}}^{2^{1-n}} \sigma^{-1} {\mu_t}^{q(t)} \frac{dt}{t} \lesssim 1$$

for any $n \in N$. And this implies that $\left(\sigma^{-\frac{1}{q(0)}} \mu_x\right)^{q(0)} \lesssim 1$ for any $n \in N, x \in [2^{-n}, 2^{1-n}]$.

Now we will prove that

$$\sum_{n=1}^{\infty} \int_{2^n}^{2^{n+1}} {\mu_x}^{q_\infty} \frac{dx}{x} \lesssim 1.$$

Clearly follows from the inequality

$${\mu_x}^{q_\infty} \lesssim \int_{2^{n-1}}^{2^{1+n}} \sigma^{-1} {\mu_t}^{q(t)} \frac{dt}{t} + 2^{-n} = \delta$$

for any $x \in [2^n, 2^{n+1}], n \in N$. Therefore, we can write the following formula

$$\left(\sigma^{-\frac{1}{q_\infty}} \mu_x\right)^{q_\infty} \leq \left(\frac{1}{\log 2} \int_{2^{n-1}}^{2^{1+n}} \sigma^{-\frac{1}{q_\infty}} \mu_t \frac{dt}{t}\right)^{q_\infty} \lesssim 1.$$

By Lemma 2.2

$$\left(\frac{\tau}{\log 2} \int_{2^{n-1}}^{2^{1+n}} \sigma^{-\frac{1}{q_\infty}} \mu_t \frac{dt}{t}\right)^{q(t)} \lesssim \int_{2^{n-1}}^{2^{1+n}} \sigma^{-\frac{q(t)}{q_\infty}} {\mu_t}^{q(t)} \frac{dt}{t} + 1,$$

where $\tau = e^{-4zc_{\log}(1/q)}$ and $z > 0$. We use the logarithmic decay condition on q at infinity to show that

$$\sigma^{-\frac{q(t)}{q_\infty}} \approx \sigma^{-1},$$

for any $t \in [2^{n-1}, 2^{1+n}], n \in N$. Therefore, from the definition of σ, we find that

$$\int_{2^{n-1}}^{2^{1+n}} \sigma^{-1} {\mu_t}^{q(t)} \frac{dt}{t} \lesssim 1,$$

for any $n \in N$ and this implies that for any $x \in [2^n, 2^{n+1}]$,

$$\left(\sigma^{-\frac{1}{q_\infty}}\mu_x\right)^{q_\infty} \lesssim 1,$$

which completes the proof of (3.3)

Step 3. We prove that

$$\| \lambda_x \|_{L^{q(\cdot)}((0,\infty),\frac{dx}{x})} \lesssim \left(\int_0^1 \lambda_x^{q(0)} \frac{dx}{x}\right)^{1/q(0)} + \left(\int_1^\infty \lambda_x^{q_\infty} \frac{dx}{x}\right)^{1/q_\infty} \tag{3.4}$$

We suppose that the right-hand side is less than or equal one. Notice that

$$\| \lambda_x \|_{L_w^q((0,\infty),\frac{dx}{x})} \approx \left\| \left(x^{-\frac{1}{q(x)}} \lambda_x \chi_{\{2^n,2^{n+1}\}} \right)_n \right\|_{\ell^{q(\cdot)}(L_w^q)}.$$

We see that

$$\lambda_x \leq \frac{1}{\log 2}\int_x^{2x} \lambda_x \frac{dt}{t} \leq \frac{1}{\log 2}\int_x^{2x} \lambda_t \frac{dt}{t} \lesssim x^{-k}\int_0^{2x} t^k\lambda_t \frac{dt}{t} \leq x^{-k}\int_0^{2^{n+2}} t^k\lambda_t \frac{dt}{t}$$

$$\leq \sum_{j=-\infty}^{n} x^{-k}\int_{2^j}^{2^{j+2}} t^k\lambda_t \frac{dt}{t} = \sum_{i=-n}^{\infty} x^{-k}\int_{2^{-i}}^{2^{2-i}} t^k\lambda_t \frac{dt}{t}$$

for any $n \leq 0$ and $x \in [2^n, 2^{n+1}]$. Let $\delta > 0$ be such that $q_+ < \delta$. We have

$$\left(\sum_{i=-n}^{\infty} x^{-k}\int_{2^{-i}}^{2^{2-i}} t^k\lambda_t \frac{dt}{t}\right)^{q(x)/\delta}$$

$$\leq 2^{nkq(x)/\delta} \sum_{i=-n}^{\infty} 2^{-(n+i)kq(x)/\delta}\left(\int_{2^{-i}}^{2^{2-i}} \lambda_t \frac{dt}{t}\right)^{q(x)/\delta}.$$

Again, by Hölder's inequality, we estimate this expression by

$$c2^{nkq(t)/\delta}\left(\sum_{i=-n}^{\infty} 2^{-(n+i)kq(x)/\delta}\left(\int_{2^{-i}}^{2^{2-i}} \lambda_t \frac{dt}{t}\right)^{q(x)}\right)^{1/\delta}.$$

Applying again Lemma 2.2 we get

$$\left(\frac{1}{(i-n+2)\log 2}\int_{2^{-i}}^{2^{n+2}} \lambda_t \chi_{\{2^{-i},2^{2-i}\}}(t)\frac{dt}{t}\right)^{q(x)}$$

$$\lesssim \frac{1}{i+n+2}\int_{2^{-i}}^{2^{n+2}} \lambda_t^{q(0)} \chi_{\{2^{-i},2^{2-i}\}}(t)\frac{dt}{t} + 2^{nz}.$$

Herewith,

$$\lambda_x^{q(x)} \lesssim \sum_{i=-n}^{\infty} 2^{-(n+i)kq(x)/\delta}(i+n+2)^{q_+-1}\int_{2^{-i}}^{2^{2-i}} \lambda_t^{q(0)}\frac{dt}{t} + h_n$$

for $n \leq 0$ and any $x \in [2^n, 2^{n+1}] \subset \left[2^{-i}, 2^{n+2}\right]$, where $h_n = 2^{nz}$. Therefore,

$$\int_{2^n}^{2^{1+n}} \lambda_x^{q(x)}\frac{dx}{x} \lesssim \sum_{i=-n}^{\infty} 2^{-(n+i)kq_-/\delta}(i+n+2)^{q_+-1}\int_{2^{-i}}^{2^{2-i}} \lambda_t^{q(0)}\frac{dt}{t} + h_n.$$

By taking z large enough such that $z > 0$ and again by Lemma 2.1 we get

$$\sum_{n=-\infty}^{0}\int_{2^n}^{2^{1+n}} \lambda_x^{q(x)}\frac{dx}{x} \lesssim \sum_{i=1}^{\infty}\int_{2^{-i}}^{2^{2-i}} \lambda_t^{q(0)}\frac{dt}{t} + c \lesssim 1.$$

Now we see that

$$\lambda_x \leq \int_x^{2x} \lambda_x \frac{dt}{t} \leq \int_x^{2x} \lambda_t \frac{dt}{t} \lesssim x^{-k}\int_1^{2x} t^k\lambda_t\frac{dt}{t} \leq x^{-k}\int_1^{2^{2+n}} t^k\lambda_t\frac{dt}{t}$$
$$\leq \sum_{i=0}^{n} x^{-k}\int_{2^i}^{2^{2+i}} t^k\lambda_t\frac{dt}{t}$$

for any $n > 0$ and $x \in [2^n, 2^{n+1}]$. Let $\delta > 0$ be such that $q_+ < \delta$. We have

$$\left(\sum_{i=0}^{n}\int_{2^i}^{2^{2+i}} t^k\lambda_t\frac{dt}{t}\right)^{q(x)/\delta} \leq \sum_{i=0}^{n}\left(\int_{2^i}^{2^{2+i}} t^k\lambda_t\frac{dt}{t}\right)^{q(x)/\delta}$$

$$\leq \sum_{i=0}^{n} 2^{ikq(x)/\delta}\left(\int_{2^i}^{2^{2+i}} \lambda_t \frac{dt}{t}\right)^{q(x)/\delta}$$

$$= 2^{nkq(x)/\delta} \sum_{i=-n}^{\infty} 2^{(i-n)kq(x)/\delta}\left(\int_{2^i}^{2^{2+i}} \lambda_t \frac{dt}{t}\right)^{q(x)/\delta}$$

Again, by Hölder's inequality, we estimate this expression by

$$c2^{nkq(x)/\delta}\left(\sum_{i=0}^{n} 2^{(i-n)kq(x)/\delta}\left(\int_{2^i}^{2^{2+i}} \lambda_t \frac{dt}{t}\right)^{q(x)}\right)^{1/\delta}.$$

Applying again Lemma 2.2 we get

$$\left(\frac{1}{(n-i+2)\log 2}\int_{2^i}^{2^{2+i}} \lambda_t \chi_{\{2^i,2^{2+i}\}}(t)\frac{dt}{t}\right)^{q(x)}$$

$$\lesssim \frac{1}{n-i+2}\int_{2^i}^{2^{2+i}} \lambda_t^{q_\infty}\chi_{\{2^i,2^{2+i}\}}(t)\frac{dt}{t} + 2^{-iz}$$

for $n > 0$ and any $x \in [2^n, 2^{n+1}] \subset \left[2^i, 2^{n+1}\right]$, Therefore,

$$\lambda_x^{q(x)} \lesssim \sum_{i=0}^{n} 2^{(i-n)kq(x)/\delta}(n-i+2)^{q_+-1}\int_{2^i}^{2^{2+i}} \lambda_t^{q_\infty}\frac{dt}{t} + h_n$$

for any $n > 0$ and $x \in [2^n, 2^{n+1}]$, where $h_n = \sum_{i=0}^{n} 2^{(i-n)kq_-/\delta}(n-i+2)^{q_+} 2^{-iz}$.

Herewith,

$$\int_{2^n}^{2^{1+n}} \lambda_x^{q(x)}\frac{dx}{x} \lesssim \sum_{i=0}^{n} 2^{(i-n)kq_-/\delta}(n-i+2)^{q_+-1}\int_{2^i}^{2^{2+i}} \lambda_t^{q_\infty}\frac{dt}{t} + h_n.$$

By taking z large enough such that $z > 0$ and again by Lemma 2.1 we get

$$\sum_{n=1}^{\infty}\int_{2^n}^{2^{1+n}} \lambda_x^{q(x)}\frac{dx}{x} \lesssim \sum_{i=0}^{\infty}\int_{2^i}^{2^{2+i}} \lambda_t^{q_\infty}\frac{dt}{t} + c \lesssim 1.$$

The proof of (3.4) is completed.

Step 4. We prove that

$$\left(\int_0^1 \lambda_x^{q(0)} \frac{dx}{x}\right)^{1/q(0)} + \left(\int_1^\infty \lambda_x^{q_\infty} \frac{dx}{x}\right)^{1/q_\infty} \lesssim \| \lambda_x \|_{L_w^q\left((0,\infty),\frac{dx}{x}\right)}.$$

We omit the proofs of this estimate, since they are essentially similar to the proof of (3.3).

Thus, the proof of theorem 3.1 will be completed.

We would like to mention that the estimates (3.1) and (3.2) are true if we assume that $\mu_t \leq \mu_x,\ 0 < t \leq x$ and $\lambda_x \leq \lambda_t,\ 0 < x \leq t$ respectively. Also we find that

$\| \mu_x \|_{L_w^q\left((0,\infty),\frac{dx}{x}\right)} \approx \| \mu_x \|_{L_w^q\left((0,\infty),\frac{dx}{x}\right)}$ and $\| \lambda_x \|_{L_w^q\left((0,\infty),\frac{dx}{x}\right)} \approx \| \lambda_x \|_{L_w^q\left((0,\infty),\frac{dx}{x}\right)}$ for any $q, p \in Q(R)$ are log-Hölder continuos both at the origin and at infinity with $1 \leq q^- \leq q^+ < \infty, 1 \leq p^- \leq p^+ < \infty$, $q(0) = p(0)$ and $q_\infty = p_\infty$.

By the proof of Theorem 3.1 we immediately arrive at the following result.

Theorem 3.2. Let $k > 0$ and $q \in Q(R)$ be log-Hölder continuos both at the origin with $1 \leq q^- \leq q^+ < \infty, 1 \leq p^- \leq p^+ < \infty$. Let w be a weight function on $(0,\infty)$. Let $\{\epsilon_x\}_x$ be a sequence of positive measurable functions. And let $\mu_x = x^k \int_x^1 t^{-k} w(t) \epsilon_t \frac{dt}{t}$ and $\lambda_x = x^{-k} \int_0^x t^k w(t) \epsilon_t \frac{dt}{t}$.

Then there exists constant $c > 0$ depending only on $k, q^-, c_{\log}(q)$ and q^+ such that

$$\| \mu_x \|_{L_w^q\left((0,1),\frac{dx}{x}\right)} \approx \left(\int_0^1 \mu_x^{q(0)} \frac{dx}{x}\right)^{1/q(0)} \qquad (3.5)$$

$$\| \lambda_x \|_{L_w^q\left((0,1),\frac{dx}{x}\right)} \approx \left(\int_0^1 \lambda_x^{q(0)} \frac{dx}{x}\right)^{1/q(0)} \qquad (3.6)$$

Moreover,

$$\| \mu_x\|_{L^q_w\left((0,1),\frac{dx}{x}\right)} + \| \lambda_x\|_{L^q_w\left((0,1),\frac{dx}{x}\right)} \lesssim \left(\int_0^1 \epsilon_x^{q(0)} w(x) \frac{dx}{x}\right)^{1/q(0)}.$$

Again, we would like to mention that the estimates (3.5) and (3.6) are true if we assume that $\mu_t \leq \mu_x$, $0 < t \leq x \leq 1$ and $\lambda_x \leq \lambda_t$, $0 < x \leq t \leq 1$, respectively. Also we find that

$$\| \mu_x\|_{L^q_w\left((0,1),\frac{dx}{x}\right)} \approx \| \mu_x\|_{L^q_w\left((0,1),\frac{dx}{x}\right)} \quad \text{and} \quad \| \lambda_x\|_{L^q_w\left((0,1),\frac{dx}{x}\right)} \approx \| \lambda_x\|_{L^q_w\left((0,1),\frac{dx}{x}\right)}$$

for any $q, p \in Q(R)$ are log-Hölder continuos both at the origin with $1 \leq q^- \leq q^+ < \infty, 1 \leq p^- \leq p^+ < \infty$, and $q(0) = p(0)$.

References

[1] L. Diening, Maximal function on generalized Lebesque spaces $L^{p(.)}$, Math. Inequal. Appl. 7 (2004), no. 2, 245.253.

[2] D. Cruz-Uribe, A. Fiorenza, and C. Neugebauer, The maximal function on variable $L^{p(.)}$ spaces, Ann. Acad. Sci. Fenn. Math. 28 (2003), 223.238; 29 (2004), 247.249.

[3] S. Samko, Convolution and potential type operators in $L^{p(.)}(R^n)$, Int. Transforms Spec. Funct. 7 (1998), no. 3.4, 261.284.

[4] V. Kokilashvili and S. Samko, On Sobolev theorem for Riesz-type potentials in Lebesgue spaces with variable exponent, Z. Anal. Anwend. 22 (2003), no. 4, 899. 910.13

[5] L. Diening and S. Samko, Hardy inequality in variable exponent Lebesgue spaces. Fract. Calc. Appl. Anal. 10 (2007), no. 1, 1.18.

[6] C. Bennett and R. Sharpley, Interpolation of operators, volume 129 of Pure and Applied Mathematics. Academic Press, Inc., Boston, MA, 1988.

[7] D. Cruz-Uribe and A. Fiorenza,Variable Lebesgue Spaces: Foundations and Harmonic Analysis, Birkhaeuser Verlag, Basel, 2013.

[8] L. Diening, P. Harjulehto, P. Hästö, Y. Mizuta and T. Shimomura, Maximal functions in variable exponent spaces: limiting cases of the exponent, Ann. Acad. Sci. Fenn. Math. 34 (2009), no. 2, 503.522.

[9] F. Mamedov, Y. Zeren, L. Akın, “Compactification of weighted Hardy operator in variable exponent Lebesgue spaces,”Asian Journal of Mathematics and Computer Science, 2017, 17(1), 38-47.

[10] L. Akın, “On two weight criterions for the Hardy-Littlewood maximal operator in BFS,” Asian Journal of Science and Technology, Vol. 09, Issue, 05, pp.8085-8089, May, 2018.

[11] L. Akın, “A Characterization of Approximation of Hardy Operators in VLS,” Celal Bayar University Journal of Science, Volume 14, Issue 3, 2018, p 333-336

[12] L. Diening, P. Harjulehto, P. Hästö and M. Ruzicka, Lebesgue and Sobolev spaces with variable exponents. Lecture Notes in Mathematics, vol. 2017, Springer-Verlag, Berlin 2011.

[13] D. Drihem, Variable Besov spaces: continuous version, arXiv:1601.00309v3.

[14] A. Kufner and L. E. Persson, “Weighted Inequalities of Hardy Type”, World Scientific, Singapore, 2003.

[15] V. Kokilashvili and S. Samko, “On Sobolev theorem for Riesz-type potentials in Lebesgue spaces with variable exponent”, Z. Anal. Anwend. 22 (2003), no. 4, 899-910.

On Some Properties of Hardy-Littlewood Maximal Operators on Hardy Spaces Built upon BFS

Lütfi AKIN[1]

CHAPTER 10

[1] Mardin Artuklu University, Department of Business Administration

1. INTRODUCTION

Operator theory studied by very mathematicians, we refer to [1,2,3,4,5]. Compactification of weighted Hardy operator in variable exponent Lebesgue spaces has been proof by [6]. Generalized duality of some Banach function spaces has been proof by [7]. On two weight criterions for the Hardy-Littlewood maximal operator in BFS has been proven, we refer to [8]. A Characterization of Approximation of Hardy Operators in VLS has been proven by [9]. We know that it is established an integral-type necessary and sufficient condition on weights which provides the boundedness of the Hardy-Littlewood maximal operator from weighted Lebesgue spaces into p-convex weighted BFS, we refer to [11].

The domain Ω be the unit circle in the complex plane $\mathbb{C}$. Let Banach algebra of all linear operators on a Banach space F will be denoted by $\mathcal{B}(F)$. Let a function $p(k) = \sum_{t=-n}^{n} b_t k^t$,

where $n \in Z_+$, $b_t \in \mathbb{C}$ for all $t \in \{-n, n\}$ and $k \in \Omega$, is called a trigonometric polynomial of order n. The set of all trigonometric polynomials is denoted by $\aleph$. Riesz projection is operator P which is defined by

$$P: \sum_{t=-n}^{n} b_t k^t \to \sum_{t=0}^{n} b_t k^t. \qquad (1.1)$$

Let $L^p = L^p(\Omega)$ be Lebesgue space on the unit circle Ω in the complex plane for $1 \leq p \leq \infty$. For $f \in L^1$, let $\tilde{f}(n)$ be the sequence of the Fourier coefficients of f and $\tilde{f}(n)$ denoted by

$$\tilde{f}(n) = \frac{1}{2\pi} \int_{-\pi}^{\pi} f(e^{i\varphi}) e^{-in\varphi} d\varphi, \quad n \in Z. \qquad (1.2)$$

Hardy spaces H^p are given by

$$H^p = \{f \in L^p : \tilde{f}(n) = 0, \forall n < 0\}. \qquad (1.3)$$

The classical Hardy-Littlewood maximal operator is defined by

$$Mf(x) = \sup_{B \ni x} \frac{1}{|B|} \int_B f(y) dy$$

where, the supremum is taken over balls B in R^n which contain the point x and $|B|$ denotes the measure of B. It is well known that the Riesz projection P extends to a bounded linear operator on L^p if and only if

$1 < p < \infty$. For $\beta \in L^{\infty}$, Hardy-Littlewood maximal operator M_{β} with symbol β on H^p, $1 < p < \infty$, is given by

$$M_{\beta} f = P(\beta f) \tag{1.4}$$

In this work, we will consider the so-called Banach function spaces Y in place of L^p.

In this work, we will use the following notations.

The unit circle Ω with Lebesgue measure $dm(\theta) = \frac{|d\theta|}{2\pi}$. L^0 is denoted by the set of all measurable functions on Ω. L_+^0 is denoted by the subset of functions in L^0 whose values lie in $[0, \infty]$. χ_D is denoted by the characteristic function of a measurable set of $D \subset \Omega$.

$p: L_+^0 \to [0, \infty]$ is called a function norm for all functions $f, g, f_n (n \in N)$ in L_+^0.

For all constants $c \geq 0$ and measurable subsets D of Ω, the following properties holds

I) $p(f) = 0 \Leftrightarrow f = 0$ a.e., $p(cf) = cp(f), p(f+g) \leq p(f) + p(g)$,
II) $0 \leq g \leq f$ a.e. $\Longrightarrow p(g) \leq p(f)$,
III) $0 \leq f_n \uparrow f$ a.e. $\Longrightarrow p(f_n) \leq p(f)$,
IV) $p(\chi_D) < \infty, \int_D f(\theta) dm(\theta) \leq C_D p(f)$,
with $C_D \in [0, \infty]$ depending on D and p but independent of f. When functions differing only on a set of measure zero are identified, the set Y of all functions $f \in L^0$ for which $p(|f|) < \infty$ is a Banach space under the norm $\|f\|_Y = p(|f|)$. If p is a function norm, its associate norm p' is defined on L_+^0 by

$$p'(g) = \sup \left\{ \int_{\Omega} f(\theta) g(\theta) dm(\theta) : f, g \in L_+^0, p(f) \leq 1 \right\} \tag{1.5}$$

The Banach function space Y' determined by the function norm p' is called the associate space of Y. The associate space Y' is a subspace of the dual space Y. The simplest examples of Banach function spaces are the Lebesgue spaces L^p, $1 \leq p \leq \infty$. The class of all Banach function spaces includes all Orlicz spaces, as well as all rearrangement-invariant Banach function spaces (see [5, Chap. 3]). We are mainly interested in non-rearrangement-invariant Banach function spaces. Two examples of non rearrangement-invariant Banach function spaces are weighted Lebesgue space and weighted variable Lebesgue spaces.

Following (see [10, p.877]), we will consider Hardy spaces $H[Y]$ built upon a Banach function space Y over the unit circle Ω as follows:

$$H[Y] = \{f \in Y : \tilde{f}(n) = 0, \forall n < 0\} \qquad (1.6)$$

This definition makes sense because Y is continuously embedded in L^1 in view of axiom (IV). It can be shown that $H[Y]$ is a closed subspace of Y. It is clear that if $1 \le p \le \infty$, then $H[L^p]$ is the classical Hardy space H^p.
It follows from axiom (IV) that $\aleph \subset L^\infty \subset Y$. We will restrict ourselves to Banach function spaces Y such that the Riesz projection defined initially on $\aleph$ by formula (1.1) extends to a bounded linear operator on the whole space Y. The extension will again be denoted by P. If $\beta \in L^\infty$ and $P \in B(Y)$, then the Hardy-Littlewood maximal operator defined by formula (1.4) is bounded on $H[Y]$ and

$$\|M_\beta\|_{\mathcal{B}(H[Y])} \le \|P\|_{\mathcal{B}(Y)} \|\beta\|_{L^\infty} \qquad (1.7)$$

We aim of this paper is to show that the Brown-Halmos theorem remains true for Hardy spaces $H[Y]$ built upon reflexive Banach function spaces Y if $P \in B(Y)$. Also, we show that, under mild assumptions on a Banach function space Y, a Hardy-Littlewood maximal operator M_β is compact on Hardy space $H[Y]$ built upon Y if and only if $\beta = 0$. These results are specified to the case of Hardy spaces built upon Lebesgue spaces with Muckenhoupt weights.

For $f \in Y$ and $g \in Y'$, we will use the following equation:

$$\langle f, g \rangle = \int_\Omega f(\theta)\overline{g(\theta)}dm(\theta) \qquad (1.8)$$

Let $n \in Z$ and $\theta \in \Omega$, put $\chi_n(\theta) = \theta^n$. For $n \in Z$, Fourier coefficients of a function $f \in L^1$ can be explained by $\tilde{f}(n) = \langle f, \chi_n \rangle$.

Theorem 1.1. *Let Y be a reflexive Banach function space over the unit circle Ω such that the Riesz projection P is bounded on Y. Suppose $B \in \mathcal{B}(H[Y])$ and there is a sequence $\{\beta_n\}_{n\in Z}$ of complex numbers such that*

$$\langle B\chi_i, \chi_t \rangle = \beta_{t-i}, \forall i, t \in Z_+ \qquad (1.9)$$

Then there is a function $\beta \in L^\infty$ such that $B = M_\beta$ and $\hat{\beta}(n) = \beta_n$ for all $n \in Z$. Moreover

$$\|\beta\|_{L^\infty} \le \|M_\beta\|_{\mathcal{B}(H[Y])} \le \|P\|_{\mathcal{B}(Y)} \|\beta\|_{L^\infty} \qquad (1.10)$$

We need the notion of a function with absolutely continuous norm to formulate the result on the noncompactness of nontrivial Hardy-Littlewood maximal operators. Following (see [5, Chap1, Definition 3.1]), a function f in a Banach function space Y is said to have absolutely continuous norm in Y, if $\|f\chi_{D_n}\|_Y \to 0$ for every sequence $\{D_n\}_{n\in N}$ of measurable sets satisfying $\chi_{D_n} \to 0$ almost everywhere as $n \to \infty$.The set of all functions in Y of absolutely continuous norm is denoted by Y_β. It is known that a Banach function space Y is reflexive if and only if Y and Y' have absolutely continuous norm (see [5, Chap.1, Corollary 4.4]).

Theorem 1.2. *Let Y be a Banach function space over the unit circle Ω such that $\chi_D \in Y_\beta$ for every measurable subset $D \subset \Omega$. If the Riesz projection P is bounded on Y and $\beta \in L^\infty$, then the Hardy-Littlewood maximal operator $M_\beta \in \mathcal{B}(H[Y])$ is compact if and only if $\beta = 0$.*

We can summarize our article as follows. In section 2 contains results on the density of the set of all trigonometric polynomials $\aleph$ in a Banach function space Y. We also show that the norm
of a function f in Y can be calculated in terms of $\langle f, p\rangle$, where $p \in \aleph$, under the assumption that Y' is separable. Furthermore, we prove that every bounded linear operator on a separable Banach function space, whose matrix is of the form $(\beta_{t-i})_{i,t\in Z}$ is an operator of multiplication by a function $\beta \in L^\infty$ and the sequence of its Fourier coefficients is exactly $(\beta_t)_{t\in Z}$. Finally, we prove that if the characteristic functions of all measurable sets $D \subset \Omega$ have absolutely continuous norms in Y, then the sequence $(\chi_t)_{t\in Z_+}$ converges weakly to zero on Hardy space $H[Y]$. In section 3, we provide proofs of our main results, using auxiliary results from the previous section.

2. AUXILIARY STATEMENTS

In order to prove our Theorem 1.1 and Theorem 1.2 in section 1, we need the following lemmas.

Lemma 2.1. Let Y be a Banach function space over the unit circle Ω. The following statements are equivalent;

(i) The set $\aleph$ of all trigonometric polynomials is dense in the space Y,
(ii) The space C of all continuous functions on Ω is dense in the space Y,
(iii) The Banach function space Y is separable.

Let $n \in Z_+$, a function of the form $\gamma(k) = \sum_{t=0}^{n} b_t k^t$, where $b_t \in \mathbb{C}$ for all $t \in \{0, \dots, n\}$ and $k \in \Omega$, is said to be an analytic polynomial on Ω. The set of all analytic polynomials is denoted by $\aleph_B$.

Lemma 2.2. (see [3, Lemma 4]) Let Y be a separable Banach functions space over the unit circle Ω. If the Riesz projection P is bounded on Y, then the set $\aleph_B$ is dense in H[Y].

Lemma 2.3. (see [3, Lemma 5]) Let Y be a Banach function space over the unit circle Ω. If the associate space Y′ is separable, then for every f ∈ Y

$$\|f\|_Y = \sup\{|\langle f, p\rangle| : p \in \aleph, \|p\|_{Y'} \leq 1\} \qquad (2.1)$$

The following result by Maligranda and Persson on multiplication operators acting on Banach function spaces.

Lemma 2.4. (see [6, Theorem 1]) Let Y be a Banach function space over the unit circle Ω. If $\beta \in L^0$, then the multiplication operator

$$M_\beta: Y \to Y, f \mapsto \beta f, \tag{2.2}$$

is bounded on Y if and only if $\beta \in L^\infty$ and $\|M_\beta\|_{\mathcal{B}(Y)} = \|\beta\|_{L^\infty}$.
Thus, we can easily do the following equation.

$$\langle M_\beta \chi_{i,}\chi_t\rangle = \langle \beta, \chi_{t-i}\rangle = \hat{\beta}(t-i), \qquad \forall i,t \in Z \tag{2.3}$$

Lemma 2.5. (see [3, Lemma 7]) Let Y be a separable Banach functions space over the unit circle Ω. Suppose $B \in \aleph(Y)$ and there exists a sequence $(\beta_n)_{n\in N}$ of complex numbers such that

$$\langle B\chi_{i,}\chi_t\rangle = \beta_{t-i}, \qquad \forall i,t \in Z \tag{2.4}$$

Then there exists a function $\beta \in L^\infty$ such that $B = M_\beta$ and $\hat{\beta}(n) = \beta_n$ *for all* $n \in Z$.

Lemma 2.6. (see [3, Lemma 8]) If Y is a Banach function space such that $\chi_D \in Y_\beta$ for every measurable subset $D \subset \Omega$, then $\{\chi_t\}_{t\in Z_+}$ converges weakly to zero on H[Y].

3. RESULTS AND DISCUSSION

In this section, we will give proof of our theorems in section 1.

3.1. *Proof of Theorem 1.1.*

We follow the scheme of the proof of [2, Theorem 4.5] (see also [4, Theorem 2.7]). Without breaking the general frame, we may assume that the Hardy-Littlewood maximal operator M is nonzero. For $n \in Z_+$ and $c_n = \chi_{-n} M \chi_n$. Then taking into account Lemma 2.4 and that $M \in \mathcal{B}(H[Y])$, we get

$$\|c_n\|_Y \le \|\chi_{-n}\|_{L^\infty} \|M\chi_n\|_Y = \|M\chi_n\|_{H[Y]} \le \|M\|_{\mathcal{B}(H[Y])} \|\chi_n\|_{H[Y]} \\ = \|M\|_{\mathcal{B}(H[Y])} \|1\|_Y \tag{3.1}$$

Consider the following subset of the associate space,

$$W = \left\{ x \in Y' : \|x\|_{Y'} < \frac{1}{\|M\|_{\mathcal{B}(H[Y])} \|1\|_Y} \right\} \tag{3.2}$$

It follows from Hölder's inequality for Banach function spaces (see [5, Chap. 1, Theorem 2.4]) and (3.1) and (3.2) that

$$|\langle c_n, x\rangle| \le \|c_n\|_Y \|x\|_{Y'} < 1, \forall x \in W, n \in Z_+ \tag{3.3}$$

Since Y is reflexive, in view of [5, Chap.1,Corollaries 4.3-4.4], we know that Y' is canonically isometrically isomorphic to Y^*. Applying the Banach-Alaoglu theorem (see [12, Theorem 3.17]) to W, Y', and $\{c_n\}_{n\in Z} \subset Y = Y^{**} = (Y')^*$, we deduce that there exists $m, c \in Y$ such that some subsequence $\{c_{n_t}\}_{t\in Z_+}$ of $\{c_n\}_{n\in Z_+}$ converges to c in the weak topology on Y.
In particular, we can write the following,

$$\lim_{t\to+\infty} \langle c_{n_t}, \chi_i\rangle = \langle c, \chi_i\rangle, \qquad \forall i \in Z \tag{3.4}$$

On the other hand, the definition of c_n and equality (1.9) imply that,

$$\langle c_{n_t}, \chi_i\rangle = \langle M\chi_{n_t}, \chi_{n_t+i}\rangle = \beta_i,\ (n_t + i) \in Z_+ \tag{3.5}$$

From (3.4) and (3.5) that

$$\langle c, \chi_i\rangle = \beta_i, \qquad \forall i \in Z \tag{3.6}$$

Let's define the mapping N as follows,

$$N: \aleph \to Y,\ \ f \mapsto cf, \tag{3.7}$$

Assume that f and g are trigonometric polynomials of orders j and s, respectively. Then

$$f = \sum_{t=-j}^{j} \hat{f}(t)\chi_t\,,\ \ g = \sum_{i=-s}^{s} \hat{g}(i)\chi_i \tag{3.8}$$

It follows from (1.9) and (3.6) that for $n \ge \max(j, s)$

$$\langle Nf, g\rangle = \sum_{t=-j}^{j}\sum_{i=-s}^{s} \hat{f}(t)\hat{g}(i)\langle c\chi_t, \chi_i\rangle = \sum_{t=-j}^{j}\sum_{i=-s}^{s} \hat{f}(t)\hat{g}(i)\beta_{i-t}$$

$$= \sum_{t=-j}^{j}\sum_{i=-s}^{s} \hat{f}(t)\hat{g}(i)\langle M\chi_{t+n}, \chi_{i+n}\rangle = \sum_{t=-j}^{j}\sum_{i=-s}^{s} \hat{f}(t)\hat{g}(i)\langle \chi_{-n}M(\chi_n\chi_t), \chi_i\rangle$$

$$= \langle \chi_{-n}M(\chi_n f), g\rangle \tag{3.9}$$

It is clear that $\chi_n f \in H[Y]$ for $n \geq \max(j, s)$.

Herewith, taking into account Lemma 2.4, we see that,

$$\left\|K_{\chi_{-n}} M K_{\chi_n} f\right\|_Y \leq \|\chi_{-n}\|_{L^\infty} \|M\chi_n f\|_{H[Y]} \leq \|M\|_{\mathcal{B}(H[Y])} \|\chi_n f\|_{H[Y]}$$

$$\leq \|M\|_{\mathcal{B}(H[Y])} \|\chi_n\|_{L^\infty} \|f\|_Y = \|M\|_{\mathcal{B}(H[Y])} \|f\|_Y \quad (3.10)$$

If we use Hölder's inequality from (3.9) and (3.10), we get the following

$$|\langle Nf, g\rangle| \leq \lim_{n\to\infty} \sup\left|\langle K_{\chi_{-n}} M K_{\chi_n} f, g\rangle\right| \leq \lim_{n\to\infty} \sup\left\|K_{\chi_{-n}} M K_{\chi_n} f\right\|_Y \|g\|_{Y'}$$

$$\leq \|M\|_{\mathcal{B}(H[Y])} \|f\|_Y \|g\|_{Y'}$$
(3.11)

Due to a Banach function space Y is reflexive and the Lebesgue measure is separable, it follows from [5, Chap.1, Corollaries 4.4 and 5.6] that the spaces Y and Y' are separable. Then Lemma 2.3 and inequality (3.11). And for all $f \in \aleph$, we can write the following

$$\|Nf\|_Y = \sup\{|\langle Nf, g\rangle| : g \in \aleph, \|g\|_{Y'} \leq 1\} \leq \|M\|_{\mathcal{B}(H[Y])} \|f\|_Y \qquad (3.12)$$

In view of Lemma 2.1, $\aleph$ is dense in Y. Then (26) implies that the linear mapping N defined in (3.7) extends to an operator $N \in \mathcal{B}(Y)$ such that

$$\|N\|_{\mathcal{B}(Y)} \leq \|M\|_{\mathcal{B}(H[Y])} \qquad (3.13)$$

We deduce from (3.6) that

$$\langle N\chi_i, \chi_t\rangle = \langle c, \chi_{t-i}\rangle = \beta_{t-i}, \forall i, t \in Z \qquad (3.14)$$

By Lemma 2.5, there exists a function $\beta \in L^\infty$ such that $N = K_\beta$ and $\beta_n = \hat{\beta}(n)$ for all $n \in Z$.

Herewith,

$$\|N\|_{\mathcal{B}(Y)} = \left\|K_\beta\right\|_{\mathcal{B}(Y)} = \|\beta\|_{L^\infty} \qquad (3.15)$$

It follows from the definition of the Hardy-Littlewood maximal operator M_β that

$$\langle M_\beta \chi_{i,} \chi_t\rangle = \hat{\beta}(t - i), \qquad \forall i, t \in Z_+ \qquad (3.16)$$

Combining this fact with equality (1.9), we obtain

$$\langle M_\beta \chi_{i,} \chi_t \rangle = \beta_{t-i} = \langle M \chi_{i,} \chi_t \rangle, \qquad \forall i, t \in Z_+ \tag{3.17}$$

Since $M_\beta \chi_,, M\chi_i \in H[Y] \subset H^1$, by the uniqueness theorem for Fourier series (see [14, Chap. I, Theorem 2.7]), it follows from (3.17) that $M_\beta \chi_, = M\chi_i$, for all $i \in Z_+$. Herewith,

$$M_\beta p = Mp, \qquad \forall p \in \aleph_M \tag{3.18}$$

In view of Lemma 2.2, the set $\aleph_M$ is dense in $H[Y]$. This fact and equality (3.18) imply that $M_\beta = M$ and

$$\|M_\beta\|_{\mathcal{B}(H[Y])} = \|M\|_{\mathcal{B}(H[Y])} \tag{3.19}$$

Combining inequality (3.13) with equalities (3.15) and (3.19), we obtain the first inequality in (1.10). The second part of inequality (1.10) is obvious.

3.2. *Proof of Theorem 1.2*

It is clear that if $\beta = 0$, then M_β is the zero operator, which is compact. Now assume that M_β is compact. Then it maps weakly convergent sequences in $H[Y]$ into strongly convergent sequences in $H[Y]$ (see [13, Section 7.5, Theorem 4]). Since $\{\chi_t\}_{t \in Z_+}$ converges to zero weakly on $H[Y]$ in view of Lemma 2.6, we have

$$\lim_{t \to \infty} \|M_\beta \chi_t\|_{H[Y]} = 0 \tag{3.20}$$

By [5, Chap. 1, Theorem 2.7 and Lemma 2.8], for $t \in Z_+$,

$$\|M_\beta \chi_t\|_{H[Y]} = \|M_\beta \chi_t\|_Y = \sup\{|\langle M_\beta \chi_t, g \rangle| : g \in Y', \|g\|_{Y'} \le 1\} \tag{3.21}$$

Since $L^\infty \subset Y'$, there exists a constant $a \in (0, \infty)$ such that

$$a^{-1} \|\chi_j\|_{Y'} \le \|\chi_j\|_{L^\infty} = 1, \quad j \in Z \tag{3.22}$$

For all $n \in Z$ and all $t \in Z_+$ such that $t + n \in Z_+$, we have

$$\hat{\beta}(n) = \langle M_\beta \chi_t, \chi_{t+n} \rangle \tag{3.23}$$

Then from (3.21)–(3.23) we obtain for all $n \in Z$ and all $t \in Z_+$ such that $t + n \in Z_+$

$$\|M_\beta \chi_t\|_{H[Y]} \ge |\langle M_\beta \chi_t, a^{-1} \chi_{t+n} \rangle| = a^{-1} |\hat{\beta}(n)| \tag{3.24}$$

Passing in this inequality to the limit as $t \to \infty$ and taking into account (3.20), we see that $\hat{\beta}(n) = 0$ for all $n \in Z$. By the uniqueness theorem for Fourier series (see, e.g., [14, Chap. I,

$$\langle M_\beta \chi_{i,} \chi_t \rangle = \beta_{t-i} = \langle M \chi_{i,} \chi_t \rangle, \qquad \forall i, t \in Z_+ \tag{3.17}$$

Since $M_\beta \chi_{,}, M\chi_i \in H[Y] \subset H^1$, by the uniqueness theorem for Fourier series (see [14, Chap. I, Theorem 2.7]), it follows from (3.17) that $M_\beta \chi_{,} = M\chi_i$, for all $i \in Z_+$. Herewith,

$$M_\beta p = Mp, \qquad \forall p \in \aleph_M \tag{3.18}$$

In view of Lemma 2.2, the set $\aleph_M$ is dense in $H[Y]$. This fact and equality (3.18) imply that $M_\beta = M$ and

$$\|M_\beta\|_{\mathcal{B}(H[Y])} = \|M\|_{\mathcal{B}(H[Y])} \tag{3.19}$$

Combining inequality (3.13) with equalities (3.15) and (3.19), we obtain the first inequality in (1.10). The second part of inequality (1.10) is obvious.

3.2. *Proof of Theorem 1.2*

It is clear that if $\beta = 0$, then M_β is the zero operator, which is compact. Now assume that M_β is compact. Then it maps weakly convergent sequences in $H[Y]$ into strongly convergent sequences in $H[Y]$ (see [13, Section 7.5, Theorem 4]). Since $\{\chi_t\}_{t\in Z_+}$ converges to zero weakly on $H[Y]$ in view of Lemma 2.6, we have

$$\lim_{t\to\infty} \|M_\beta \chi_t\|_{H[Y]} = 0 \tag{3.20}$$

By [5, Chap. 1, Theorem 2.7 and Lemma 2.8], for $t \in Z_+$,

$$\|M_\beta \chi_t\|_{H[Y]} = \|M_\beta \chi_t\|_Y = \sup\{|\langle M_\beta \chi_t, g\rangle| : g \in Y', \|g\|_{Y'} \le 1\} \tag{3.21}$$

Since $L^\infty \subset Y'$, there exists a constant $a \in (0, \infty)$ such that

$$a^{-1}\|\chi_j\|_{Y'} \le \|\chi_j\|_{L^\infty} = 1, \quad j \in Z \tag{3.22}$$

For all $n \in Z$ and all $t \in Z_+$ such that $t + n \in Z_+$, we have

$$\hat{\beta}(n) = \langle M_\beta \chi_t, \chi_{t+n} \rangle \tag{3.23}$$

Then from (3.21)–(3.23) we obtain for all $n \in Z$ and all $t \in Z_+$ such that $t + n \in Z_+$

$$\|M_\beta \chi_t\|_{H[Y]} \ge |\langle M_\beta \chi_t, a^{-1}\chi_{t+n}\rangle| = a^{-1}|\hat{\beta}(n)| \tag{3.24}$$

Passing in this inequality to the limit as $t \to \infty$ and taking into account (3.20), we see that $\hat{\beta}(n) = 0$ for all $n \in Z$. By the uniqueness theorem for Fourier series (see, e.g., [14, Chap. I, Theorem 2.7]), this implies that $\beta = 0$ a.e. on Ω.

3.3. Corollaries

3.3.1. Let $1 < p < \infty$ and $w \in M_p(\Omega)$. If $M \in \mathcal{B}(H^p(w))$ and there exists a sequence
$\{\beta_n\}_{n \in Z}$ of complex numbers satisfying (1.9), then there exists a function $\beta \in L^\infty$ such that $M = M_\beta$ and $\hat{\beta}(n) = \beta_n$ for all $n \in Z$. Moreover

$$\|\beta\|_{L^\infty} \leq \|M_\beta\|_{\mathcal{B}(H^p(w))} \leq \|P\|_{\mathcal{B}(L^p(w))} \|\beta\|_{L^\infty} \tag{3.25}$$

This inequality is the result of the Theorem 1.1.

3.3.2. Let $1 < p < \infty$ and $w \in M_p(\Omega)$. If $\beta \in L^\infty$, then the Hardy-Littlewood maximal
operator $M_\beta \in \mathcal{B}(H^p(w))$ is compact if and only if $\beta = 0$.

References

[1] A. Brown and P. R. Halmos, “Algebraic properties of Toeplitz operators,” *Journal Für Die Reine Und Angewandte Mathematik*, vol. 213, pp. 89–102, 1964.

[2] A. Yu. Karlovich, “Norms of Toeplitz and Hankel operators on Hardy type subspaces of rearrangement-invariant spaces, ”*Integral Equations and Operator Theory*, vol. 49, no.1, pp. 43–64, 2004.

[3] A. Yu. Karlovich, “Toeplitz Operators on Abstract Hardy Spaces Built upon Banach Function Spaces,” *Journal of Function Spaces,* Volume 2017, Article ID 9768210, 8 pages
https://doi.org/10.1155/2017/9768210.

[4] A. Böttcher and B. Silbermann, “Analysis of Toeplitz Operators”, Springer, Berlin, Germany, 2nd edition, 2006.

[5] C. Bennett and R. Sharpley, “Interpolation of Operators,” vol. 129 of *Pure and Applied Mathematics*, Academic Press, New York, NY, USA, 1988.

[6] F. Mamedov, Y. Zeren, L. Akın, “Compactification of weighted Hardy operator in variable exponent Lebesgue spaces,” *Asian Journal of Mathematics and Computer Science,* 2017, 17:1, 38-47.

[7] L. Maligranda and L. E. Persson, “Generalized duality of some Banach function spaces,” *Indagationes Mathematicae (Proceedings)*, vol. 92, no. 3, pp. 323–338, 1989.

[8] L. Akın, “On two weight criterions for the Hardy-Littlewood maximal operator in BFS,” *Asian Journal of Science and Technology,* Vol. 09, Issue, 05, pp.8085-8089, May, 2018.

[9] L. Akın, “A Characterization of Approximation of Hardy Operators in VLS,” *Celal Bayar University Journal of Science,* Volume 14, Issue 3, 2018, p 333-336

[10] Q. H. Xu, “Notes on interpolation of Hardy spaces,” *Annales de l’Institut Fourier*, vol.
42, no. 4, pp. 875–889, 1992.

[11] R. A. Bandaliyev, “On a two-weight criteria for multidimensional Hardy type operator
in p-convex Banach function spaces and some application,” *Ukrainian Mathematical Journal*, DOI: 10.1007/s11253-015-1085-1 · Source: arXiv.

[12] W. Rudin, “Functional Analysis,” McGraw-Hill, 1991.

[13] W. Cheney, “Analysis for Applied Mathematics,” vol. 208 of *Graduate Texts in Mathematics*, Springer-Verlag, New York, 2001.

[14] Y. Katznelson, “*An Introduction to Harmonic Analysis*,” Dover Publications, Inc., New York, corrected edition, 1976.

The Cobalt Diffusion in MgB_2 Superconductors During Heat Treatment

Asaf Tolga ÜLGEN[1]

CHAPTER 11

[1] Şırnak University, Faculty of Engineering, Electrical-Electronics Department, Şırnak, Turkey

INTRODUCTION

The conduction electrons one direction moving in metal, when a voltage difference occurs between the ends of a metal. Since these electrons interact with the lattice, they lose some of their energies during this movement. If the atoms that make up the lattice collide/scatter with electrons, they will be so great at their speed. So, less colliding/scattering electrons generate a greater current, in other words, the resistivity of metal is low. The phenomenon of superconductivity is absolute near zero electrical resistance and exclusion of the magnetic field happening in certain materials when cooled below a characteristic critical temperature (T_c). These materials showing near-zero resistivity (ρ) under T_c are called superconductors.

Kamerling Onnes observed that the immunity of mercury fell to 4.2 K at zero (Onnes, 1911), and this study was the first to describe the superconductivity. In 1933, when Meissner and Ochsenfeld applied an external magnetic field to a critical temperature superconducting material, the superconducting material proved to exclude this magnetic field (Meissner and Ochsenfeld, 1933). So, it has been found that superconducting materials are not only excellent conductors, but also excellent diamagnet materials. In 1935, the Heinz and Fritz London brothers defined the depth of infiltration as the externally applied static magnetic flux can infiltrate a superconducting material (London, 1935). In the early 1950s, Herbert Fröhlich saw that good conductors such as gold (Au) and silver (Ag) at room temperature were not superconductors at low temperatures, and superconducting T_c proved to be inversely proportional to the square root of masses of ions in pure metals (Fröhlich, 1950). In 1957, Alexei Abrikosov and his discovered a new type of superconducting class (Abrikosov, 1957). In 1971, Nb_3Ga (Webb et al., 1971), which had a T_c = 21 K, was discovered in the Nb_3Ge (Gavaler, 1973) superconducting thin film which had a transition temperature of 23.2 K two years later. In 1987, Bednorz and Müller, who worked on oxide-based superconductors, discovered that the La-Ba-Cu-O system was a high-temperature superconductor of 35 K ceramic material and received the Nobel Prize (Bednorz et al., 1987). However, (Hinks et al., 1987) Bi-Sr-Cu-O superconductors with a transition temperature of 7-20 K were discovered. In the same year, Wu et al T_c = 91K discovered that the Y-Ba-Cu-O superconductors are based on oxide-based type-II of work on the superconductors accelerated (Wu et al., 1987). The MgB_2 metal-alloy superconductor, which excites many research groups and contains the boron mineral which is an important ore for our country, was discovered in 2001. (Nagamatsu et al., 2001).

MgB_2 has important applications in the fields of research and development (R&D) of superconductors from the discovery of these superconducting material to the present day (Savaskan et al., 2018; Erdem et al. 2017). These applications; high-field magnet applications, nuclear magnetic resonance (NMR) spectroscopy and magnetic resonance imaging (MRI) and scanner magnets (Lvovsky et al., 2013), particle accelerator magnets, transmission cables, transformers, electric power sector, motors, generators, leakage current limiters, adiabatic demagnetization coolers for space applications (Tomsic et al., 2007; Tuttle et al., 2004). The biggest advantage of MgB_2 superconducting materials is that the T_c value is three times lower than the high temperature superconductors (HTS), and the critical current density (J_c) in MgB_2 are three times higher than HTS (Guner et al., 2019; Turgay and Yildirim, 2018; Ulgen et al., 2018; Zalaoglu et al., 2018, Guner et al., 2012). The MgB_2 superconducting material is easy to find and inexpensive is also an important advantage, as well as a low anisotropy compared to the HTS and a simple crystal hexagonal structure as seen in Figure 1 (green spheres represent Mg atoms and orange spheres represent B atoms).

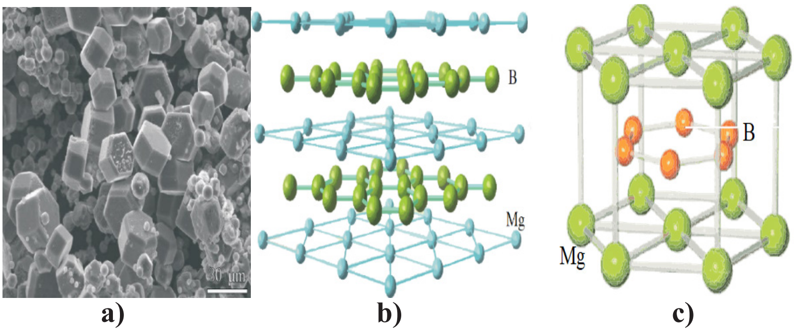

Figure 1. a) The crystal structure of MgB_2 superconductor, b) intra-inter layers (Larbalestier et al., 2001) and c) MgB_2 grains observed in MgB_2 powder (scale bar 30 μm) using scanning electron microscope (Chen et al., 2007).

The fabrication of high density MgB_2 is called diffusion technique, where a wire sample is first prepared with boron and then magnesium is made to diffuse into it during synthesis (Canfield et al., 2001). For practical and industrial superconductivity applications, long-length conductor materials are requisite in the form of bulks (Ulgen and Belenli, 2017; Yilmazlar et al., 2004; Dogruer et al., 2003), tapes (Mikhailov et al., 2018; Flükiger et al., 2003) and wires (Ulgen et al., 2019; Mroczek et al., 2019; Karaboga et al., 2018). The fabrication techniques for superconducting wire and tape fabrication are the powder-in-tube (PIT) process and continuous tube forming and filling (CTFF). The coated conductor technique is widely used for the fabrication of commercially available superconductors.

The present work investigates in some principal characteristic features such as the crystallinity quality and diffusivity between the superconducting grains in the cobalt (Co) coated MgB_2 superconducting materials. In this study, the production of superconducting ex-situ MgB_2 bulk produced by ex-situ methods was successfully performed by solid state reaction process. One surface of the MgB_2 bulk materials was coated with Co metals before heat treatment and then the coated MgB_2 bulk materials was sintered at various temperatures from 650°C to 850°C for 1h. One surface of each bulk material was coated approximately 50 μm with the Co transition metals having high electrical conductivity by using metal evaporation system. So, the interface interactions of the superconducting bulk materials as MgB_2-Co obtained from ex-situ bulk samples coated with transition metals were investigated in detailed.

MATERIALS AND METHODS

All the polycrystalline MgB_2 superconducting bulk samples were fabricated by standard solid-state reaction technique using high purity ex-situ powders with 99.95% purity (Courtesy of Pavezyum Advanced Chemicals Company from Turkey). So, the mixture (minimize the oxidation and produce homogeneous powder) of MgB_2 powders were shuffled and grounded in agate mortar for 30 minutes in a glove box under argon (Ar) atmosphere. After that, ex-situ MgB_2 powders were further ball-milled under high purity Ar atmosphere for 3 hours with a speed of 240 rpm in a cylindrical hard glass grinding vessel and a combination of different diameter agate balls. Two-thirds of the vessel was filled by agate balls and powder leaving one third of the vessel empty for efficient milling. The MgB_2 superconductor powders were pressed into rectangular bars of 25x4x2 mm^3 with a pressure of 300 Bar/15 min ambient conditions, as shown in Figure 2. The MgB_2 rectangular bulk samples were annealed for 1 hour at different temperatures of 650°C, 700°C, 750°C, 800°C and 850°C (see, bottom right of Figure 2) in 5 bar Ar atmosphere. Also, a stainless-steel tube with vacuum and Ar gas inlets was used for sintering process of the ex-situ MgB_2 superconductor bulk samples. Set annealing temperature of the system was determined measuring the real temperature inside the steel tube at the position where the MgB_2 bulk samples are ensconced and after then the controllable furnace was set to the determined temperature for heat treatments. A temperature-time process for the annealing of MgB_2 bulk heating and cooling rates are adjusted to be 5°C/min.

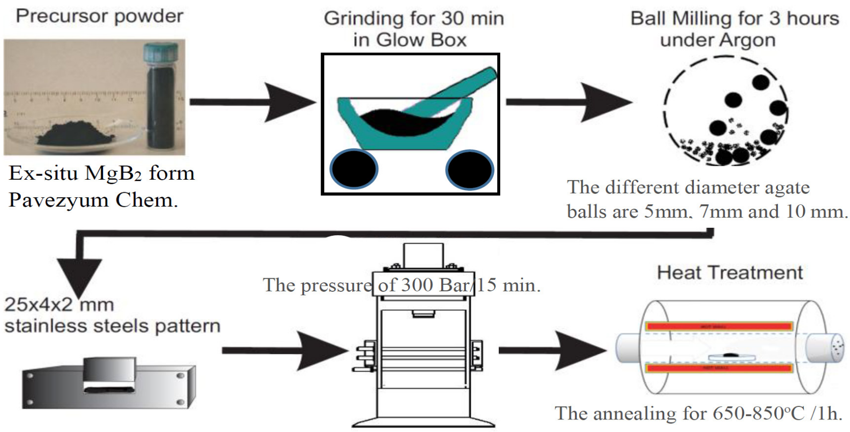

Figure 2. Schematic diagram of fabrication superconductor bulk samples.

The Co coating (about 50-60 μm) is applied on a surface bulk superconducting samples by evaporation of metal films using instructions for the (BOC) Edwards AUTO 306 Vacuum Coater Systems under $1x10^{-4}$ Pa vacuum. These systems are designed for physical vapour deposition processes under high vacuum conditions, at the same time resistance evaporation is most effective deposition technique. In this deposition technique, commonly used metals such as gold, titanium, magnesium, etc. and many others are readily evaporated.

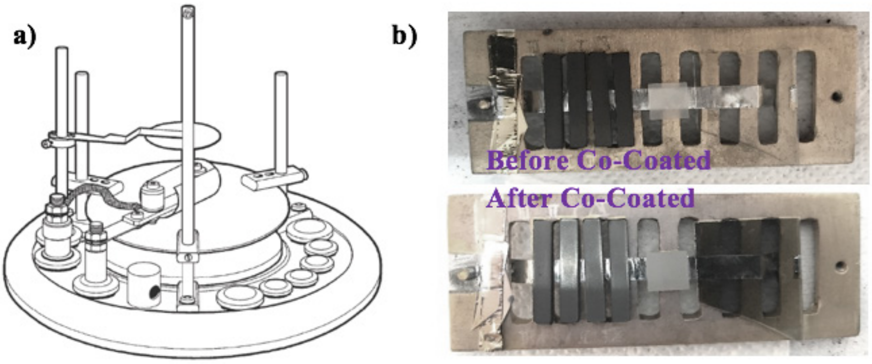

Figure 3. a) Schematic diagram of the deposition region in Edwards AUTO 306 Vacuum Coater Systems, and b) The ex-situ MgB_2 rectangular four pellets before and after Co coating.

Figure 3.a show that the single resistance source for filament/boat evaporation and Figure 3.b show surfaces of Co coated and un-coated MgB_2 ex-situ bulk samples on the aluminium grid.

RESULTS AND DISCUSSION

Figure 4.a shows the X-ray diffraction patterns (XRD) of Co coated Al_2O_3 substrate and Figure 4.b illustrates the XRD of Co into MgB_2 fabricated sintering process at 650 - 800°C for 1 hours. The XRD of the following examples which are noncoated (bare) and Co Coated Al_2O_3 substrate that can be seen Figure 4.a in the range 2theta = 10−70° at a scan speed of 5°/min and step increment of 0.02° at room temperature. It can be said that main phase (101) of the MgB_2 matrix can be obtained from the XRD analyses in the range 2theta = 20−70° of all samples in Figure 4.b.

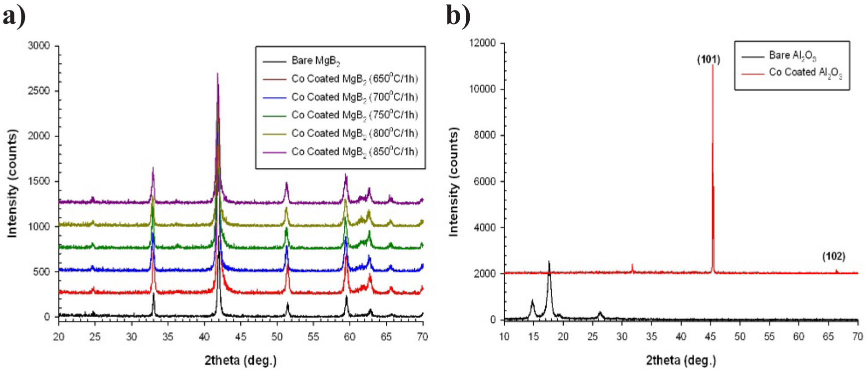

Figure 4. a) The X-ray diffraction patterns for the Co-coated and bare Al_2O_3 substrate, b) Co-coated ex-situ MgB_2 bulk samples for all annealed temperature.

All superconductor samples studied in this work exhibit polycrystalline superconducting phase. After a depth of about 50 μm Co coated samples, Figure 4.b shows that the peaks near 46° which represent Co and MgB_2 are not observed in these samples. Both bare and Co coated bulk samples of lattice parameter *a* are very close value. Table 1 summarizes the lattice parameter *a*, lattice parameter *c* and grain size for different sintering temperature. We used Debye-Scherrer method (Taylor and Sinclair, 1945) to calculate the lattice parameters (*a* and *c*) of the ex situ MgB_2 superconducting bulks, and the values of all lattice parameters are numerically tabulated in Table 1. The crystallite (grain) size of the ex situ MgB_2 samples is calculated to be within the angstrom scale (Å) by using equation of Scherrer (Patterson, 1939). It is observed that the Co-coated ex-situ MgB_2 bulk samples annealed at 850°C for 1 h had the highest grain size and the differences between Co-coated and bare samples can be seen in Table 1. The careful examination of our results (not included in this study) revealed that the lattice parameter *a* tends to stay almost constant along the all annealing temperature, so these parameter value of coated superconductor bulk samples are close and approximately around 3.08 Å. On the other hand, the value of lattice parameter *c* varies between 3.529±.001 Å and 3.540±.001 Å for these samples and Co coated samples have broadest *c* parameters for all annealing temperatures. Effect of the Co diffusion on *c* parameter value has been resembling temperature dependence for all superconductor bulk samples. The grain size values of bare and coated samples sintered at different temperatures were calculated from XRD patterns (in Figure 4.b) and these values were given in Table 1. It is calculated that the Co coated MgB_2 bulk for sintering temperature of 850°C/1h sample have highest grain size (299.55±.01Å), and the differences between Co coated and bare samples are apparent.

Samples	Annealing Conditions	Lattice Parameter *a*	Lattice Parameter *c*	Grain Size
Bare Mg_B2	800°C/1h	3.080±.001	3.529±.001	277.25±.01
Co Coated ex-situ MgB_2 Bulks	650°C/1h	3.084±.001	3.532±.001	282.16±.01
	700°C/1h	3.081±.001	3.535±.001	288.91±.01
	750°C/1h	3.086±.001	3.536±.001	293.37±.01
	800°C/1h	3.078±.001	3.538±.001	296.04±.01
	850°C/1h	3.081±.001	3.540±.001	299.55±.01

Table 1. Lattice parameter *a* and *c*, grain size values of different annealing temperatures for bare and Co-coated ex situ MgB_2 bulk samples.

The atoms of the crystal lattice in a solid oscillate with around their equilibrium (balance) positions (Mehrer, 2007). Atoms move through solids by several different mechanisms (such as vacancy, interstitial, interstitialcy and self-interstitial diffusion mechanism). Lattice diffusion process of atoms in solid phases takes place through the motion of point defects. The variation of point defects gives rise to different mechanisms of diffusion. The diffusion mechanism depending upon agents such as crystal structure, solute size and intermolecular forces (Ulgen, 2016). The mathematical analysis of diffusivity (concentrations ratio) and material ratios for a system of diffusion can be calculated by Fick's 2nd law. The finite thin film the diffusion coefficient calculation is given by following equation (Abdullaev and Dzhafarov, 1987);

$$N(x,t) = N_0\left[1 - \operatorname{erf}\left(\frac{x}{2\sqrt{Dt}}\right)\right] \qquad (1)$$

where $\operatorname{erf}(x/2(Dt)^{1/2})$ is the error function and $y = x/2(Dt)^{1/2}$ is solved by following equation;

$$\operatorname{erf}(y) = \left(\frac{2}{\sqrt{\pi}}\right)\int_0^y \exp(-y^2) \qquad (2)$$

The $N_0 = N(0,t)$ is the concentration constant over the calculated sample (MgB_2 bulk) surface. In these equations, $N(x,t)$ is the concentration of foreign materials, where x is represent to distance from the coated surface, the diffusion coefficient is D and the annealing time to provide diffusion t.

We have also calculated the diffusion coefficients and the activation energies of Co diffusion in superconductor bulk samples of ex-situ MgB_2. Ground a surface of the Co coated sample was cleaned after grinding process (removal about 25 μm) with pressurized air stream before XRD. It is obvious from Figure 5 that the XRD pattern of the Co coated ex-situ MgB_2 samples was annealed for 800°C/1h. As a Figure 5, these steps were repeated eight times to study the depth profile (concentration of Co metal) on the Co coated surface, down to a depth of 200 μm in eight steps.

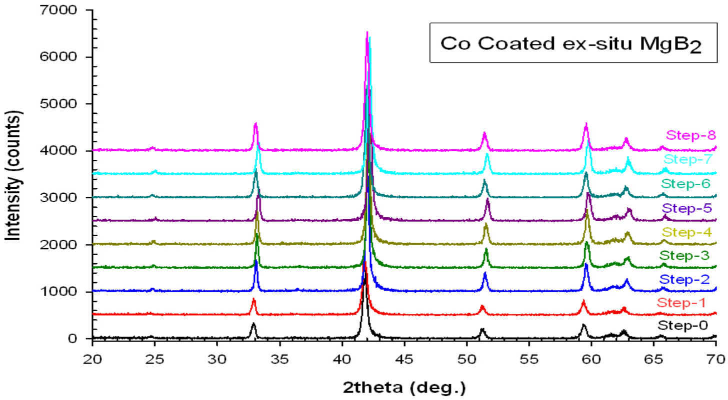

Figure 5. The XRD patterns of all removal steps in Co diffused samples of annealed for 800°C/1 hour.

The concentration profile (diffusivity) depends on the sintering temperature (650-850°C /1h). Figure 6 give the change of parameter *c* ($\Delta c/c_0$) in superconductor sample, as a function of thickness of sample subjected to Co diffusion at different annealing temperatures. After then we calculated diffusion coefficients from diffusivity profiles (as can be seen Figure 6.a) using the Equation 1, values of these coefficients are given in Table 2.

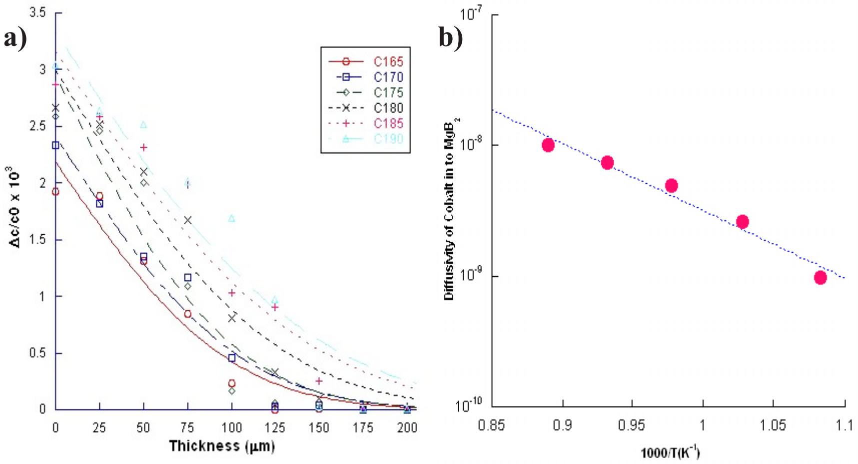

Figure 6. a) Concentration profile of coated Co metal versus the thickness for all MgB_2 superconductor bulk samples calculated by changes in lattice parameter *c*, and b) Temperature-dependent of Co diffusivity at the annealing temperatures between 650°C and 850°C for the bulk MgB_2 superconducting material.

Sintering Conditions	Co diffusion coefficients
650°C/1h	9.9984x10^{-10} cm^2/s
700°C/1h	2.6418x10^{-9} cm^2/s
750°C/1h	5.0161x10^{-9} cm^2/s
800°C/1h	7.3895x10^{-9} cm^2/s
850°C/1h	1.0037x10^{-8} cm^2/s

Table 2. Diffusion coefficient (cm^2/s) of different annealing temperatures for Co coated ex-situ MgB_2 bulk samples.

It is observed that the Co metal diffusion coefficient decreases with increasing annealing temperature and the diffusion coefficient between the Mg_2 superconductor materials coated with Co is between 9.9984E-10 cm^2/s and 1.0037E-8 cm^2/s. Diffusivity relations are seen in Figure 6.b as lines approximated from measured diffusion coefficients of D_{Co} express activation energies values 1.17 eV. The poor activation energies can be pertaining to individual Co atoms or ions migrating into the bulk of MgB_2 samples through the defects such as inner surfaces of voids and grain boundaries, slightly changing the lattice parameter *c* (Ulgen and Belenli, 2016

CONCLUSIONS

In this recent study, we investigated that the surface of a Co coated MgB_2 superconducting sample has changed due to diffusion effects and mechanics. The lattice parameter *c* and grain size values of MgB_2 superconducting bulk samples were improved by a 50 micrometers thickness of Co coating thin layer. The diffusion coefficients (diffusivity) and activation energies of Co diffusion into these samples are inferred from the lattice parameters calculated with the aid of the XRD patterns along the depth profile. The lattice parameter *c* value of the unit cell raises with coating/diffusion of Co and *c* value is increases in Co diffused samples compared to bare MgB_2 samples. The Co coated MgB_2 superconductor material have slightly larger grain size of 299.55 Å with up to 8.5% highest due to bare samples. Increasing of annealing temperature value causes the diffusion coefficient and the grain size to increase. The result of temperature dependent on Co diffusivity relies on the fact that the minimum activation energy value is 1.17 eV for transition metal Co atoms/ions into the bulk MgB_2 crystal lattice.

ACKNOWLEDGEMENTS

This work is supported by the Scientific and Technological Research Council of Turkey, (Project no:117F263) and in part by Sirnak University Research Fund Grant No:2017.03.02.01.

REFERENCES

1. Abdullaev, G.B., Dzhafarov, T.D., (1987), *Atomic diffusion in semiconductor structures*, Harwood, New York.
2. Abrikosov, A.A., (1957), *On the magnetic properties of superconductors of the second group*, Sov. Phys. JETP, 5, 1174-1182.
3. Bednorz, J.G., Takashige, M., Müller, K.A., (1987), *Susceptibility measurements support high-Tc superconductivity in the Ba-La-Cu-O system*, EPL (Europhysics Letters), 3 (3), 379.

4. Canfield, P.C., Finnemore, D.K., Bud'Ko, S.L., Ostenson, J.E., Lapertot, G., Cunningham, C.E., Petrovic, C., (2001), *Superconductivity in dense MgB_2 wires*, Physical Review Letters, 86 (11):2423.

5. Chen, W., Liu, W., Chen, C., Wang, R., Feng, Q., (2011), *Single-crystal MgB_2 hexagonal microprisms via hybrid physical-chemical vapor deposition*. Cryst.Eng.Comm., 13 (12), 3959-3961.

6. Dogruer, M., Karaboga, F., Yildirim, G., Terzioglu, C., (2013), *Comparative study on indentation size effect, indentation cracks and superconducting properties of undoped and MgB_2 doped Bi-2223 ceramics*, Journal of Materials Science: Materials in Electronics, 24 (7), 2327-2338.

7. Erdem, O., Abdioglu, M., Guner, S. B., Celik, S., and Kucukomeroglu, T., (2017), *Improvement in levitation force performance of bulk MgB_2 superconductors through coronene powder adding*, Journal of Alloys and Compounds, 727, 1213-1220.

8. Fick, A. (1855), Annalen der Physik und Chemie 94:59.

9. Flükiger, R., Suo, H. L., Musolino, N., Beneduce, C., Toulemonde, P., Lezza, P. (2003), *Superconducting properties of MgB_2 tapes and wires*, Physica C: Superconductivity, 385 (1-2), 286-305.

10. Fröhlich, H., (1950), *Isotope effect in superconductivity*, Proceedings of the Physical Society. Section A, 63 (7), 778.

11. Gavaler, J.R., (1973) *Superconductivity in Nb–Ge films above 22 K*, Applied Physics Letters, 23 (8), 480-482.

12. Guner, S. B., Zalaoglu, Y., Turgay, T., Ozyurt, O., Ulgen, A. T., Dogruer, M., Yildirim, G., (2019), *A detailed research for determination of Bi/Ga partial substitution effect in Bi-2212 superconducting matrix on crucial characteristic features*, Journal of Alloys and Compounds, 772, 388-398.

13. Guner, S.B., Gorur, O., Celik, S., Dogruer, M., Yildirim, G., Varilci, A., Terzioglu, C., 2012, *Effect of zirconium diffusion on the microstructural and superconducting properties of $YBa_2Cu_3O_{7-\delta}$ superconductors*, Journal of Alloys and Compounds, 540, 260-266.

14. Hinks, D.G., Soderholm, L., Capone, D.W., Dabrowski, B., Mitchell, A. W., Shi, D., (1988), *Preparation of Bi-Sr-Ca-Cu-O superconductors from oxide-glass precursors*, Applied physics letters, 53 (5), 423-425.

15. Karaboğa, F., Ulgen, A. T., Yetiş, H., Akdoğan, M., Pakdil, M., Belenli, I. (2018), *Mechanical properties and uniformity of Fe-MgB2 wires upon various wire drawing steps*, Materials Science and Engineering: A, 721, 89-95.

16. Larbalestier, D., Gurevich, A., Feldmann, D. M., Polyanskii, A., (2001), *High-T_c superconducting materials for electric power applications*, Nature, 414 (6861), 368.

17. London, F., London, H., (1935), *The electromagnetic equations of the supraconductor*, Proc. Roy. Soc., A 149:71.

18. Lvovsky, Y., Stautner, E.W., and Zhang, T., (2013), *Novel technologies and configurations of superconducting magnets for MRI*, Supercond. Sci. Technol., 26, 093001, 71-78.

19. Mehrer, H. (2007), *Diffusion in Solids: Fundamentals, Methods, Materials, Diffusion-Controlled Processes*, Berlin: Springer-Verlag.

20. Meissner, W., Ochsenfeld, R., (1933), *Ein neuer effekt bei eintritt der supraleitfahigkeit*, Naturwissenschaften, 21 (44):787-788.

21. Mikhailov, B., Mikhailova, A., Nikulin, V. Y., Borovitskaya, I., Silin, P. (2018), *Properties and Structural Transformations of MgB_2-tapes under the Action of Plasma Shock Waves*, KnE Materials Science, 4 (1), 250-258.

22. Mroczek, Z., Morawski, A., Czujko, T., Karaboğa, F., Akdoğan, M., Zaleski, A. J., Małecka, M., Cetner, T., Yetiş, H., Gajda, D., Belenli, I., (2019), *Influence of the lamella structure and high isostatic pressure on the critical current density in in situ* MgB_2 *wires without a barrier*, Journal of Alloys and Compounds, 776, 636-645.
23. Nagamatsu, J., Nakagawa, N., Muranaka, T., Zenitani, Y., and Akimitsu, J., (2001), *Superconductivity at 39K in magnesium diboride*, Nature, 410 (6824), 63.
24. Onnes, H.K., (1911), Commun. Phys. Lab. Univ. Leiden. Suppl. 29.
25. Patterson, A.L., (1939), *The Scherrer formula for X-ray particle size determination*, Physical review, 56 (10), 978.
26. Savaşkan, B., Güner, S.B., and Koparan, E.T., (2018), MgB_2 *Külçe Örneklerine SiC Eklenmesi ile Manyetik Kaldırma ve Kılavuzlama Kuvvetinin İyileştirilmesi*, Karaelmas Fen ve Mühendislik Dergisi, 8 (2), 595-601.
27. Taylor, A., Sinclair, H., (1945), *On the determination of lattice parameters by the Debye-Scherrer method*, Proceedings of the Physical Society, 57 (2), 126.
28. Tomsic, M., Rindfleisch, M., Yue, J., McFadden, K., and Phillips, J., (2007), *Overview of* MgB_2 *superconductor applications*, Int. J. Appl. Ceram.Technol., 4, 250–259.
29. Turgay, T., and Yıldırım, G., (2018), *Effect of Diffusion Annealing Temperature on Crack-initiating Omnipresent Flaws, Void/crack Propagation and Dislocation Movements Along Ni Surface-layered Bi-2223 Crystal Structure*, Sakarya University Journal of Science, 22 (5), 1211-1220.
30. Tuttle, J., Pourrahimi, S., Shirron, P., Canavan, E., DiPirro, M., and Riall, A., (2004), *10K magnet for spaceright ADRs*, Cryogenics 44 383–388.
31. Ulgen, A.T., (2016), *The Diffusion of Iron (Fe) in Superconducting* MgB_2 *Polycrystalline Samples*, PhD Thesis, Abant İzzet Baysal University, pp180.
32. Ulgen, A.T., Turgay, T., Terzioglu, C., Yildirim, G., and Oz, M., (2018), *Role of Bi/Tm substitution in Bi-2212 system on crystal structure quality, pair wave function and polaronic states*, Journal of Alloys and Compounds, Vol 764, Pages 755-766.
33. Ulgen, A.T., and Belenli, I., (2017), *The Effect of Fe Diffusion on Some Physical and Superconducting Properties of* MgB_2, Journal of Superconductivity and Novel Magnetism, 30 (4), 1089-1095.
34. Ulgen, A. T., Karaboğa, F., Karakaya, M., Podila, R., Rao, A. M., Belenli, I., (2019), *Improved transport properties of* MgB_2 *superconducting round wires via minute addition of gold nanoparticles*, Ceramics International, 45 (1), 1031-1036.
35. Webb, G.W., Vieland, L.J., Miller, R.E., and Wicklund, A., 1971, *Superconductivity above 20K in stoichiometric* Nb_3Ga, Solid State Communications, 9 (20), 1769-1773.
36. Wu, M.K., Ashburn, J.R., Torng, C.J., Hor, P.H., Meng, R.L., Gao, L., Huang, Z.J., Wang, Y.Q., and Chu, C.W., (1987), *Superconductivity at 93K in a new mixed-phase Y-Ba-Cu-O compound system at ambient pressure*, Phys. Rev. Lett. 58, 908.
37. Yilmazlar, M., Terzioglu, C., Dogruer, M., Karaboga, F., Soylu, N., Zalaoglu, Y., Yildirim, G., Ozturk, O., (2014), *Evaluation of Microstructural and Mechanical Properties of Ag-Diffused Bulk MgB2 Superconductors,* J. Supercond. Nov. Magn., 27: 77.
38. Zalaoglu, Y., Terzioglu, C., Turgay, T., Yildirim, G., (2018), *Detailed survey on minimum activation energy for penetration of Ni nanoparticles into Bi-2223 crystal structure and temperature-dependent Ni diffusivity*, Journal of Materials Science: Materials in Electronics, 29(4), 3239-3249.

Nearness and Near Sets via Normal Subgroups

Nurettin BAĞIRMAZ[1]

Hatice TAŞBOZAN[2]

CHAPTER 12

1 Mardin Artuklu University, Mardin, Turkey

2 Hatay Mustafa Kemal University, Hatay, Turkey

INTRODUCTION

The theory of near sets, which states that objects with similar characteristics to some extent are perceptually near to each other, were introduced by Peters in [6] . Since its inception, near set theory has evolved in many ways and has found applications in different areas [8-12,14]. The algebraic properties of near sets are described in [7]. In recent years, many studies have focused on establishing a relationship between near sets and algebraic structures. In [5], Özcan and Bağırmaz obtained some of the key features of near sets. In [3], Bağırmaz defined the concept of near subsemigroups, near ideals on near approximation spaces. In [4], İnan and Öztürk introduced the notion of near groups. In [2], Bağırmaz examined the concept of near approximations in a group. In [1], Abd El-Monsef at al. studied the lower and upper approximations of near sets with topological structures. In [13], Hatice et al. have defined near soft topology on nearness approximations spaces.

PRELIMINARIES

In this section, we will give some definitions and properties regarding perceptual near sets as in [7].

Definition 1. (Perceptual Object) A perceptual object is something perceivable that has its origin in the physical world.

Definition 2. (Probe Function) A probe function is a real-valued function representing a feature of a perceptual object.Simple examples of probe functions are the colour, size or weight of an object.

Definition 3. (Perceptual System) A perceptual system (O, F) consists of a non-empty set O of sample perceptual objects and a non-empty set F of real-valued functions $\varphi \in F$ such that $\varphi: O \to \mathbb{R}$.

Definition 4. (Object Description) Let (O, F) be a perceptual system, and let $B \subseteq F$ be a set of probe functions. Then, the description of a perceptual object $x \in O$ is a feature vector given by

$$\varphi_B(x) = (\varphi_1(x), \varphi_2(x), \dots, \varphi_i(x), \dots, \varphi_l(x))$$

where l is the length of the vector φ_B, and each $\varphi_i(x)$ in $\varphi_B(x)$ is a probe function value that is part of the description of the object $x \in O$.

Definition 5. Indiscernibility relation) Let (O, F) be a perceptual system. For every $B \subseteq F$ the indiscernibility relation $\sim_B$ is defined as follows:

$$\sim_B = \{(x, y) \in O \times O \mid \forall \varphi_i \in B, \varphi_i(x) = \varphi_i(y)\}.$$

If $B = \{\varphi\}$ for some $\varphi \in F$, instead of $\sim_{\{\varphi\}}$ we write $\sim_\varphi$.

The indiscernibility relation $\sim_B$ is an equivalence relation on object descriptions.

Lemma 6. Let (O, F) be a perceptual system. Then for every $B \subseteq F$ and for every $\varphi \in F$

$$\sim_B = \bigcap_{\varphi \in B} \sim_\varphi$$

Definition 7. (Equivalence Class) Let (O, F) be a perceptual system and let $x \in O$. For a set $B \subseteq F$ an equivalence class is defined as

$$[x]_B = x/\sim_B = \{y \in O \mid y \sim_B x\}.$$

Definition 8. (Quotient Set) Let (O, F) be a perceptual system. For a set $B \subseteq F$ a quotient set is defined as

$$O/\sim_B = \{x/\sim_B \mid x \in O\}.$$

Definition 9. Let (O, F) be a perceptual system. Then

$$\prod(O, F) := \bigcup_{B \quad F} O/\sim_B,$$

i.e., $\prod(O, F)$ is the family of equivalence classes of all indiscernibility relations determined by a perceptual information system (O, F).

Definition 10. (Nearness relation). Let (O, F) be a perceptual system and let $X, Y \subseteq O$. A set X is near to a set Y within the perceptual system (O, F) $(X \bowtie_F Y)$ iff there are $F_1, F_2 \subseteq F$ and $f \in F$ and there are $A \in O/\sim_{F_1}$, $B \in O/\sim_{F_2}$, $C \in O/\sim_f$ such that $A \subseteq X, B \subseteq Y$ ve $A, B \subseteq C$. If a perceptual system is understood, then we say briefly that a set X is near to a set Y.

Example 11. Let (O, F) be a perceptual system such that

$O = \{x_1, x_2, \dots, x_6\}$, $F = \{\varphi_1, \varphi_2\}$, $\varphi_1(x_1) = \varphi_1(x_2) = \varphi_1(x_3)$, $\varphi_1(x_4) = \varphi_1(x_5) = \varphi_1(x_6)$, $\varphi_1(x_1) \neq \varphi_1(x_4)$ and $\varphi_2(x_1) = \varphi_2(x_2), \varphi_2(x_3) = \varphi_2(x_4)$, $\varphi_2(x_5) = \varphi_2(x_6)$, $\varphi_2(x_1) \neq \varphi_2(x_4) \neq \varphi_2(x_5)$.

Thus $O/\sim_{\varphi_1} = \{\{x_1, x_2, x_3\}, \{x_4, x_5, x_6\}\}$, $O/\sim_{\varphi_2} = \left\{\{x^1, x^2\}, \{x^3, x^4\}, \{x^5, x^6\}\right\}$, $O/\sim_{\{\varphi_1, \varphi_2\}} = \{\{x_1, x_2\}, \{x_3\}, \{x_4\}, \{x_5, x_6\}\}$.

Let $X = \{x_1, x_2, x_3, x_5\}, Y = \{x_2, x_4, x_5, x_6\}$. Thus there are $A = \{x_4\} \in O/\sim_{\{\varphi_1, \varphi_2\}}$, $B = B\{x_5, x_6\} \in O/\sim_{\varphi_2}$, $C = (A \cup B) \in O/\sim_{\varphi_1}$ such that $A \subseteq X, B \subseteq Y$. Therefore $X \bowtie_F Y$.

Definition 12. (Perceptual near sets) Let (O, F) be a perceptual system and let $X \subseteq O$. A set X is a perceptual near set iff there is $Y \subseteq O$ such that $X \bowtie_F Y$. The family of near sets of a perceptual system (O, F) is denoted by $Near_F(O)$.

Nearness and Near sets via normal subgroups

In this section, we will get natural results similar to the definitions in the previous section within a group structure. Then, we give some new definition and propositions which are related to some propositions in [5] and [7].

Let G be a group. Well it is known that there is a one-to-one correspondence between normal subgroups of G and congruence relations on G. On the other hand, a congruence relation defines an equivalence relation in G. Therefore, we can identify the notion (O, F) and (G, F), where F denote a set of normal subgroups of G.

Definition 13. (Cosets as equivalence classes) Let G be a group with a normal subgroup N. Then, the equivalence class of $x \in G$ is $[x]_N == xN$.

Lemma 14. Let (G, F) be a perceptual system and B⊆F. The equivalence class of x∈G

$$[x]_B = xB = \bigcap_{N \in B} xN = x(\bigcap_{N \in B} N).$$

Definition 15. Let (G, F) be a perceptual system and let $X, Y \subseteq G$. A set X is near to a set Y within the perceptual system (G, F) $(X \bowtie_F Y)$ iff there are $F_1, F_2 \subseteq F$ and $N \in F$ and there are $A \in G/F_1, B \in G/F_2, C \in G/N$ such that $A \subseteq X, B \subseteq Y$ ve $A, B \subseteq C$.

Example 16. Let $G = (Z_{12}, \oplus) = \{0,1,2,3,4,5,6,7,8,9,10,11\}$ and $B = \{N_1, N_2\}$ where $N_1 = \{0,6\}, N_2 = \{0,3,6,9\}$. Since all subgroups of a commutative group are normal subgroups, we obtain that N_1, N_2 and N_3 are normal subgroups of G.

Let $X = \{0,4,10\}$ and $Y = \{1,3,7,8\}$ and $Z = \{2,5\}$

Then by a simple calculation we have

$$[0]_{N_1} = 0 \oplus N_1 = \{0,6\}, [1]_{N_1} = \{1,7\}, [2]_{N_1} = \{2,8\},$$

$$[3]_{N_1} = \{3,9\}, [4]_{N_1} = \{4,10\}, [5]_{N_1} = \{5,11\},$$

$$[0]_{N_2} = \{0,3,6,9\}, [1]_{N_2} = \{1,4,7,10\}, [2]_{N_2} = \{2,5,8,11\}.$$

Thus $A = \{4,10\} \in G/N_1 \subseteq X,\ B = \{1,7\} \in G/N_1 \subseteq Y$

and

$$C = A \cup B = \{1,4,7,10\} \in G/N_2$$

Therefore $X \bowtie_B Y$.

But there is no $C = A \cup B \in G/N_1 \cup G/N_2$, such that $A \subseteq X,\ B \subseteq Z$. Therefore, the set X is not near to the set Z.

On the other hand, X, Y, Z are a near set.

Definition 17. Let (G, F) be a perceptual system and let $X \subseteq G$. A set X is a perceptual near set iff there is $Y \subseteq G$ such that $X \bowtie_F Y$. The family of near sets of a perceptual system (G, F) is denoted by $Near_F(G)$.

Definition 18. Let (G, F) be a perceptual system and $x \in G$. Then

$$\prod(G,F) := \bigcup \{xB \mid \forall B \subseteq F\}$$

i.e., $\prod(G,F)$ is the family of cosets of all normal subgroups determined by a perceptual system (G, F).

This definition is slightly different Definition 9 because each coset has the same size and divides the perceptual system into equal sections.

Proposition 19. Let (G, F) be a perceptual system.Then

$$X \bowtie_F X \Leftrightarrow \textit{there is } A \in \prod(G,F) \textit{ such that } A \subseteq X.$$

Proof. It is clear from Definition 15.

Corollary 20. Let (G, F) be a perceptual system.Then

$$X \in \prod(G,F) \Rightarrow X \bowtie_F X,$$

i.e., the relation $\bowtie_F$ is reflexive within the family $\prod(G,F)$.

From the above corollary, we can say every coset in $\prod$(G,F) is a near set.

Proposition 21. Let (G, F) be a perceptual system. Let $e \in F$ and $X, Y \subseteq G$. Then

$$X \cap Y \neq \emptyset \Rightarrow X \bowtie_F Y.$$

Proof. Let $X \cap Y \neq \emptyset$ and $x \in G$. Then, there is $[x]_e \in G/F$ such that $[x]_e \subseteq X \cap Y$. From Definition 15, $X \bowtie_F Y$.

Proposition 22. Let (G, F) be a perceptual system and $X, Y \subseteq G$. If there is $A \in \prod(G,F)$ such that $A \subseteq X \cap Y$, then $X \bowtie_F Y$.

Proof. It is clear from Proposition 21.

By Proposition 22, we obtain the following corollary.

Corollary 23. Let (G, F) be a perceptual system and $X, Y \subseteq G$. Then if there is $A \in \prod(G, F)$ such that $A \subseteq X$, then $X \subseteq Y \Rightarrow X \bowtie_F Y$.

Proposition 24. Let (G, F) be a perceptual system and $X, Y \subseteq G$. Then

$$X \bowtie_F Y \Rightarrow X \neq \emptyset \wedge Y \neq \emptyset.$$

Proof. It is clear from Definition 15.

Proposition 25. Let (G, F) be a perceptual system and $X, Y, Z \subseteq G$. Then

$$X \bowtie_F Y \wedge Y \subseteq Z \Rightarrow X \bowtie_F Z.$$

Proof. It is clear from Definition 15.

By Definition 15 and Definition 17, we obtain the following proposition.

Proposition 26. Let (G, F) be a perceptual system. For every $X \subseteq G$, the following conditions are equivalent:

(a) $X \in Near_F(G)$,

(b) there is $A \in \prod(G, F)$ such that $A \subseteq X$,

(c) there is $A \in G/F$ such that $A \subseteq X$.

Corollary 27 and 28 follows directly from Proposition 26.

Corollary 27. Let (G, F)be a perceptual system. Let $e \in F$ and $X \subseteq G$. Then $X \in Near_F(G)$.

Corollary 28. Let (G, F) be a perceptual system. Then $\emptyset \notin Near_F(G)$.

Proposition 29. Let (G, F) be a perceptual system and $X \subseteq Y \subseteq G$. Then

$$X \in Near_F(G) \Rightarrow Y \in Near_F(G).$$

Proof. It is clear from Proposition 26.

Proposition 30. Let (G, F) be a perceptual system and $X, Y \subseteq G$. Then

$$X, Y \in Near_F(G) \Rightarrow X \cup Y \in Near_F(G).$$

Proof. Let $X, Y \subseteq G$. Since $X, Y \subseteq X \cup Y$ from Proposition 29, $X \cup Y \in Near_F(G)$.

Proposition 31. Let (G, F) be a perceptual system and $X, Y \subseteq G$. Then always there are $X, Y \in Near_F(G)$ such that $X \cap Y \notin Near_F(G)$.

Proposition 32. Let (G, F) be a perceptual system. *Let* $e \in F$ and $X, Y \subseteq G$ Then

$$X \cap Y \neq \emptyset \Rightarrow X \cap Y \in Near_F(G).$$

Proof. Let $X \cap Y \neq \emptyset$ and $x \in G$. Then, there is $[x]_e \in G/F$ such that $[x]_e \subseteq X \cap Y$. From Proposition 26, $X \cap Y \in Near_F(G)$.

From Lemma 14, we can give following corollary.

Corollary 33. Let (G,F) be a perceptual system and $F = B_n = \{N_1, N_2, \ldots, N_n\}$. Then for all $B_i \subseteq F$, $1 \leq j, i \leq n$, $B_j \subseteq B_i \Rightarrow [x]_{B_i} \subseteq [x]_{B_j}$.

Proposition 34. Let (G,F) be a perceptual system and $F = B_n = \{N_1, N_2, \ldots, N_n\}$. Then for all $B_i \subseteq F$, $1 \leq j, i \leq n$, the following condition hold:

(a) $\prod(G, B_j) \subseteq \prod(G, B_i)$,

(b) $Near_{B_j}(G) \subseteq Near_{B_i}(G)$,

(c) $X \bowtie_{B_j} Y \Rightarrow X \bowtie_{B_i} Y$.

Proof. (a) Since $B_j \subseteq B_i$, from Definition 18, $\prod(G, B_j) \subseteq \prod(G, B_i)$.

(b) Let $X \subseteq G$ and $X \in Near_{B_j}(G)$. Then from Proposition 26, there is $A \in \prod(G, B_j)$ such that $A \subseteq X$. Thus from item (a), $A \in Near_{B_i}(G)$. Therefore $X \in Near_{B_i}(G)$.

(c) Follow from Proposition 4.9 in [5].

Let (G,F) be a perceptual system and $F = B_n = \{N_1, N_2, \ldots, N_n\}$. Then we can form the ascending subsets normal subgroups of G as follows:

$$B_1 \subseteq B_2 \subseteq \ldots \subseteq B_n.$$

From Proposition 34, we can give following corollary.

Corollary 35. Let (G,F) be a perceptual system and $F = B_n = \{N_1, N_2, \ldots, N_n\}$. Then for all $B_i \subseteq F$, $1 \leq j, i \leq n$, the following condition hold:

(a) $\prod(G, B_1) \subseteq \prod(G, B_2) \subseteq \ldots \subseteq \prod(G, F)$,

(b) $Near_{B_1}(G) \subseteq Near_{B_2}(G), \subseteq \ldots \subseteq Near_F(G)$,

$(c) X \bowtie_{B_1} Y \Rightarrow X \bowtie_{B_2} Y \Rightarrow \cdots \Rightarrow X \bowtie_F Y$.

Homomorphisms of near sets

In this section we mainly study the image and inverse image of near sets with respect to a homomorphism between two groups. It is proven that the image of a near set is invariant under a group homomorphism.

Proposition 36. Let (G_1, F_1), (G_2, F_2) be two perceptual system. Let f be a homomorphism from G_1 to G_2 and $f(F_1) \subseteq F_2$. Then

$$X \bowtie_{F_1} Y \Rightarrow f(X) \bowtie_{f(F_1)} f(Y).$$

Proof. Let $H_1, H_2 \subseteq F_1$ and $N \in F_1$. From Definition 15, there are $A \in G_1/H_1, B \in G_1/H_2, C \in G_1/N$ such that $A \subseteq X, B \subseteq Y$ ve $A, B \subseteq C$. Since f is a homomorphism, then

$$f(A) \subseteq f(X), f(B) \subseteq f(Y), f(A), f(B) \subseteq f(C)$$

and

$$f(H_1), f(H_2) \subseteq f(F_1) \subseteq F_2, f(N) \in F_2.$$

Thus

$$f(A) \in G_2 / f(H_1), f(B) \in G_2 / f(H_2), f(C) \in G_2 / f(N)$$

Therefore, again from Definition 15, we have $f(X) \bowtie_{f(F_1)} f(Y)$.

Proposition 37. Let (G_1, F_1), (G_2, F_2) be two perceptual system. Let f be a homomorphism from G_1 to G_2 and $f(F_1) \subseteq F_2$. Then

$$X \in Near_{F_1}(G_1) \Rightarrow f(X) \in Near_{F_2}(G_2).$$

Proof. Let $X \in Near_{F_1}(G_1)$. Then from Proposition 26, there is $A \in \prod(G_1, F_1)$ such that $A \subseteq X$. Since f is a homomorphism and $f(F_1) \subseteq F_2$, there is $f(A) \in \prod(f(G_1), f(F_1)) \subseteq \prod(G_2, F_2)$ such that $f(A) \subseteq f(X)$. Therefore, again from Proposition 26, we have $f(X) \in Near_{F_2}(G_2)$.

Proposition 38. Let (G_1, F_1), (G_2, F_2) be two perceptual system. Let f be a homomorphism from G_1 to G_2 and $f(F_1) \subseteq F_2$. Then

$$X \cap Y \in Near_{F_1}(G_1) \Rightarrow f(X) \cap f(Y) \in Near_{F_2}(G_2).$$

Proof. Well it is known that $f(X \cap Y) = f(X) \cap f(Y)$. Then, from Proposition 37, we have $f(X) \cap f(Y) \in Near_{F_2}(G_2)$.

Proposition 39. Let (G_1, F_1), (G_2, F_2) be two perceptual system. Let f be a homomorphism from G_1 to G_2 and $f(F_1) \subseteq F_2$. Then

$$X \cup Y \in Near_{F_1}(G_1) \Rightarrow f(X) \cup f(Y) \in Near_{F_2}(G_2).$$

Proof. Well it is known that $f(X \cup Y) = f(X) \cup f(Y)$. Then, from Proposition 37, we have $f(X) \cup f(Y) \in Near_{F_2}(G_2)$.

CONCLUSION

Investigation of the characteristics of near sets in a group is an important research topic of near set theory. In this study, we gave near set and nearness concepts and their important features in a group. We have also shown that homomorphic images of a near sets in a group are also near sets.

REFERENCES

1. Abd El-Monsef, M. E., Kozae, A.M., Marei, E.A., Near set theory and its generalization, Journal of King Saud University -Science, Vol. 23, Issue 1, 41-45, 2011.
2. Bağırmaz, N., Near approximations in groups, Applicable Algebra in Engineering, Communication and Computing, https://doi.org/10.1007/s00200-018-0373-z.
3. Bağırmaz, N., Near ideals in near semigroups, European Journal of Pure and Applied Mathematics, Vol .11 (2), 505-516, 2018.
4. Inan, E., Öztürk, M., Near groups on nearness approximation spaces, Hacettepe Journal of Mathematics and Statistics, Vol. 4, 545-558, 2012.
5. Özcan, A. F., Bağırmaz, N., Comparison of near sets by means of a chain of features, Hacettepe Journal of Mathematics and Statistics, Vol.45 (1) , 69 - 76, 2016.
6. Peters, J. F., Near sets, General theory about nearness of objects, Appl. Math. Sci. Vol. 1 (53) , 2029-2609, 2007.
7. Peters, J. F. and Wasilewsk, P., Foundations of near sets, Information Sciences, Vol. 179 , 3091-3109, 2009.
8. Peters, J. F. Fuzzy Sets, Near Sets, and Rough Sets for Your Computational Intelligence Toolbox, Foundations of Comput. Intel. Vol. 2, pp. 3-25, 2009.
9. Peters, J. F. and Ramanna, R. Feature selection: a near set approach, (in: ECML & PKDD Workshop on Mining Complex Data, Warsaw, 2007), 1-12.
10. Peters, J. F., Naimpally, S., Applications of near sets, Notices of the Amer. Math. Soc., Vol. 59 (4), 536-542, 2012.
11. Peters, J. F. and Pal, S. K., Cantor, Fuzzy, Near , and Rough Sets in Image Analysis, (In: Pal, S.K. and Peters, J. F.(eds.) Rough Fuzzy Image Analysis: Foundations and Methodologies, CRC Pres ,Taylor and Francis Group, Boca Raton, U.S.A, 2010), 1.1-1.16.

12. Peters, J. F., Topology of Digital Images. Visual Pattern Discovery in Proximity Spaces, Intelligent Systems Reference Library, Springer, ISBN 978-3-642-53844-5, Vol. 63, 1-342, 2014.
13. Tasbozan, H., İçen, İ., Bağırmaz, N., Özcan, A. F., Soft Sets and Soft Topology on Nearness Approximation Spaces, Filomat, Vol. 31(13), 4117-4125, 2017.
14. Wolski, W., Perception and classification. A note on near sets and rough sets, Foundamenta Informaticae, 101, 143-155, 2010.

In Vitro Synthesis of mRNA for Gene Therapy Applications

Betül AYDIN[1]

CHAPTER 13

[1] Research Assistant Dr., Gazi University, Faculty of Science, Department of Molecular Biology and Genetic, Ankara, Turkey

1. INTRODUCTION

Gene therapy applications by using plasmid DNA (pDNA) drugs has been developed in the past two decades. After the improvement of in vitro transcription (IVT) methods, IVT mRNA based gene therapy has become a more useful alternative to pDNA for production of desired protein in the cells. One of the advantages of the IVT mRNA usage in gene therapy is not to integrate into the host genome which increased the risk of mutation. Another advantage is that there is no need to entrance in the nucleus for translation (Kwon et al., 2018; Meng et al., 2017; Ramanathan, Robb, & Chan, 2016; Steinle, Behring, Schlensak, Wendel, & Avci-Adali, 2017). Moreover, the production of IVT mRNA is comparatively cheap and easy (Sahin, Karikó, & Türeci, 2014).

Synthetic mRNAs are used for genome engineering (Na et al., 2013; Wang et al., 2015), cancer immunotherapy (Fotin-Mleczek et al., 2012; Kranz et al., 2016; McNamara, Nair, & Holl, 2015), regenerative medicine (Kwon et al., 2018), vaccination against infectious diseases (Petsch et al., 2012; Van Gulck et al., 2012), replacement therapy (Kormann et al., 2011; Youn & Chung, 2015), genetic reprogramming (Carlsten & Childs, 2015; Carlsten et al., 2016) and allergies (Hattinger et al., 2015; Zeyer et al., 2016).

There are two main approaches of using synthetic mRNA in therapeutic applications; ex vivo transfection and direct vaccination. In ex vivo transfection approach; synthetic mRNA is transferred into the patient's cells, and then these transfected cells are administered back to the patient. In direct vaccination, synthetic mRNA is transferred to the patient's body directly (Sahin et al., 2014).

2. SYNTHETIC MESSENGER RNA STRUCTURE

mRNA is the intermediate step between the translation of protein-encoding DNA and the production of proteins by ribosomes in the cytoplasm. The structure of mature mRNAs in eukaryotic cells can be divided into five major portions (Figure 1): (i) cap structure – m7GpppN or m7Gp3N (N: any nucleotide); (ii) 5′ untranslated region (5′UTR); (iii) protein-encoding open reading frame (ORF); (iv) 3′ untranslated region (3′UTR); (v) tail of 100–250 adenosine residues (3′ poly(A) tail) (Lee, Kim, Seo, & Lee, 2018; Pardi, Hogan, Porter, & Weissman, 2018). Also, synthetic mRNA should contain all of these components for an efficient protein translation. The position of these elements at the beginning of the translation are shown in Figure 2.

Figure 1. The structure of mRNA

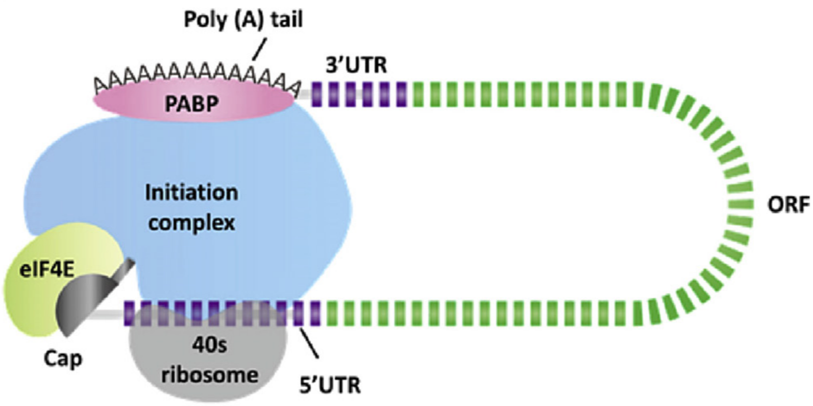

Figure 2. Initation of translation (Kwon et al., 2018)

The standard in vitro transcription (IVT) procedure for mRNA generation begins with a linearized plasmid, PCR product or synthesized DNA that contains at least four elements: a promoter that is recognized by a phage polymerase, such as T7, T3 or SP6, the coding sequence of the protein (ORF), UTR and poly (T) sequence (Kwon et al., 2018; Weissman, 2015; Zhong et al., 2018).

First, the promoter, the coding sequence of the protein (ORF) and UTR regions are amplified using polymerase chain reaction (PCR). The generated DNA template contains all the important elements of the mRNA. Second, in vitro transcription (IVT) is performed, which synthesizes multiple copies of mRNA from the amplified PCR product DNA using the T7,T3 or SP6 RNA polymerase. Then, the DNA template is digested with DNase treatment to terminate transcription. After the purification steps by conventional methods of nucleic acid isolation, the mRNA is ready to use (Figure 3) (Michel, Wendel, & Krajewski, 2016; Weissman, 2015).

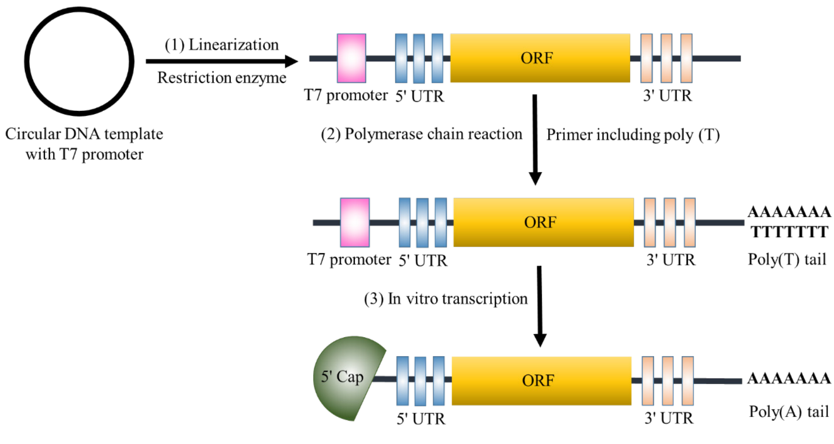

Figure 3. Synthetic mRNA production steps

2.1. Cap

A functional 5' cap structure is an essential element for the translation process of mRNA (Proudfoot, Furger, & Dye, 2002). Therefore in nature, all eukaryotic mRNA consists of a 7-methylguanosine (m7G) residue linked to the 5' end of mRNA through a 5' to 5'-triphosphate bridge (ppp) (m7GpppN structure) (Ramanathan et al., 2016). There are three types of cap structure in eukaryotic mRNA as shown in Figure 4.

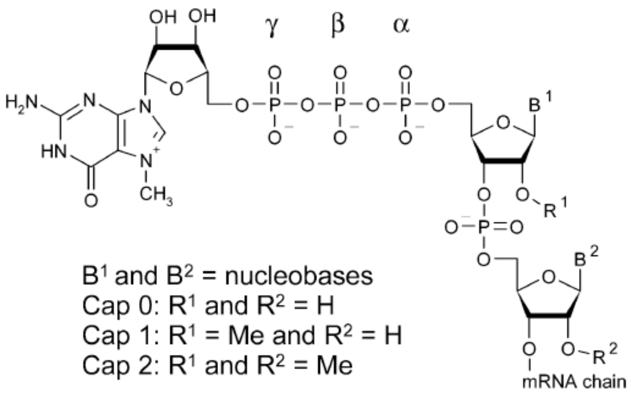

Figure 4. mRNA caps in eukaryotes (Jemielity, Kowalska, Rydzik, & Darzynkiewicz, 2010)

As the DNA template does not encode the 5' cap, a synthetic cap analogue must be added to the IVT mRNA. There are several functions of the 5' cap for translation and protection of mRNA. First of all, the mRNA cap is essential for the cap-dependent initiation of the translation through its binding to eukaryotic translation initiation factor 4E (eIF4E) (Figure 2), whereas its binding to the mRNA decapping enzymes DCP1, DCP2 or DCPS regulates mRNA decay. Second, the 5' cap prevents the mRNAs from 5' to 3' cleavage by the exonucleases (Kwon et al., 2018; Michel et al., 2016; Ramanathan et al., 2016; Sahin et al., 2014; Sergeeva, Koteliansky, & Zatsepin, 2016; Weissman, 2015). Third, the cap structure is also important to prevent recognition of the mRNA by innate immune sensors (Zhong et al., 2018).

There are two main strategies to adding a 5' cap to in vitro synthesized mRNA: post-transcriptional capping and co-transcriptional capping.

Post-Transcriptional Capping

Recombinant Vaccinia virus derived enzymes are used in this process. This type of enzymes make a 5' cap-1 that is same as the cap structure that is most frequently found in eukaryotic mRNAs. First, the triphosphate of the first nucleotide at the 5'end of the synthesized mRNA is hydrolyzed to a diphosphate by the RNA triphosphatase (RTP). Then, 5′ to 5′- triphosphate linkage is generated from fusion of a GMP moiety from GTP to the β-phosphate of the resulting 5′-diphosphate end by guanylyltransferase (GT). Finally, the N7 position of the transferred GMP is methylated by a methyltransferase (MT) using S-adenoysl-L-methionine (SAM) generating a standard type of cap structure (m7GpppN ; cap0). Moreover, in applications where the innate immune response is to be minimized, the methylation can be induced 2'-O position of the first (m7GpppNmpN …; cap1) or the first and second nucleotides (m7GpppNmpNm …; cap2) of the transcript using a cap-specific 2'O methyltransferase (Jemielity et al., 2010; Muttach, Muthmann, & Rentmeister, 2017).

Co-Transcriptional Capping

Co-transcriptional capping is another approach to prepare the 5' capped IVT mRNA. In this approach, cap analogues are included directly in the in vitro transcription reaction. Notwithstanding there are advantages and disadvantages to both approaches, co-transcriptional capping is a more general and relatively inexpensive capping procedure. Post-transcriptional capping is more difficult compared to co-transcriptional capping and adding the cap after transcription requires a second reaction in this process. Another advantage of the co-transcriptional capping is various modified cap structures can be incorporated with a more diverse cap design (Kwon et al., 2018; Proudfoot et al., 2002).

Nevertheless, including a cap analog during transcription results in a decrease in the total amount of mRNA produced and a portion of the mRNA made will not contain a cap analog, and this situation is an important disadvantage of this capping mechanism. This is because the cap analog competes with GTP as initiator nucleotide in the transcription reaction that initiated by RNA polymerases with nucleophilic attack by the 3′-OH of GTP on the α-phosphate of the next nucleoside triphosphate specified by the DNA template. Due to this competitive reaction, uncapped mRNAs are undesirably generated. To solve this problem, a cap analog is present in the reaction mixture 4–10-fold molar excess in respect to GTP, thus, the transcription is initiated mainly by attack of 3′-OH of the cap dinucleotide rather than that of GTP, and this reaction results in formation of capped transcripts(Figure 5) (Strenkowska et al., 2010).

Figure 5. Schematic representation of co-transcriptional capping

Primary mRNA investigation was done using mRNAs produced with m7GpppG cap analogue. And the most commonly used cap analogue is m7GpppG. However, there is a problem of using this cap analogue for generating IVT mRNA. In vitro transcription executed in the presence of m7GpppG cap analog may be initiated by an RNA polymerase from either guanosine (G) or m7G to generate correctly-capped (m7GpppG) or reversely-capped (Gpppm7G) mRNA, respectively. One third to one half of the mRNA can contain the cap in a reversed orientation and this reversely-capped mRNAs decreased the translational activity of mRNA (Weissman, 2015). This problem was overcome by developing anti-reverse cap analogues (ARCA) bearing either 3′-O-methyl, 3'-H or 2′-O-methyl modifications in the N7-methylguanosine ribose and containing a 5'-5' triphosphate bridge (Figure 6) (Stepinski, Waddell, Stolarski, Darzynkiewicz, & Rhoads, 2001). ARCA-capped mRNAs exhibit higher translational efficiency than m7GpppG capped mRNAs in a variety of cell types (Muttach et al., 2017; Pasquinelli, Dahlberg, & Lund, 1995; Strenkowska et al., 2010; Youn & Chung, 2015).

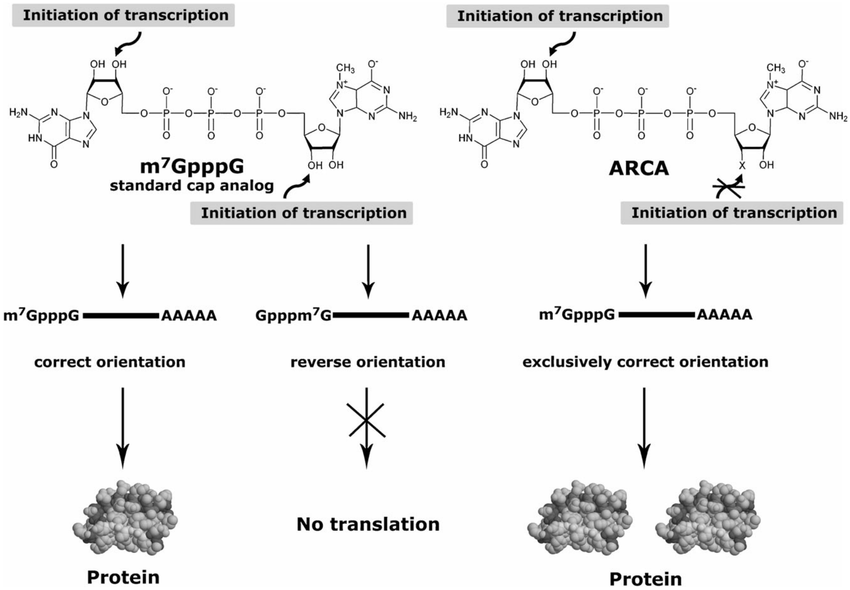

Figure 6. The concept of anti-reverse cap analogs (ARCA) (Jemielity et al., 2010)

2.2. UTRs

Eukaryotic cells use the 5′- and 3′-untranslated regions (UTRs) to regulate posttranscriptional gene expression and to inhibit the decapping and degradation of the mRNA for providing the stability. Therefore, templates for IVT mRNA can be constituted by the integration of cellular or viral 5'- and 3'- UTRs including specific regulatory sequence regions (Kwon et al., 2018; Steinle et al., 2017). The 5' UTRs found in many orthopoxvirus mRNAs have been demonstrated to inhibit both decapping and 3'-5' exonuclease degradation (Weissman, 2015). Many IVT mRNAs contain the 3′-UTRs derived from α- and β-globin mRNAs that enhance the stability and translation of the mRNA (Michel et al., 2016; Tavernier et al., 2011). On the contrary, if limited lengths of protein production may be desired, rapid mRNA degradation is possible by incorporating AU-rich sequences into 3′-UTR region (Sahin et al., 2014; Weissman, 2015).

2.3. ORF

An open reading frame (ORF) should be included in the IVT mRNA because it contains genetic information for translation process. Sometimes this protein-coding region of the mRNA enables the mRNA degradation. For this reason, this region of the mRNA has to be optimized. This optimization can be provided in two ways. One of them is to use optimized codons to lead to better translation of the sequence into the desired protein. Besides, it is still unclear which codon combination usages is ideal for increasing the translation activity and stability of mRNAs. Further studies are needed to confirm the effect of codon adaptation. And the other one is to reduce endonucleolytic degradation by optimization of the bases (Michel et al., 2016). For instance, to protect the mRNA from degradation, the frequency of UU and UA dinucleotides in the ORFs can be reduced (Kwon et al., 2018; Sahin et al., 2014; Youn & Chung, 2015).

2.4. Poly(A) Tail

In eukaryotic cells, most actively translated mRNAs have 100-250 adenosine residues at the 3' end (Zhong et al., 2018). The presence and length of the 3' poly(A) tail which binds to the polyadenosyl-binding-protein (PABP), is also crucial for efficient translation and stability of mRNAs (Kwon et al., 2018). The eIF4F complex bound to the cap as part of the translation initiation complex interacts with the PABP bound to the poly(A) tail (Figure 2) (Sergeeva et al., 2016). Also, suitable length of the poly(A) tail is significant for this interaction to provide the stability of mRNA. If the poly(A) tail is too short, the cap structure is cleaved and the mRNA is degraded (Youn & Chung, 2015). There are two main approaches for poly (A) tailing reaction when producing the synthetic mRNAs. First approach is to use a DNA template which has poly (T) sequence for in vitro transcription. The DNA template can be generated via the polymerase chain reaction (PCR) by using a primer containing a long poly (T). Other approach for preparing the poly (A) tailed mRNA is to use a separate enzymatic reaction by recombinant poly(A) polymerase after transcription (Quabius & Krupp, 2015; Sahin et al., 2014; Weissman, 2015).

3. PURIFICATION OF SYNTHETIC mRNA

After the IVT, the DNA template enzymatically digested by DNase. In order that reduce the possible immune response, 5' triphosphate group of the mRNAs is removed using heat-labile antarctic phosphatase. Furthermore, unreacted ribonucleotides, RNA polymerase, capping enzymes, free cap molecules, residual salts, double-strand (ds) RNAs, short abortive RNA transcripts should be removed to obtain pure IVT mRNA. There are various techniques such as commercially available mRNA purification kits, reversed-phase high performance liquid chromatography (HPLC), anion-exchange chromatography, size exclusion chromatography (SEC), cross-flow filtration to separate the IVT mRNA from these molecules that can activate an undesired innate immune response (Kwon et al., 2018; Zhong et al., 2018).

4. DELIVERY METHODS OF THE SYNTHETIC mRNA

For in vivo delivery of the IVT mRNA different approaches are used such as delivery of naked mRNA (Wolff et al., 1990), gene gun mediated delivery of mRNA (Qiu, Ziegelhoffer, Sun, & Yang, 1996), lipid-based carriers (Lu, Benjamin, Kim, Conry, & Curiel, 1994; Zhou et al., 1999), in vivo electroporation of mRNA (Bugeon et al., 2017; Johansson, Ljungberg, Kakoulidou, & Liljeström, 2012), lipid nanoparticles (Kauffman et al., 2015), lipidoids and polymer-based carriers (Gonçalves, Akhter, Pichon, & Midoux, 2016; Zhong et al., 2018).

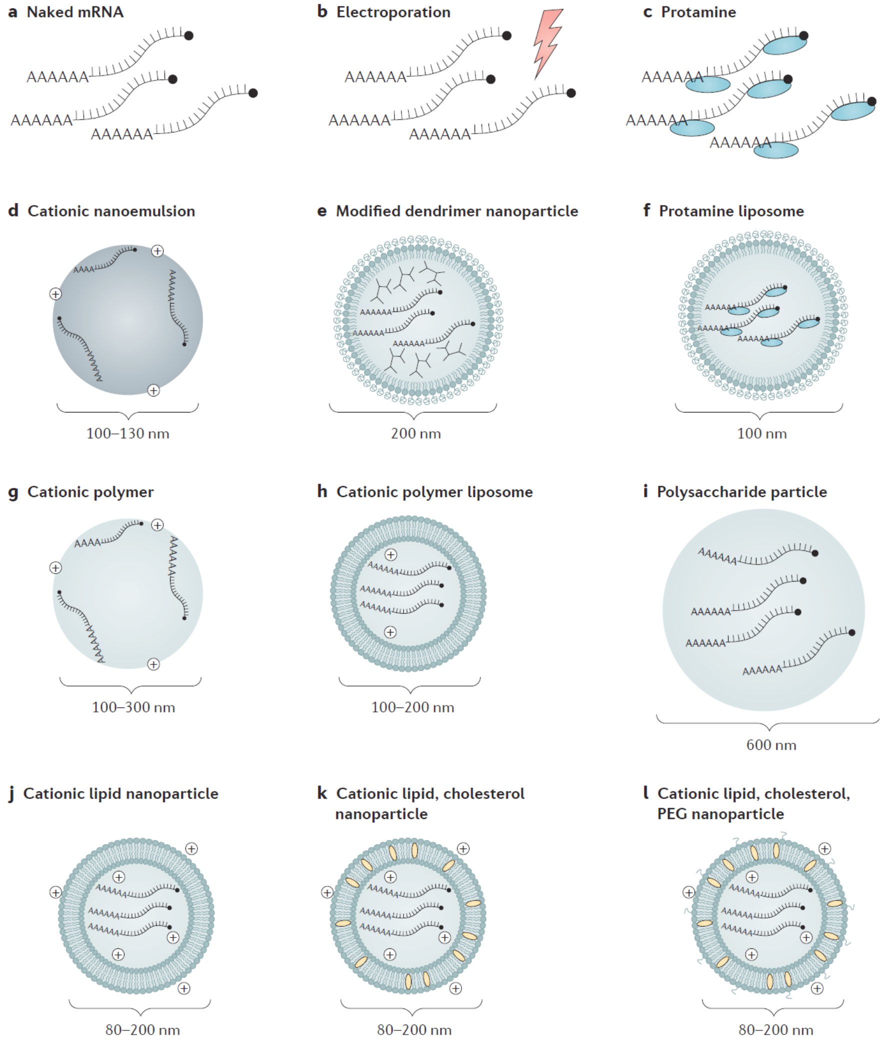

Figure 7. Main delivery methods for synthetic mRNA (Pardi et al., 2018)

5. CONCLUSION

The use of mRNA-based gene therapy could be a great help for patients suffering from various diseases such as cancer, infectious diseases, genetic disorders. To allow patients to produce their own therapeutic proteins makes the synthetic mRNA to a unique and attractive therapeutic molecule. It is hoped that this molecule will be used in more clinical applications in the coming years.

REFERENCES

1. Bugeon, S., de Chevigny, A., Boutin, C., Coré, N., Wild, S., Bosio, A., . . . Beclin, C. (2017). Direct and efficient transfection of mouse neural stem cells and mature neurons by in vivo mRNA electroporation. *Development*, dev. 151381.

2. Carlsten, M., & Childs, R. W. (2015). Genetic manipulation of NK cells for cancer immunotherapy: techniques and clinical implications. *Frontiers in immunology, 6*, 266.
3. Carlsten, M., Levy, E., Karambelkar, A., Li, L., Reger, R., Berg, M., . . . Childs, R. W. (2016). Efficient mRNA-based genetic engineering of human NK cells with high-affinity CD16 and CCR7 augments rituximab-induced ADCC against lymphoma and targets NK cell migration toward the lymph node-associated chemokine CCL19. *Frontiers in immunology, 7*, 105.
4. Fotin-Mleczek, M., Zanzinger, K., Heidenreich, R., Lorenz, C., Thess, A., Duchardt, K. M., & Kallen, K. J. (2012). Highly potent mRNA based cancer vaccines represent an attractive platform for combination therapies supporting an improved therapeutic effect. *The journal of gene medicine, 14*(6), 428-439.
5. Gonçalves, C., Akhter, S., Pichon, C., & Midoux, P. (2016). Intracellular availability of pDNA and mRNA after transfection: A comparative study among polyplexes, lipoplexes, and lipopolyplexes. *Molecular pharmaceutics, 13*(9), 3153-3163.
6. Hattinger, E., Scheiblhofer, S., Roesler, E., Thalhamer, T., Thalhamer, J., & Weiss, R. (2015). Prophylactic mRNA vaccination against allergy confers long-term memory responses and persistent protection in mice. *Journal of immunology research, 2015*.
7. Jemielity, J., Kowalska, J., Rydzik, A. M., & Darzynkiewicz, E. (2010). Synthetic mRNA cap analogs with a modified triphosphate bridge–synthesis, applications and prospects. *New Journal of Chemistry, 34*(5), 829-844.
8. Johansson, D. X., Ljungberg, K., Kakoulidou, M., & Liljeström, P. (2012). Intradermal electroporation of naked replicon RNA elicits strong immune responses. *PloS one, 7*(1), e29732.
9. Kauffman, K. J., Dorkin, J. R., Yang, J. H., Heartlein, M. W., DeRosa, F., Mir, F. F., . . . Anderson, D. G. (2015). Optimization of lipid nanoparticle formulations for mRNA delivery in vivo with fractional factorial and definitive screening designs. *Nano letters, 15*(11), 7300-7306.
10. Kormann, M. S., Hasenpusch, G., Aneja, M. K., Nica, G., Flemmer, A. W., Herber-Jonat, S., . . . Schams, A. (2011). Expression of therapeutic proteins after delivery of chemically modified mRNA in mice. *Nature biotechnology, 29*(2), 154.
11. Kranz, L. M., Diken, M., Haas, H., Kreiter, S., Loquai, C., Reuter, K. C., . . . Hefesha, H. (2016). Systemic RNA delivery to dendritic cells exploits antiviral defence for cancer immunotherapy. *Nature, 534*(7607), 396.
12. Kwon, H., Kim, M., Seo, Y., Moon, Y. S., Lee, H. J., Lee, K., & Lee, H. (2018). Emergence of synthetic mRNA: In vitro synthesis of mRNA and its applications in regenerative medicine. *Biomaterials, 156*, 172-193.
13. Lee, K., Kim, M., Seo, Y., & Lee, H. (2018). Development of mRNA vaccines and their prophylactic and therapeutic applications. *Nano Research*, 1-20.
14. Lu, D., Benjamin, R., Kim, M., Conry, R., & Curiel, D. (1994). Optimization of methods to achieve mRNA-mediated transfection of tumor cells in vitro and in vivo employing cationic liposome vectors. *Cancer gene therapy, 1*(4), 245-252.
15. McNamara, M. A., Nair, S. K., & Holl, E. K. (2015). RNA-based vaccines in cancer immunotherapy. *Journal of immunology research, 2015*.
16. Meng, Z., O'Keeffe-Ahern, J., Lyu, J., Pierucci, L., Zhou, D., & Wang, W. (2017). A new developing class of gene delivery: Messenger RNA-based therapeutics. *Biomaterials science, 5*(12), 2381-2392.

17. Michel, T., Wendel, H.-P., & Krajewski, S. (2016). Next-Generation Therapeutics: mRNA as a Novel Therapeutic Option for Single-Gene Disorders. In *Modern Tools for Genetic Engineering*: InTech.
18. Muttach, F., Muthmann, N., & Rentmeister, A. (2017). Synthetic mRNA capping. *Beilstein journal of organic chemistry, 13*(1), 2819-2832.
19. Na, D., Yoo, S. M., Chung, H., Park, H., Park, J. H., & Lee, S. Y. (2013). Metabolic engineering of Escherichia coli using synthetic small regulatory RNAs. *Nature biotechnology, 31*(2), 170.
20. Pardi, N., Hogan, M. J., Porter, F. W., & Weissman, D. (2018). mRNA vaccines—a new era in vaccinology. *Nature Reviews Drug Discovery, 17*(4), 261.
21. Pasquinelli, A., Dahlberg, J. E., & Lund, E. (1995). Reverse 5'caps in RNAs made in vitro by phage RNA polymerases. *Rna, 1*(9), 957-967.
22. Petsch, B., Schnee, M., Vogel, A. B., Lange, E., Hoffmann, B., Voss, D., . . . Stitz, L. (2012). Protective efficacy of in vitro synthesized, specific mRNA vaccines against influenza A virus infection. *Nature biotechnology, 30*(12), 1210.
23. Proudfoot, N. J., Furger, A., & Dye, M. J. (2002). Integrating mRNA processing with transcription. *Cell, 108*(4), 501-512.
24. Qiu, P., Ziegelhoffer, P., Sun, J., & Yang, N. (1996). Gene gun delivery of mRNA in situ results in efficient transgene expression and genetic immunization. *Gene therapy, 3*(3), 262-268.
25. Quabius, E. S., & Krupp, G. (2015). Synthetic mRNAs for manipulating cellular phenotypes: an overview. *New biotechnology, 32*(1), 229-235.
26. Ramanathan, A., Robb, G. B., & Chan, S.-H. (2016). mRNA capping: biological functions and applications. *Nucleic acids research, 44*(16), 7511-7526.
27. Sahin, U., Karikó, K., & Türeci, Ö. (2014). mRNA-based therapeutics—developing a new class of drugs. *Nature Reviews Drug Discovery, 13*(10), 759.
28. Sergeeva, O., Koteliansky, V., & Zatsepin, T. (2016). mRNA-based therapeutics–Advances and perspectives. *Biochemistry (Moscow), 81*(7), 709-722.
29. Steinle, H., Behring, A., Schlensak, C., Wendel, H. P., & Avci-Adali, M. (2017). Concise review: application of in vitro transcribed messenger RNA for cellular engineering and reprogramming: progress and challenges. *Stem Cells, 35*(1), 68-79.
30. Stepinski, J., Waddell, C., Stolarski, R., Darzynkiewicz, E., & Rhoads, R. E. (2001). Synthesis and properties of mRNAs containing the novel "anti-reverse" cap analogs 7-methyl (3′-O-methyl) GpppG and 7-methyl (3′-deoxy) GpppG. *Rna, 7*(10), 1486-1495.
31. Strenkowska, M., Kowalska, J., Lukaszewicz, M., Zuberek, J., Su, W., Rhoads, R. E., . . . Jemielity, J. (2010). Towards mRNA with superior translational activity: synthesis and properties of ARCA tetraphosphates with single phosphorothioate modifications. *New Journal of Chemistry, 34*(5), 993-1007.
32. Tavernier, G., Andries, O., Demeester, J., Sanders, N. N., De Smedt, S. C., & Rejman, J. (2011). mRNA as gene therapeutic: how to control protein expression. *Journal of controlled release, 150*(3), 238-247.
33. Van Gulck, E., Vlieghe, E., Vekemans, M., Van Tendeloo, V. F., Van De Velde, A., Smits, E., . . . Mertens, L. (2012). mRNA-based dendritic cell vaccination induces potent antiviral T-cell responses in HIV-1-infected patients. *Aids, 26*(4), F1-F12.

34. Wang, J., Exline, C. M., DeClercq, J. J., Llewellyn, G. N., Hayward, S. B., Li, P. W.-L., . . . Holmes, M. C. (2015). Homology-driven genome editing in hematopoietic stem and progenitor cells using ZFN mRNA and AAV6 donors. *Nature biotechnology, 33*(12), 1256.
35. Weissman, D. (2015). mRNA transcript therapy. *Expert review of vaccines, 14*(2), 265-281.
36. Wolff, J. A., Malone, R. W., Williams, P., Chong, W., Acsadi, G., Jani, A., & Felgner, P. L. (1990). Direct gene transfer into mouse muscle in vivo. *science, 247*(4949), 1465-1468.
37. Youn, H., & Chung, J.-K. (2015). Modified mRNA as an alternative to plasmid DNA (pDNA) for transcript replacement and vaccination therapy. *Expert opinion on biological therapy, 15*(9), 1337-1348.
38. Zeyer, F., Mothes, B., Will, C., Carevic, M., Rottenberger, J., Nürnberg, B., . . . Kormann, M. S. (2016). mRNA-mediated gene supplementation of toll-like receptors as treatment strategy for asthma in vivo. *PloS one, 11*(4), e0154001.
39. Zhong, Z., Mc Cafferty, S., Combes, F., Huysmans, H., De Temmerman, J., Gitsels, A., . . . Sanders, N. N. (2018). mRNA therapeutics deliver a hopeful message. *Nano Today*.
40. Zhou, W.-Z., Hoon, D., Huang, S., Fujii, S., Hashimoto, K., Morishita, R., & Kaneda, Y. (1999). RNA melanoma vaccine: induction of antitumor immunity by human glycoprotein 100 mRNA immunization. *Human gene therapy, 10*(16), 2719-2724.